Development and verification of an ECG processing algorithm for fast post-hoc analysis of large datasets collected with VREACT

Diplomarbeit

zur Erlangung des akademischen Grades eines

Diplom-Ingenieur (Dipl.-Ing.)

im Rahmen des Studiums

Biomedical Engineering

ausgeführt am

Institut für Biomedizinische Elektronik

an der

Technischen Universität Wien

unter der Anleitung von

Univ.Ass. Dipl.-Ing. Klaus Zeiner

Univ.Prof. Dipl.-Ing. Dr.techn. Eugenijus Kaniusas

eingereicht von

Dr. med. univ. Michael Desch BSc

(Matrikelnummer 1226622)

Abstract

With todays possibilities of easy and fast medical data collection the amount of gathered data increases at a fast pace. Hence, also the need for quick and reliable analysis algorithms to get an overview and first insights of a dataset is very high. The goal of this diploma thesis was to develop signal processing algorithms with the objective of analyzing the heart rate variability (HRV) of already recorded electrocardiograms (ECGs). The patient data was provided by the Department of Anaesthesia of the Medical University of Vienna and was recorded from patients under general anaesthesia during different surgical procedures. In order to achieve this goal the ECG data first had to be preprocessed and signal distortions and artefacts needed to be eliminated. Then an automated QRS complex detection algorithm was used to detect the exact position of every heart beat and subsequently the beat to beat intervals were calculated. By applying some further signal quality improvement algorithms (artefact detection based on the beat to beat intervals and detection of ectopic heart beats) a mean heart beat detection positive predictive value (PPV) of 98.89% and sensitivity of 97.38% were achieved as compared with the original QRS complex detection algorithm, which achieved a mean PPV of 97.92% and sensitivity of 97.93%. From the beat to beat intervals subsequently the following HRV parameters were calculated in the time domain: the standard deviation of normal to normal heartbeat intervals (SDNN), the root mean square of successive heartbeat interval differences and the percentage of successive normal to normal heartbeat intervals differing by more than 50ms. These parameters were calculated for the whole dataset and for standard 5 minute data-segments and were then statistically analyzed. A correlation between the SDNN and the following metadata was found: American Society of Anesthesiologists physical status classification, diabetes mellitus and inflammation. Furthermore the time under general anaesthesia seems to influence the HRV as most of the patients show a drop in the SDNN by aproximately 50% about 10 min after the ECG recording is started. Overall the quality of the beat detection and thus the HRV data produced by the algorithms developed in this work proved to be more than sufficient for the investigation of the present dataset. However the dataset lacks some metadata and details like the mode of the artificial ventilation and drugs given to the patients. Thereby, if there were more sufficient information available, there might be even more statistically/clinically relevant conclusions gained from the HRV investigation. The next step will be a handover of the developed tools to healthcare professionals in order to investigate other ECG datasets and gather feedback from the end users.

Kurzfassung

Mit den heutigen Möglichkeiten der einfachen Aufzeichnung medizinischer Biosignale nimmt die Datenmenge dieser schnell zu. Um einen ersten Einblicke in einen Datensatz zu erhalten ist daher auch der Bedarf an schnellen und zuverlässigen Analysealgorithmen hoch. Das Ziel dieser Diplomarbeit bestand darin, Signalverarbeitungsalgorithmen zu entwickeln, um die Herzfrequenzvariabilität (HRV) bereits aufgezeichneter Elektrokardiogramme (EKGs) zu analysieren. Die dafür genutzten Patientendaten wurden vom Department für Anästhesie der Medizinischen Universität Wien zur Verfügung gestellt und stammten von narkotisierten Patienten während chirurgischer Eingriffe. Zu diesem Zweck mussten die EKGs zunächst vorverarbeitet werden um Signalverzerrungen und Artefakte zu beseitigen. Anschließend wurde ein QRS-Komplex Detektionsalgorithmus verwendet um die genaue Position jedes Herzschlags zu ermitteln und daraus wurden die Schlag-zu-Schlag-Intervalle berechnet. Durch weitere Algorithmen zur Verbesserung der Signalqualität (Artefakterkennung basierend auf den Schlag-zu-Schlag-Intervallen und Erkennung von ektoptischen Schlägen) wurde eine Schlagdetektionssensitivität von 97,38% und ein positiver Vorhersagewert von 98,89% erreicht. Im Vergleich dazu wurde mit dem originalen Algorithmus eine Sensitivität von 97.93% und ein positiver Vorhersagewert von 97.92% gemessen. Aus den Schlag-zu-Schlag-Intervallen wurde anschließend folgende HRV Parameter im Zeitbereich berechnet: die Standardabweichung der Schlagintervalle (SDNN), das quadratische Mittel aufeinanderfolgender Intervalle und der Prozentsatz aufeinanderfolgender Intervalle, die sich um mehr als 50 ms unterscheiden. Es wurde eine Korrelation zwischen der SDNN und den folgenden Metadaten festgestellt: American Society of Anesthesiologists Risikoklassifikation, Diabetes mellitus und Entzündungswerte. Darüber hinaus scheint die Dauer der Vollnarkose die HRV zu beeinflussen, da die meisten Patienten etwa 10 min nach Beginn der EKG-Aufzeichnung einen Abfall der SDNN von etwa 50% aufweisen. Insgesamt erwies sich die Qualität der in dieser Arbeit entwickelten Algorithmen zur Herzschlagdetektion und somit die erzeugten HRV-Daten mehr als ausreichend für die Untersuchung der vorliegenden Daten. Allerdings fehlen in dem Datensatz einige Metadaten und Details wie beispielsweise der Modus der Beatmung und die verabreichten Medikamente. Daher könnte bei Vorhandensein zusätzlicher Informationen noch mehr statistisch/klinisch relevante Erkenntnisse aus der HRV-Untersuchung gewonnen werden. Der nächste Schritt besteht nun darin, die entwickelten Tools an Ärzte zu übergeben, um andere EKG-Datensätze zu untersuchen und Feedback von diesen zu sammeln.

Acknowledgments

I would like to express my gratitude to Prof. Eugenijus Kaniusas and Klaus Zeiner for providing me with the opportunity to complete my master's thesis in this fascinating field. I am truly grateful for their unwavering support, valuable suggestions, and constructive feedback throughout the entire project. Their abundance of patience and understanding, as well as the flexibility to pursue this thesis alongside my regular work at the hospital, are deeply appreciated.

Furthermore, I would like to thank all colleagues and friends I have acquired during my studies, particularly for the collaborations that played a vital role in the successful completion of both my degrees. Most importantly, I would like to express my deepest gratitude to my family and my girlfriend, Rosmarie, for their unwavering support and presence whenever I needed it.

Contents

Acronyms

AC alternating current

AIT Austrian Institute of Technology

ANS autonomic nervous system

ASA American Society of Anesthesiologists

ATP adenosine triphosphate

AV node atrioventricular node

BMI body mass index

BNP B-type natriuretic peptide

Ca^{++} calcium ion

Cl^{-} chloride ion

CRP C-reactive protein

DC direct current

ECG electrocardiogram

HbO_2 oxygenated hemoglobin

Hb (deoxygenated) hemoglobin

HF high frequency

HRV heart rate variability

ICU intensive care unit

K^{+} potassium ion

LED light-emitting diode

LF low frequency

MET metabolic equivalent

Na^+ sodium ion

NSQIP National Surgical Quality Improvement Program

NYHA New York Heart Association

pNN50 percentage of successive normal to normal heartbeat intervals differing by more than 50ms

PPG photoplethysmogram

PPV positive predictive value

RCRI Revised Cardiac Risk Index

RMSSD root mean square of successive heartbeat interval differences

SA node sinoatrial node

SDANN standard deviation of the average normal-to-normal intervals

SDNN standard deviation of normal to normal heartbeat intervals

SpO_2 peripheral oxygen saturation

ULF ultra low frequency

VLF very low frequency

VREACT Vital-signs REal-time Analysis for Clinical Translation

VT ventricular tachycardia

1. Introduction

The main physiological processes of the human body (like breathing, heart beats, oxygen transport and many more) are associated with so-called biosignals. These signals reflect properties of their underlying biological systems and can contain clinically significant information about physiological or pathological condition of patients [1].

The signals which are of electrical, optical, chemical or acoustic origin can either be sensed using a simple tool like a stethoscope, or the detection may require complex measuring systems and signal processing setups. As biosignals are often considerably complex the information conveyed in those signals may not be immediately perceivable and therefore has to be decoded or extracted in some way before the signals can be given meaningful interpretations. Thus, biomedical signal processing has become an indispensable tool for physicians to extract clinically significant information hidden in the biosignals [1].

A typical application that requires the continuous measurement of different biosignals is the perioperative environment, where patients are under general anaesthesia and their bodily functions need to be maintained from the outside. Although advances in modern anaesthesia are constantly improving clinical patient safety, the perioperative period represents a high-risk setting for patients and a major threat associated with general anaesthesia are cardiovascular complications [2, 3]. Current monitoring set-ups in the perioperative setting provide basic parameters like an electrocardiogram (ECG), blood pressure or peripheral oxygen saturation (SpO_2). While these signals are important for general health status tracking, they lack to offer a predictive value regarding cardiovascular complications.

There is evidence that a compromised function of the autonomic nervous system (ANS) shows a strong correlation with adverse cardiovascular events. Therefore, assessment of ANS activity in the perioperative period might be used as a risk indicator. A possible method to observe the ANS activity is the so called heart rate variability (HRV) [4, 5, 6]. In this work, the HRV of patients during general anesthesia was computed retrospectively by analyzing the standard ECG records of the patient monitoring system. Using the

scientific computing environment MATLAB, the time interval from one heart beat to the next was automatically detected and the HRV parameters were then calculated as the standard deviation of normal to normal heartbeat intervals (SDNN) in the time domain.

1.1. Anatomical and physiological background

To understand how biosignals like the ECG arise and what factors have an influence on them, it is necessary to first understand some basic physiological principles. Those principles as well as the basics of the human hearts anatomy are explained in the following sections.

1.1.1. Autonomic nervous system (ANS)

The function of the ANS is to keep the internal milieu of the body constant (homeostasis) or adjust it as required by changing circumstances (e.g. mechanical work, pain, food intake, water deprivation, heat or cold). For this purpose, the ANS controls and regulates bodily functions, such as the heart rate, the heart's contractibility, tonus of the smooth musculature, vascular tone, digestion, respiratory rate, pupillary response, urination, sexual arousal and the activity of other internal organs such as glands [7].

The ANS is also called the vegetative nervous system and it is a control system that acts largely unconsciously. Thereby it is distinguished from the somatic nervous system, which is subject to voluntary control and accessible to consciousness [7].

1.1.1.1. Structure of the ANS

The ANS consists of three different parts: the **sympathetic**, the **parasympathetic** and the **enteric nervous system**.

The enteric nervous system is a network of neurons in the wall of the gastrointestinal tract, that is capable of operating independently of the brain and spinal cord, but has innervation from the vagus nerve and prevertebral ganglia. Its function is to regulate secretions in the gut as well as the gastric and intestinal peristalsis [7, 8].

The basic elements in the (peripheral) sympathetic and the parasympathetic systems are a set of two neuron populations (see Figure 1). These so called autonomic ganglions receive afferent fibers (input) via preganglionic neurons which originate in different parts of the spinal cord.

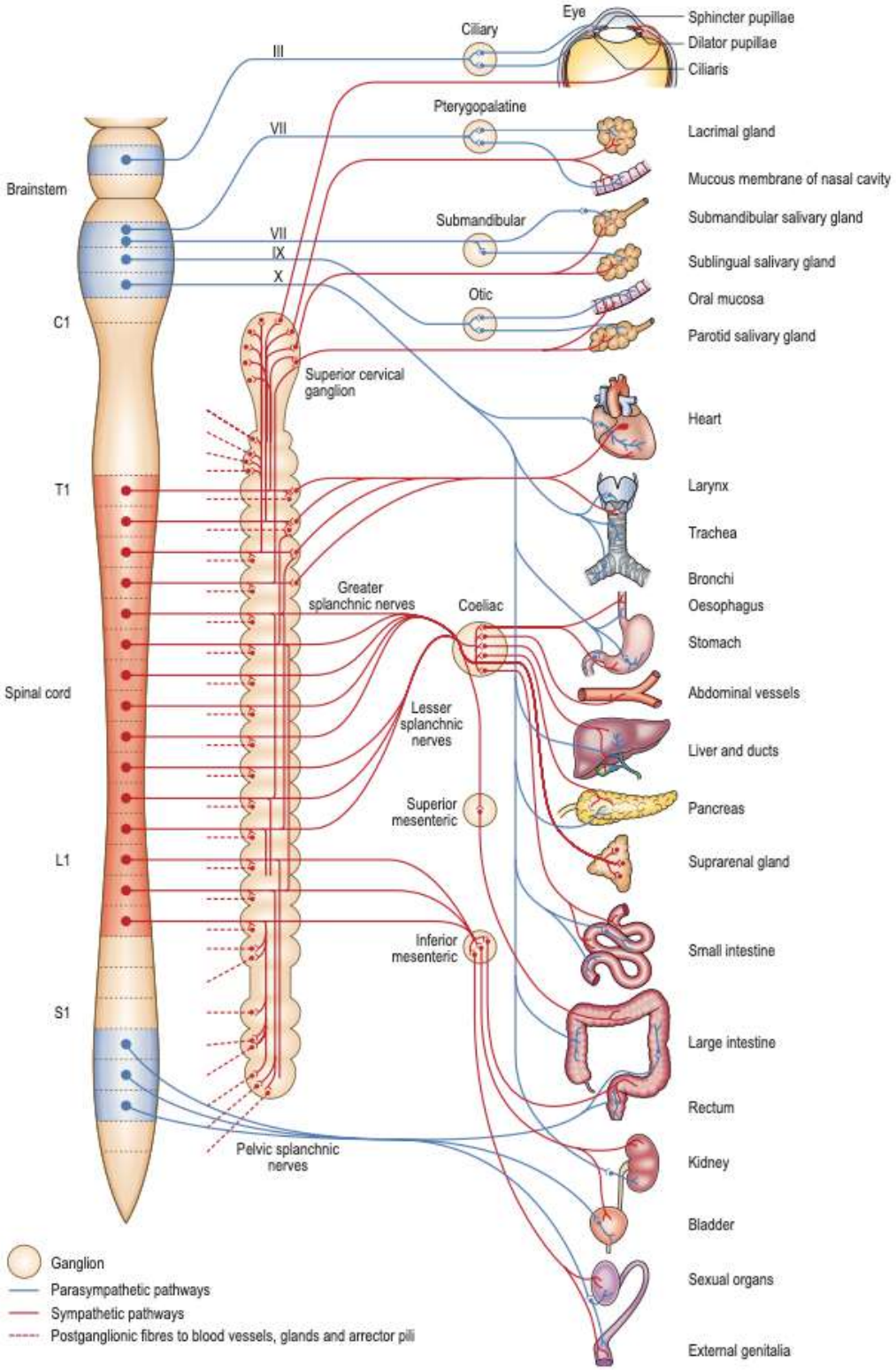

Figure 1.: Arrangement of the peripheral ANS as well as the effector organs [8].

Sympathetic system The sympathetic trunks consist of two ganglionated nerve cords that extend on either side of the vertebral column (paravertebral ganglia) and the unpaired prevertebral abdominal ganglia (collateral ganglia, or preaortic ganglia)[8]. Preganglionic axons (thin, unmyelinated or myelinated, conduction velocity $1\,\mathrm{m\,s^{-1}}$ to $10\,\mathrm{m\,s^{-1}}$[7]) join those ganglia from the thoracic spinal cord and the upper 2-3 segments of the lumbar spinal cord through the white rami communicantes and therefore the sympathetic system is also called the thoracolumbar system. Unmyelinated postganglionic axons leave sympathetic ganglia in the grey rami communicantes or special nerves to the effector organs in the head, thorax, abdomen or pelvis [7]. The nerves from the prevertebral ganglia often form plexuses (branching networks) before terminating at the effector organs. There are between 10 and 12 (usually 11) thoracic ganglia, 4 lumbar ganglia, and 4 or 5 ganglia in the sacral region [8].

The sympathetic system innervates the smooth muscles in all organs (vessels, viscera, excretory organs, lungs, hair, pupils). In addition, sympathetic postganglionic fibers influence the heart, some of the glands (sweat, salivary and digestive glands), adipose cells, liver cells, the renal tubules and lymphatic tissue (e.g., thymus, spleen, Peyer's patches and lymph nodes)[7]. Furthermore, the adrenal medulla consists of cells that are homologous the postganglionic neurones of the sympathetic system. Therefore when these cells get activated by preganglionic neurones from the thoracic spinal cord (T5-T11) they do not activate further effector cells in the adrenal medulla but release a mixture of adrenaline and noradrenaline into the bloodstream [7].

Parasympathetic system The cell bodies of the preganglionic parasympathetic neurons are in the sacral spinal cord and the brainstem and therefore the parasympathetic system is also called craniosacral system. From there the parasympathetic fibers for the muscles in the eye and for the glands in the head leave the brainstem in cranial nerves III (oculomotor), VII (facial) and IX (glossopharyngeal). The fibers to the organs in the thorax and abdomen run in the vagus nerve (cranial nerve X). The sacral parasympathetic fibers to the pelvic organs run in the pelvic nerve [8, 9]. The postganglionic nerves are situated right next to the effector organs. Thus, the unmyelinated or myelinated preganglionic nerves need to be quite long [7].

The effectors supplied by the parasympathetic system are the atria of the heart, the tear and salivary glands, and the intraocular muscles. It also innervates the smooth musculature and glands of the gastrointestinal tract, the excretory organs, the genitalia and the lungs. But it does not innervate the smooth muscles in blood vessels, except for

the arteries of the genitalia, the gastrointestinal wall and some parts of the brain and skin [7].

Central ANS At the level of the central nervous system there are different vegetative reflexes which are controlled by higher supra spinal centers in the medulla oblangata as well as in the Hypothalamus. The medulla oblangata also regulates the sympathetic tone and the respiratory and circulatory functions according to the requirements. From the hypothalamus there are many connections to other brain centers and it regulates the endocrine functions of the pituitary gland as well as the integration of emotional responses with the rest of the ANS [7, 9].

1.1.1.2. Neurotransmitters

A neurotransmitter is a molecule secreted by a neuron to affect another target cell across a synapse. In the body, this principle is used to transmit signals from one organ (or nerve) to another. The primary neurotransmitter used by the ANS are **acetylcholine** and **noradrenalin** respectively **adrenalin**, but to a lesser degree also **adenosine triphosphate (ATP)**, **nitric oxide (NO)** or **neuropeptides** are used for signal transduction [7].

Acetylcholine In the human body, there are different types of acetylcholine receptors [7]. The two main groups are:

- **nicotinic acetylcholine receptors:** at least four different kinds of ligand-gated ion channels
- **muscarinic acetylcholine receptors:** five different G-protein-coupled receptors

In the ANS acetylcholine is released at all (sympathetic and parasympathetic) preganglionic autonomic nerve endings (activating postsynaptic nicotinic receptors at the postganglionic neuron) and also by most postganglionic parasympathetic neurons (activating muscarinic receptors at the effector organ) [7]. There are also some exceptions like sweat glands and probably vasodilator neurons to the resistance vessels in the skeletal musculature where sympathetic postganglionic neurons also release acetylcholine [7].

Drugs that have the same action on effector cells as the parasympathetic nervous system are called parasympathomimetics or cholinergic drugs (e.g., nicotine, cholinesterase inhibitors). Drugs that block or weaken the action of acetylcholine on autonomic effector

cells are called parasympatholytics. The latter substances are anticholinergic drugs like atropine or glycopyrrolate.

Noradrenalin, adrenalin: α-/β-receptor concept Noradrenalin and adrenalin are so called catecholamines. Postganglionic sympathetic nerve endings release mostly noradrenalin as transmitter substance. Therefore, these neurons are called noradrenergic neurons. The responses of organs to noradrenalin and adrenalin are mediated by interaction of the catecholamines with so called adrenergic receptors. These are all G protein-coupled receptors and can be divided in two main groups of adrenoreceptors: α- and β-receptors. The most important subtypes are:

- **α_1-adrenoreceptors** (G_q coupled, activate phospholipase C) Are located postsynaptic in effector organs and mediate mostly smooth muscle contraction (mydriasis, vasoconstriction in the skin, mucosa and abdominal viscera).
- **α_2-adrenoreceptors** (inhibitory G_i coupled, inactivate adenylyl cyclase) Are located postsynaptic in effector organs in the central nervous system or at the presynaptic terminal of sympathetic neurones and thereby act as a negative feedback loop (autoreceptor).
- **β_1-adrenoreceptors** (G_s coupled, activate adenylyl cyclase) are situated mostly in the heart (positive chronotropic, dromotropic and inotropic effects) and also meditate the effect of the sympathetic system on the release of renin and lipolysis.
- **β_2-adrenoreceptors** (G_s or G_i coupled, activate or inactivate adenylyl cyclase) enhance glycogenolysis as well as lipolysis and meditate the relaxation of smooth muscles (for example bronchodilation).
- **β_3-adrenoreceptors** (G_s or G_i coupled, activate or inactivate adenylyl cyclase) Enhance lipolysis in adipose tissue and thermogenesis in skeletal muscle.

Most of the organs and tissues affected by catecholamines contain both α and β receptors in their cell membranes, and in most organs the two mediate opposite (antagonistic) effects. Under physiological conditions the response of an organ to catecholamines depends on whether the α- or the β-adrenergic action predominates [7].

There are also some drugs that imitate the action of sympathetic adrenergic neurons. These are called sympathomimetic (adrenomimetic) drugs. Drugs like β-/α-blockers block the action of sympathetic adrenergic neurons and are called sympatholytic (antiadrenergic) drugs [7].

1.1.1.3. Visceral afferents

In order to regulate internal organs like lungs, heart, circulatory system, gastrointestinal tract, excretory and genital organs, the ANS needs to obtain some information about the current state of vital values and organs (e.g., blood pressure, filling of the urinary bladder, blood oxygen concentration).

Sensors in the body measure stretching of the walls of the hollow organs via mechanosensors to monitor the intraluminal pressure (e.g., the arterial pressoreceptors and the urinary bladder) or the volume within an organ (e.g., the afferents from the muscles of the gastrointestinal tract, from the right atrium and from the lung). Furthermore, there are chemosensitive sensors measuring for example blood oxygen, carbon dioxide, pH in the walls of aorta and the carotids, osmotic concentration in the liver or glucose concentration in the intestinal mucosa [7].

This information is then transmitted to the central nervous system via the so called visceral afferents coming from the different sensors in the body. The nerve fibers from the internal organs run through the vagal ganglia (vagal afferents, vagus nerve) and in the spinal ganglia (spinal afferents). The fibers from the arterial presso- and chemosensors in the carotid bifurcation run in the glossopharyngeal nerve (cranial nerve IX). Most of these afferents end in the brainstem and the sacral cord [7]. There, this information is used to manipulate the activity of the parasympathetic and sympathetic system in order to set corrective action to adjust internal milieu of the body as required by changing circumstances. Therefore, the ANS can be considered as a closed loop control system [7].

Strong stretching and contraction of the gastrointestinal tract and the urinary bladder, mesenterial tension or ischemic stimuli have the ability to activate pain receptors within the internal organs. Thereby, these stimuli can lead to the perception of visceral pain sensations [7].

1.1.1.4. Effects on various organs

Most of the internal organs receive both sympathetic and parasympathetic innervation. These systems are functionally integrated but the effect of the two systems are widely antagonistic. For example, stimulation of sympathetic nerves causes increase in heart frequency and stroke volume. Excitation of parasympathetic fibers (electrical stimulation of the vagus nerve) has the opposite effects: decrease in heart rate and the contractile force of the atria [9].

Target organ	Parasympathetic	Sympathetic
Digestive system	Increases peristaltic, stimulates the activity of the pancreas, stimulates the gall bladder	Inhibits the activity of the digestive organs, decreases activity of the pancreas
Liver and fat cells	No effect	Release of glucose and lipolysis
Lungs	Constricts bronchioles	Dilates bronchioles
Urinary tract	Relaxes sphincter and constricts urinary badder	Constricts sphincter and relaxes urinary bladder
Kidneys	No effects	Decrease urine production
Heart	Decreases heart rate	Increases heart rate, force of contraction and provides vasodilation for the coronary vessels of the heart
Blood vessels	Dilating blood vessels leading to the GI tract	Constricts blood vessels in viscera, blood flow to skeletal muscles and the lungs is enhanced (increases blood pressure)
Salivary glands	Increases production of saliva and tears	Inhibits (result in dry mouth and dry eyes)
Eye (iris)	Constrict pupils	Dilates pupils
Adrenal Medulla	No effect	Stimulate the secretion of epinephrine and norepinephrine
Genitalia	Stimulates erection	Stimulates orgasm

Table 1.: Effects of the parasympathetic and sympathetic system on various organs [7].

Normally it is always the sum of these opposed effects that act complementary and regulate the activity of the organs. Under physiological conditions, the innervation the parasympathetic regulation mostly predominates over the sympathetic system [7]. In Table 1 the main effects of the sympathetic and parasympathetic system on various organs are listed. Of course, this list is not complete as both of these systems act on an enormous amount of effector organs.

1.1.2. Heart

The pump that drives the blood through the vessels is the heart. It can be seen as two parallel pumps - the right and the left half. Each half comprises an atrium and a ventricle. The right half receives oxygen-depleted blood from the entire body and sends it to the lungs, where it is charged with oxygen. The oxygenated blood is returned to the left half of the heart and is then distributed to all organs of the body.

The pumping action of the heart is based on a rhythmic sequence of relaxation (diastole) and contraction (systole) of the hearts chambers (atria and ventricles). During diastole the heart chambers fill with blood, and during systole they expel it into the large arteries.

1.1.2.1. Anatomy

The anatomy of the human heart is shown in Figure 2. A typical adult heart has a mass of 250 g to 350 g and is about the size of a fist. It is cone shaped, with its apex pointed downwards and the base positioned upwards and is situated in the middle mediastinum. In the thorax it is usually slightly offset to the left side and therefore the left lung is usually smaller than the right lung [8].

As already mentioned, each half of the human heart consists of an atria and a ventricle and therefore the heart has a total of four chambers: two atria and two ventricles. Between the two atria lies the interatrial septum and the interventricular septum separates the two ventricles. The right atrium and the right ventricle together are referred to as the right heart. Similarly, the left atrium and the left ventricle together are called the left heart [8].

Furthermore, the heart consists of four valve in order to allow blood pumping action only in one direction. The two valves between the atria and ventricles are called the atrioventricular valves, which are situated in the atrioventricular septum. Between the right atrium and the right ventricle is the tricuspid valve, which has three cusps. The mitral valve lies between the left atrium and left ventricle. It is also known as the bicuspid valve because it has two cusps. Both of these vales are attached to so called papillary muscles to give them more stability [8].

Two additional semilunar valves are situated at the exit of each of the ventricles. The pulmonary valve is located at the origin of the pulmonary artery and the semilunar aortic valve is situated at the base of the aorta. These valves close, when the ventricle relaxes and blood flows back into these pocket-like valves. Both of these valves usually

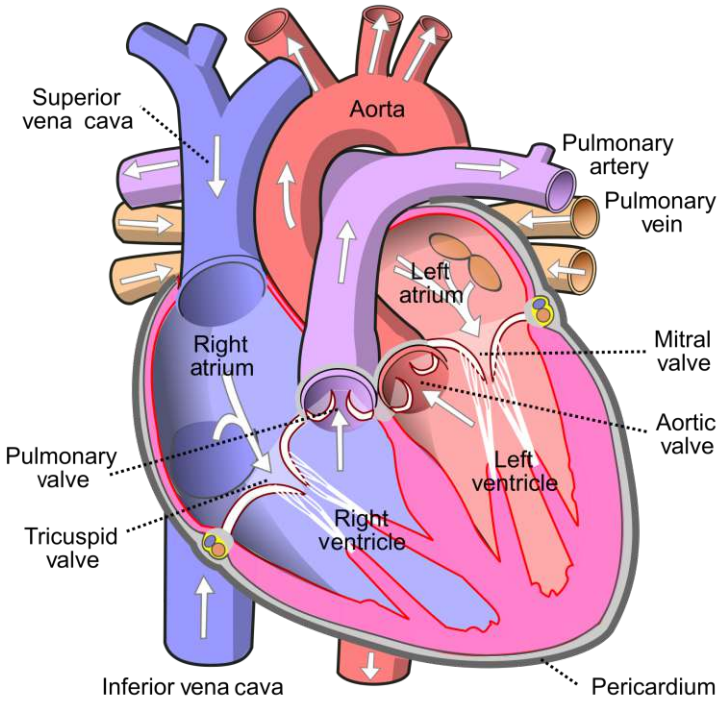

Figure 2.: Anatomy (coronal section) of the human heart [10].

have three cusps [8].

The heart wall is made up of three layers. The innermost single layered squamous epithelium is called the endocardium and covers the heart chambers as well as the valves and is continuous with the endothelium of the veins and arteries. The middle layer is the myocardium, which consists of involuntary striated muscle tissue surrounded by a framework of collagen. The outermost layer of the heart is called epicardium. These three layers are surrounded by a double-membraned sac called the pericardium [8].

1.1.2.2. Blood flow

During the diastole the right atrium receives deoxygenated blood from the body's two biggest veins, the superior and inferior venae cavae. In the systole, the right atrium pumps the blood to the right ventricle and the right ventricle further ejects the blood into the pulmonary trunk, which branches into the left and right pulmonary arteries that carry the blood to each lung [8].

At the same time, in the diastole the left atrium receives oxygenated blood back from the lungs via one of the four pulmonary veins. In the systole, the left atrium pumps the

blood to the left ventricle through the mitral valve. The left ventricle then pumps blood to the body through the aortic valve into the aorta. The left ventricle is much thicker compared to the right ventricle, due to the increased force required to pump blood to the entire body and the higher pressure it needs to overcome [8].

The circulatory system can therefore be seen as two consecutive circuits: the systemic circulation to and from the body and the pulmonary circulation to and from the lungs. The right heart therefore pumps out only deoxygenated blood from the vena cavae into the lungs, and the left half only oxygenated blood from the pulmonal veins into the aorta.

The heart tissue itself receives oxygen and nutrients mainly during the diastolic phase via blood from the left and the right coronary artery. These two arteries originate from two small openings in the aorta just above the aortic valve [8].

1.1.2.3. Electrical conduction system of the heart

The rhythmic pulsation of the heart is generated by excitatory signals generated within the heart itself. This property is called autorhythmicity. The spontaneous rhythmic triggering of excitation is performed by specialized pacemaker cells [9].

In a healthy human the heartbeat is initiated in the sinoatrial node (SA node) - also called sinus node - in the the upper part of the right atrium. From the SA node the excitation then spreads to and through the myocardium of both atria. To get to the ventricles the signal then needs to conduct through the atrioventricular node (AV node), because the rest of the atrioventricular septum consists of unexcitable connective tissue. In the AV node, the excitation is delayed by about 100 ms before it then propagates to the ventricle through the bundle of His and its left and right bundle branches and their terminal network, the Purkinje fibers. From the subendocardial endings of the Purkinje fibers the excitation spreads over to the ventricular musculature [8, 9]. The delay in the AV node is necessary because otherwise the atria and ventricles would contract at the same time, and there would be no time for the blood to flow from the atria into the ventricles. This electrical conduction system of the heart is shown in Figure 3.

When the SA node fails to initiate an excitation pace-making cells further down the conduction system can take over its function as the pacemaker. All of this pace-making centers have an intrinsic frequency F_c which decreases from SA node ($F_c = 70\,\mathrm{min}^{-1}$) to the bundle of His ($F_c = 30\,\mathrm{min}^{-1}$). So, in principle the heart can work completely without any nerve supply from the rest of the body [9].

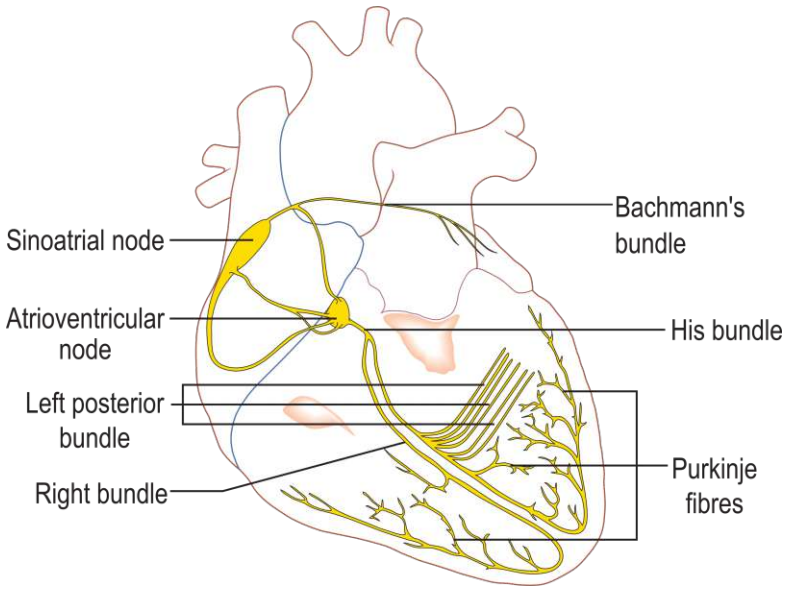

Figure 3.: Electrical conduction system of the human heart [11].

1.1.2.4. Membrane potentials and excitation

The voltage across a cell membrane is referred to as membrane potential (also transmembrane potential or membrane voltage). It is caused by differences in the concentrations of ions inside and outside of the cell. This concentration gradients are generated by actively pumping ions and by different ion permeabilities of the cell membrane [7].

The smooth muscle cells in the heart are electrically excitable, but without an outside stimulus they stay in a stable resting state. During this resting state the cell membrane is most permeable to potassium ions (K^+), which can travel into or out of cell through leak channels. All other ions cannot go through the cell wall that easily [7]. The concentrations of the most important ions in a resting heart cell are shown in Table 2. Therefore the inside of these cells is negatively charged compared to the outside. The resulting membrane potential is referred to as resting potential or resting voltage. Under normal circumstances the resting potential of heart cells is about $-90\,\mathrm{mV}$ [7].

The heart muscle cells are interconnected via gap junctions that allow some ion transport between the cells. This means once a heart cell gets electrically excited it will also lead to some shift of charge to or from neighboring cells. This will lead to some depolarization of the neighboring cells.

Once the depolarization of a heart muscle cell reaches a value of about $-70\,\mathrm{mV}$, voltage-dependent fast sodium ion (Na^+) channels open rapidly and the inwardly rectifying K^+ channels get inactivated. This allows for a rapid flow of Na^+ into the cell,

Ion	$c_{Outside}$ ($mmol\,l^{-1}$)	c_{Inside} ($mmol\,l^{-1}$)
K^+	4.4	140
Na^+	143	12
Ca^{++}	1.25	0.0001
Cl^-	115	4
HCO_3^-	27	12

Table 2.: Ion concentrations inside and outside of a resting cell.

depolarizing the membrane completely and initiating an action potential.

During this phase, the membrane is almost exclusively permeable by Na^+ and therefore the membrane potential rises towards the equilibrium potential of Na^+ of about 60 mV (intracellular Na^+ concentration $12\,mmol\,l^{-1}$, extracellular Na^+ concentration $143\,mmol\,l^{-1}$, see Table 2). However, this value is not reached because the voltage-dependent fast Na^+ channels start to close and lock (become inactive) after about 1 ms when the membrane potential is about −40 mV. Therefore, the maximum value of the membrane potential is only about 20 mV (overshoot). After that, the muscle cell starts to partially repolarize due to a transient K^+ efflux (K^+ channels open and close rapidly) and a chloride ion (Cl^-) influx.

This short repolarisation is followed by a long plateau phase where the membrane potential is about 0 mV. This is due to the balance of repolarizing currents and the slow calcium ion (Ca^{++}) influx via L-type Ca^{++} channels. These channels slowly open above −40 mV but stay open longer than the voltage-dependent fast Na^+ channels. Thus, the plateau phase can last about 200 ms to 400 ms depending on the heart frequency.

As the Ca^{++} channels close and the repolarizing K^+ currents predominate the final rapid repolarization phase begins. Two of the most important channels in this phase are the slow delayed rectifier K^+ channels and the rapid delayed rectifier K^+ channels.

These two rectifier K^+ channels close when the membrane potential is restored to about −85 mV to −90 mV, while inwardly rectifying K^+ channels remain conducting. This restores the resting membrane potential.

This change of the distribution of ions can be measured using electrodes on the body's surface. The working principle of this so-called ECG is described in subsection 1.2.3 and can give information about the physiological or pathological mechanisms in the heart.

Refractory period During the plateau phase the heart muscle cell cannot produce another action potential therefore this time is called the absolute refractory period. This is due to the voltage-dependent fast Na^+ channels being completely inactive above $-40\,mV$.

This period is followed by the relative refractory period, during which the voltage-dependent fast Na^+ channels are only partially inactive and a stronger-than-usual stimulus can produce another action potential. Such stimuli in the so called vulnerable phase can lead to circulating arrhythmia.

Na^+/K^+-ATPase During one action potential ions get shifted between the inside and outside of the cells. To regain the original ion gradient it is necessary to actively pump ions. This is done by the Na^+/K^+-ATPase, which pumps 3 Na^+-ions to the outside and 2 K^+-ions to the inside of the cell by using one ATP molecule as energy source.

Furthermore, other membrane proteins like the Na^+/Ca^{++}-exchanger are necessary to restore the same ion distribution as before the action potential.

Pacemaking cells Due to leak channels, pacemaker cells have an unstable resting potential. This means their resting potential gradually rises until a depolarization is initiated. This then triggers an action potential and spreads out to neighboring cells [9].

1.1.2.5. Electromechanical coupling

In a healthy human, whenever an action potential reaches a myocardial cell it causes a contraction and thereby a heart stroke [9]. This process is explained briefly in this section.

As already mentioned in subsubsection 1.1.2.4, the action potential comprises an inward flow of both Na^+ and Ca^{++}. The comparatively small flow of Ca^{++} through the L-type Ca^{++} channels triggers a much larger release of Ca^{++} from the sarcoplasmic reticulum. This process is called calcium-induced calcium release [9].

The two main myofilaments in cardiac muscle are actin and myosin. When Ca^{++} is present in the myocardial cell, it binds to a protein called troponin, which itself is bound to the actin filament. This binding causes a shape change in the troponin which enables the head of the myosin filament to bind to the actin. As a source of energy, ATP is then split up into adenosine diphosphate and inorganic phosphate and thereby used to change the shape of the myosin head. As a result, the actin is pushed along the myosin filament and shortens the muscle. This is called a power stroke [7].

Myosin then detaches from the actin by binding another ATP molecule and resets itself back to its original position. It then binds to another part of the actin and produces another power stroke, shortening the muscle further. This process continues, with the myosin head moving in a motion similar to that of rowing a boat.

Contraction ends when the Ca^{++} is removed from the cell. When this happens, the troponin changes back to its original shape, blocking the binding sites on actin and preventing the formation of crossbridges [9].

1.1.2.6. Autonomic Innervation

The heart receives nerve signals from both the parasympathetic and from the sympathetic system which arise from two paired cardiovascular centers in the medulla oblongata and pons (see subsection 1.1.1).

The sympathetic nerve supply is nearly uniformly distributed to all parts of the heart whereby the parasympathetic nerves branching off from the vagus nerves on both sides in the cervical region pass primarily to the right atrium (SA node and the AV node)[8, 9]. The autonomous nervous system can influence, but not control, the heart rate (chronotropic action) and the velocity of atrioventricular conduction (dromotropic action). Sympathetic nerves also influence the systolic force of heart contraction (inotropic action) whereby the parasympathetic innervation of the ventricles is sparse and its influence on systolic force is indirect, by inhibition of the sympathetic action [9].

Effect	Sympathetic	Parasympathetic
Cardiac output	β_1, (β_2): increases	M_2: decreases
Heart rate (SA node)	β_1, (β_2): increases	M_2: decreases
Conduction speed through the AV node	β_1: increases	M_2: decreases (can cause an AV block)
Atrial contractility	β_1, (β_2): increases	M_2: decreases
Ventricular contractility	β_1, (β_2): increases	—

Table 3.: The targets of the autonomous innervation of the heart as well as the corresponding receptors and their effects. M_2 is one of the subgroups of the muscarinic acetylcholine receptor.

1.2. Biosignals

A biosignal is any signal in living beings that can be continually measured and monitored. It can be defined as a description of a physiological phenomenon [12].

Biosignals can be classified based on different characteristic. For example some signals arise from spontaneous, ongoing activity within the body (permanent biosignals), while others only occur as the result of external stimulation (induced biosignals)[1]. Also the origin of biosignals can be used as a basis for their classification. For example, there are electric, magnetic, mechanic, optic, acoustic, chemical and thermal biosignals [12].

Bioelectrical signals can now be acquired using affordable equipment that effectively amplifies and digitizes the signals. The obtained biosignals can be conveniently printed or displayed on a screen, enabling basic examination by a physician. Additionally, algorithms can be utilized to perform further analysis to enable physicians to gain insight into complex processes.

As a result, many clinical procedures based on bioelectrical signals are in widespread use in hospitals all around the world. In the following sections the biosignals used in this work are explained briefly.

1.2.1. Photoplethysmogram (PPG)

In response to a heart stroke, a pulsatile pressure wave propagates along arterial vessels. This results in periodical changes of the local widening of these arterial vessels according to the heart activity. The local arterial radius (or local arterial volume) is at its minimum at the end of diastole and is at its maximum closely before the end of systole [13].

When light is shining on an arterial vessel (for example the light from a light-emitting diode (LED)) the amount of light being absorbed while transversing the vessel can be calculated using the Beer-Lambert law (see Equation 1). In this formula the absorbance A changes in direct relation to the absorption coefficient μ_A multiplied by the path length of the light (vessels radius r). In this equation I denotes the transmitted light intensity and I_0 the incident light intensity [13].

$$A = \log \frac{I}{I_0} = \mu_A * r \tag{1}$$

Consequently, the transmitted light intensity shows consecutive peaks and troughs with the same rate as the vessel radius and therefore the heart rate (see also Figure 4).

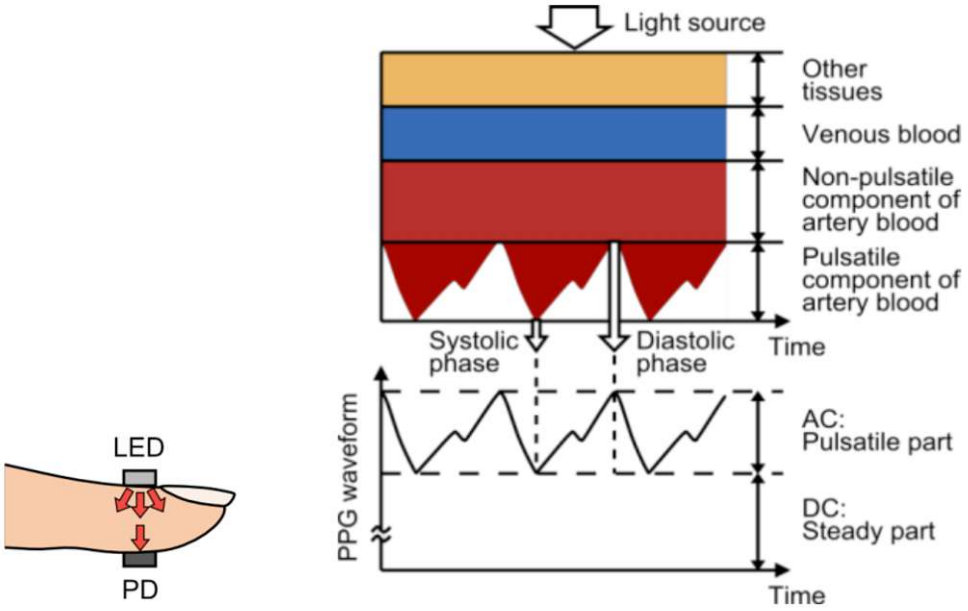

Figure 4.: PPG measuring system (left): The light source (LED) and the the sensor (photodiode (PD)) are placed on opposite sides of a finger. The waveform (right) consists of a DC component (induced by venous blood, the non-pulsatile component of the arterial blood and other tissue like bones, skin, fat and muscle tissue) and an AC component (induced by the pulsatile component of the arterial blood) [14].

These changes in intensity can be measured by using a photodiode and thereby the heart rate can be identified [13]. The PPG can be measured on different sites of the body but fingers and ear lobes are the most common.

Figure 4 shows a typical measurement system and the associated PPG waveform. It can be seen that a PPG is an induced optical biosignal whose waveform consists of a direct current (DC) component and an alternating current (AC) component. To determine the heart rate only the AC component is needed [14].

1.2.1.1. Pulse oximetry

Pulse oximetry is a non-invasive method for monitoring a person's peripheral oxygen saturation (SpO_2). This is done by using two instead of one light source and measuring the resulting PPG. Typically one LED is red, with a wavelength of about 660 nm, and the other LED is infrared with a wavelength of about 800 nm to 940 nm [13].

Due to the fact that oxygenated hemoglobin (HbO_2) and (deoxygenated) hemoglobin

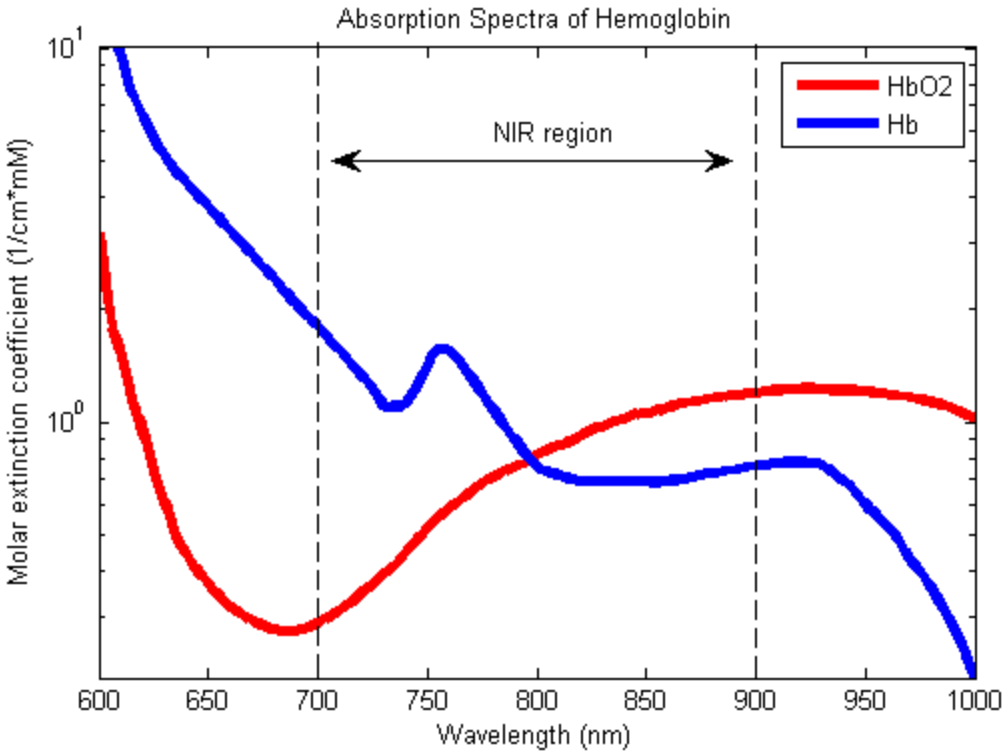

Figure 5.: Absorption spectra of HbO_2 and Hb for near-infrared wavelengths (NIR) [15].

(Hb) have different absorption spectra (see Figure 5), the percentage of oxygenated blood can be calculated according to Equation 2 [13].

$$SpO_2 = \frac{HbO_2}{HbO_2 + Hb} \tag{2}$$

Healthy individuals usually exhibit SpO_2 values between 96% and 99%, and the SpO_2 should generally be above 94%.

1.2.2. Blood pressure

Blood pressure values are generally reported in millimeters of mercury (1 mmHg = 133.322 Pa) and for each heartbeat, blood pressure varies between systolic and diastolic pressures. Normal resting blood pressure in an adult is approximately 120 mmHg systolic over 80 mmHg diastolic.

1.2.2.1. Non-invasive blood pressure measurement

The non-invasive blood pressure measurement typically uses an inflatable cuff encircling an extremity (upper arm) at roughly the same vertical height as the heart. This cuff is then inflated until the artery is completely occluded.

In the auscultatory method the pressure in the cuff is then slowly released while listening with the stethoscope to the brachial artery at the antecubital area of the elbow. When blood starts to flow in the artery, the turbulent flow creates the so called first Korotkoff sound. The pressure at which this sound is first heard is the systolic blood pressure. The cuff pressure is then further released until the artery is no longer constricted. When this happens, no more sound can be heard and this then is the diastolic arterial pressure [12].

The oscillometric method uses the principle that pulsatile blood flow produces radial oscillations of the arterial vessel walls, which are then transmitted to the cuff and measured by a pressure sensor within the cuff. When deflating the cuff, as soon as the intra-arterial blood pressure exceeds the cuff pressure, the oscillations of the vessels walls are strengthened due to turbulent blood flow. The cuff pressure at the time of the initial increase in the oscillations amplitude corresponds to the systolic blood pressure. The maximal amplitude of the oscillations is observed when the cuff pressure is at the mean arterial pressure. The diastolic pressure corresponds to the rapid decrease in the oscillations when further deflating the cuff [12].

Because the cuff needs to be inflated and deflated to do one measurement only a non continuous monitoring of the blood pressure can be achieved. Typically the measurement is done automatically in a preset interval of approximately every two to five minutes.

1.2.2.2. Invasive blood pressure measurement

The continuous invasive blood pressure measurement is done by direct measurement of arterial pressure by placing a cannula needle or catheter in an artery (usually radial, femoral or brachial). This needle/cannula is then connected to an electronic pressure transducer.

The advantage of this system is that pressure can be constantly monitored and a waveform can be displayed [12]. However, the invasiveness of this measurement method is related to the risk of complications and therefore with stable, low-risk patients it is not as popular for routine use as the non-invasive method. The continuous invasive blood pressure measurement should be done with critically ill patients who are at risk

for hemodynamic instability.

1.2.3. Electrocardiogram (ECG)

As already mentioned in subsubsection 1.1.2.4, the impulse conduction and excitation of the heart works by displacement of electrical charge. As excitation spreads over the heart, a diectrical field is produced that can be sensed on the surface of the body. The ECG is a representation of the changes in magnitude and direction of the dielectrical field as a function of time measured between various sites on the body surface [9].

Numerous diagnoses and findings can be made based upon electrocardiography. For example it is possible to identify:

- Rhythm disturbances or arrhythmias
- Heart block and conduction problems
- Electrolytes disturbances and intoxication
- Ischemia and infarction
- Structural abnormalities of the heart and surrounding tissue

To measure the dielectrical field conductive pads, so called electrodes, are attached to the body's surface in standardized positions. For an ECG recording, the difference in voltage between a pair of electrodes is referred to as a lead. The typical position of these electrodes is shown in Figure 6 as well as the names of the corresponding leads.

The electrode wires are then connected to a differential amplifier, while patient safety is ensured by considering insulation. An ECG requires a high-gain amplifier with a wide dynamic range (bandwidth typically within the range of 0.05 to 100-500 Hz, depending on the specific ECG application) [1]. Next, the ECG signals are filtered and further processed or recorded based on the requirements [1, 9].

Furthermore, some extra electrodes can be placed on the patients chest to obtain a full 12-lead ECG (precordial leads). This allows the physician to further interpret the cardiac cycle in the transverse (horizontal) plane. In anesthesia and in intensive care units (ICUs) traditionally only three to five electrodes on the patient's chest are used and only one or two leads (mostly lead II) are displayed on the monitor. In those situation, one is typically interested in the heart rhythm and frequency and therefore it is not necessary to obtain a full 12-lead ECG continuously.

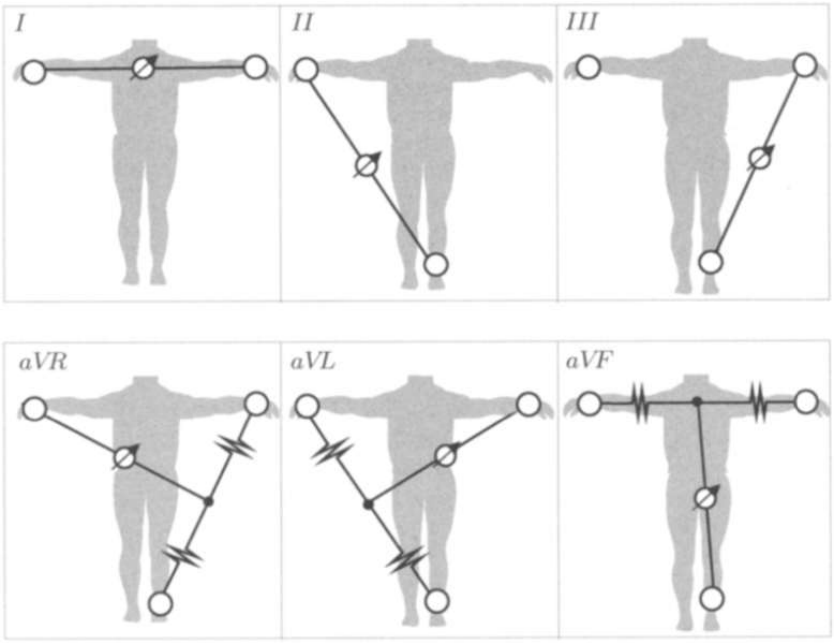

Figure 6.: The typical position of electrodes and direction of the vector of the limb leads (I, II and III) and augmented limb leads (aVR, aVL, and aVF) [1].

1.2.3.1. Physical background

In a resting heart cell, the inside of the cell is negatively charged compared to the outside (see subsubsection 1.1.2.4), when the heart cell gets activated, it depolarizes and the charges get reversed. As the depolarization spreads out over the heart a dielectric field arises from this shift of charge.

Figure 7 shows the main vector of the dielectrical field along with the heart's excitation in one cardiac cycle. Furthermore, the image of this vector as one of the ECG leads is displayed in this figure. The direction and amplitude of the sum vector of the dielectrical field consists of the following phases:

- **P wave**: represents depolarization of the atria. The vector points downward as the excitation spreads from the SA node to the AV node.
- **QRS complex**: represents depolarization of the ventricles. Ventricles contain more muscle mass than the atria, therefore the QRS complex is considerably larger than the P wave.
- **T wave**: represents repolarization of the ventricles

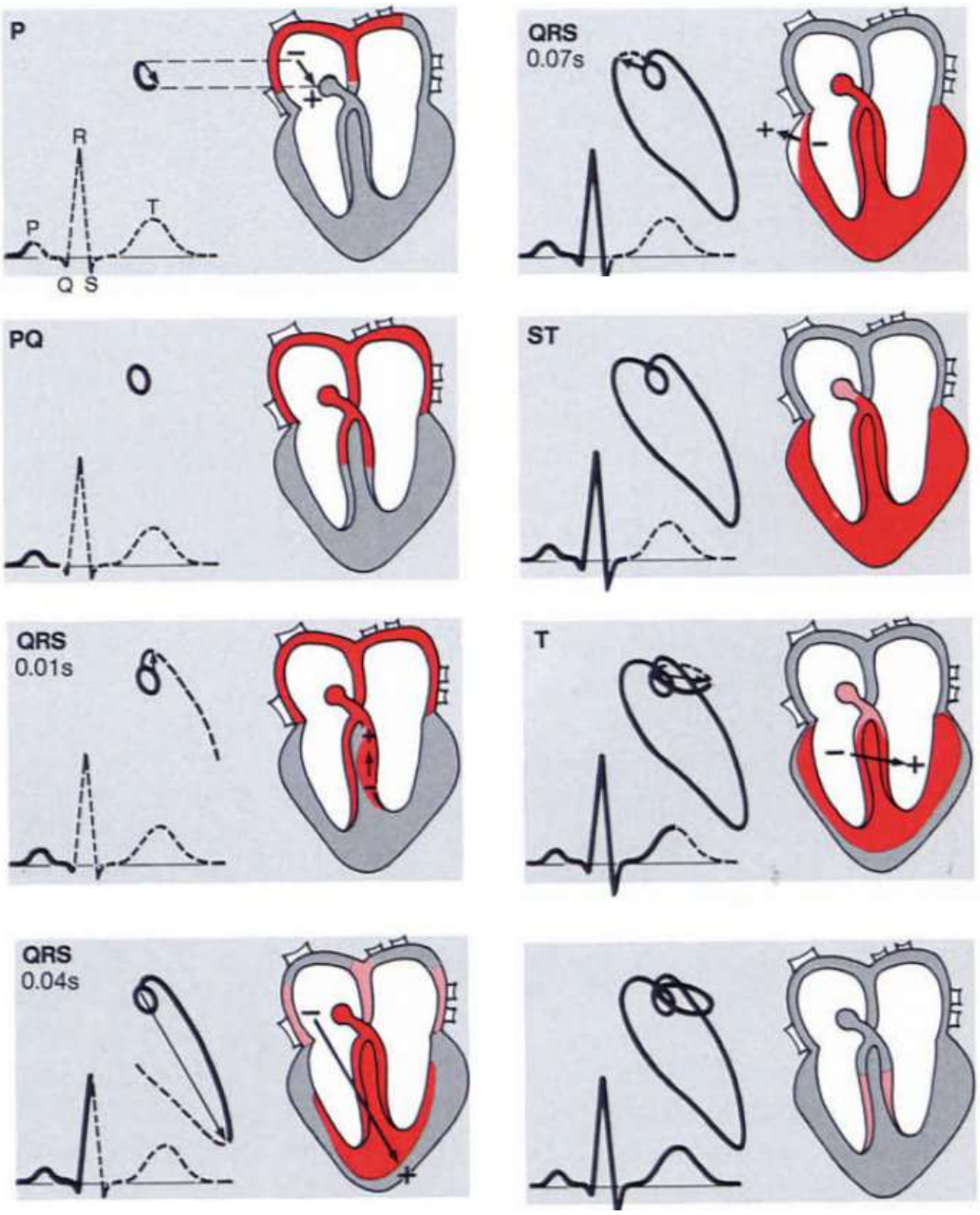

Figure 7.: ECG cycle [9]: When the heart starts to depolarize the vector of the dielectrical field points in the direction of the spreading excitation. When the heart relaxes, the vector points away from the spreading repolarisation but the polarization is reversed. ECG lead II is displayed along with the dielectric field vector.

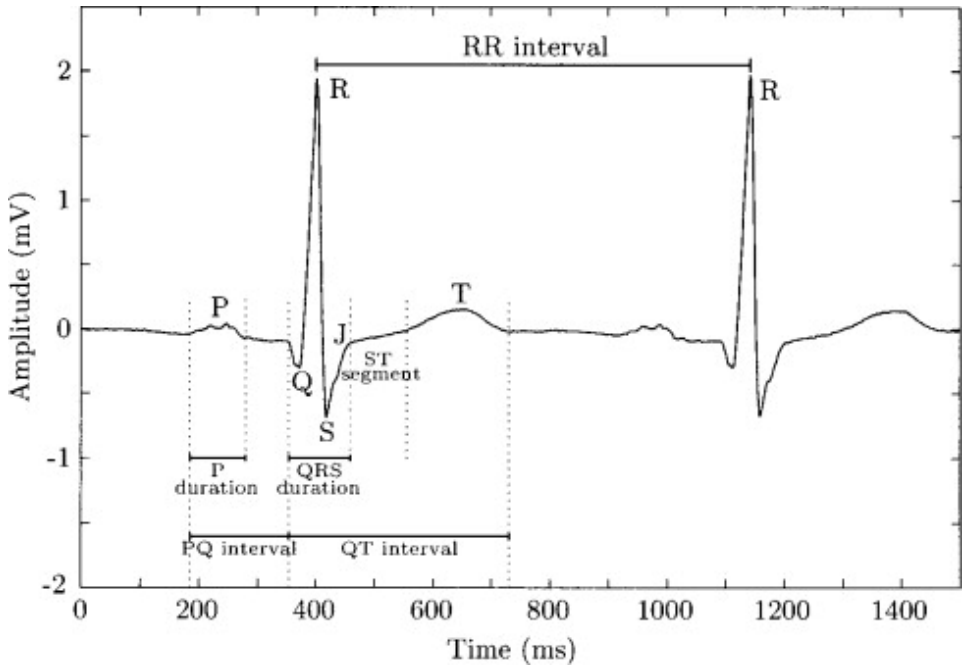

Figure 8.: Sinus rhythm with the beat to beat interval (RR interval) marked out [1].

1.2.3.2. Heart rate

To calculate the heart rate it is necessary to identify the exact position of a periodically recurring component of the ECG. Technically, this could be the P wave but in most cases it is easier to identify two successive QRS complexes due to their size and sharp peak. Furthermore, there are some arrhythmias or conduction problems where the P wave is not followed by an actual beat of the ventricle (see also section 1.3).

Figure 8 shows the time between two successive heart beats (QRS complexes), the so called RR interval. The heart rate frequency is typically given in min^{-1} and not s^{-1} and can be calculated using the Equation 3.

$$f = \frac{1}{RRinterval} \tag{3}$$

1.2.3.3. Artefacts

In the following paragraphs some important ECG artefacts are described. Figure 9 shows the typical spectral properties of the ECG.

Baseline wander may result from a variety of noise sources including perspiration, respiration, body movements, and poor electrode contact. It is a low-frequency activity

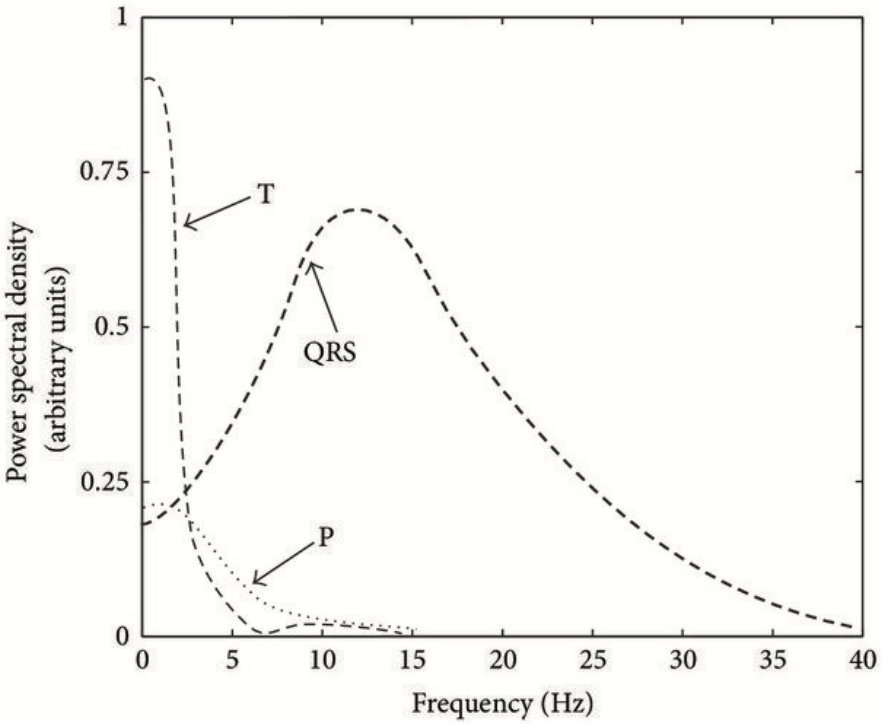

Figure 9.: Representative power spectrum of an ECG in human beings [16].

in the ECG and the magnitude of the undesired wander may exceed the amplitude of the QRS complex by several times. Its spectral content is usually well below 1 Hz.

Powerline interference (50/60 Hz) is caused by improper grounding of the ECG equipment and interference from nearby equipment. Such interference can be removed in many situations by means of filtering.

Electrode motion artefacts are mainly caused by skin stretching which alters the impedance of the skin around the electrode. Motion artefacts resemble the signal characteristics of baseline wander, but are more problematic to combat since their spectral content considerably overlaps that of the QRS complex. They occur mainly in the range from 1 Hz to 10 Hz. In the ECG, these artefacts are manifested as large-amplitude waveforms which are sometimes mistaken for QRS complexes.

Electrical activity of skeletal muscles during periods of contraction causes electromyographic noise (EMG noise). The frequency components of EMG considerably overlap those of the QRS complex. As a result there are difficulties in removing EMG noise from the ECG signal without introducing distortions.

Respiratory activity influences electrocardiographic measurements not only through heart rate but also through beat morphology. Such beat-to-beat variations in morphology are caused by chest movements, changes in the position of the heart, and changes in lung conductivity. Although variations in QRS amplitude represent an undesirable signal characteristic, it may be exploited for estimation of the respiratory frequency.

1.2.4. Standard monitoring in anaesthesia

In anesthesia, biosignals are used to monitor the body functions and the effects of different drugs given to the patients. Thereby, the pain level and stress and indirectly the depth of anesthesia of a patient can be estimated from different biosignals like the heart rate and blood pressure. Another example is the fluid need of a patient in order to compensate for the blood loss. All of these biosignals are thereby extremely important for the outcome of a patient during anesthesia and surgery. Figure 10 shows a typical patient monitor during general anaesthesia.

The Committee on Standards and Practice Parameters of the American Society of Anesthesiologists (ASA) lists a minimum of biosignals that need to be measured during all anesthesia [17]. The standard monitoring in anesthesia typically includes the following parameters:

- **Blood Pressure:** Either measured invasively or non-invasively.
- **Heart Rate:** Continuous monitoring of heart rate using an **ECG** or an **PPG** to assess cardiac function. Furthermore, the ECG can be used to detect any abnormalities or changes in cardiac rhythm.
- **Oxygen analyzer:** the concentration of oxygen in the patient breathing system shall be measured by an oxygen analyzer with a low oxygen concentration limit alarm in use.
- **SpO_2:** Non-invasive measurement of oxygen saturation in the blood to monitor adequate oxygenation. The variable pitch pulse tone and the low threshold alarm shall be audible to the anesthesiologist or the anesthesia care team personnel.
- **Capnography**: Measurement of exhaled (end-tidal) carbon dioxide ($EtCO_2$) levels to assess ventilation and proper airway placement. Furthermore **quantitative monitoring of the volume of expired gas** is strongly encouraged. The **respiratory rate** can then be derived from these measurements.

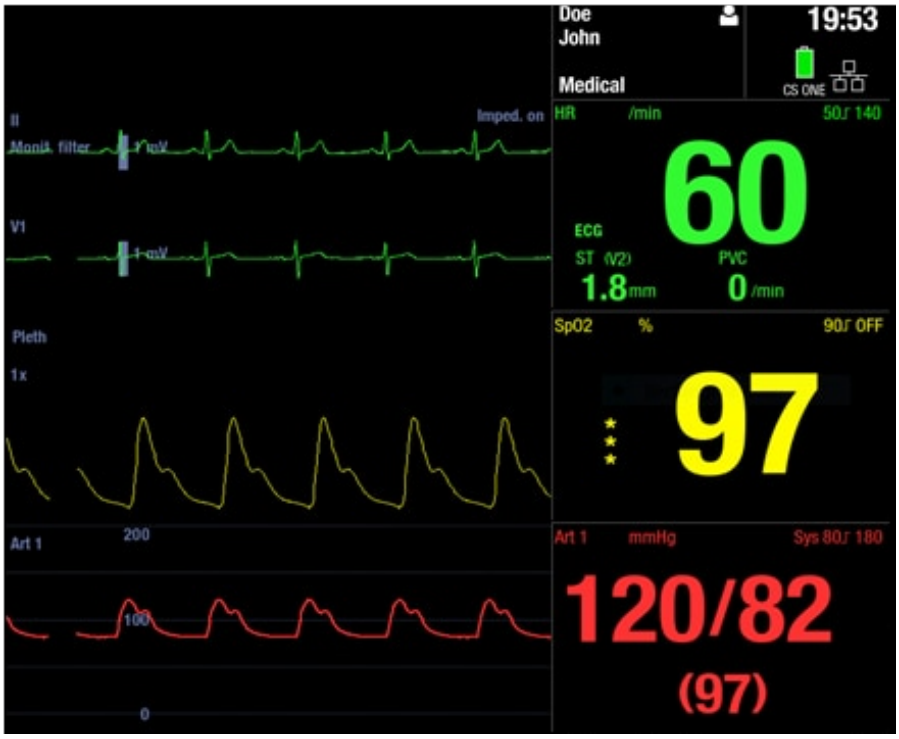

Figure 10.: Biosignals on a display of a monitor used during anaesthesia.

- **Body temperature:** Either continuously measured by using a Foley catheter or by an ear thermometer whenever clinically significant changes in body temperature are intended, anticipated or suspected. The goal is to maintain normothermia during the sugery.
- **Inhalational anesthetic concentration:** Monitoring the concentration of inhalation anesthetics to ensure proper depth of anesthesia. This measurement needs to be done whenever inhalation anesthetics are used.
- **Neuromuscular Monitoring:** Assessing the degree of neuromuscular blockade using train-of-four (TOF) monitoring to guide administration of muscle relaxants.

These parameters provide essential information about the patient's vital signs, oxygenation, ventilation, anesthetic depth, and overall physiological status during anesthesia. Additional monitoring may be used based on the patient's specific needs and the complexity of the procedure.

- **Depth of Anesthesia:** Assessing the level of anesthesia to reduce the incidence of intraoperative awareness using parameters such as bispectral index (BIS) or entropy monitors.

- **Advanced hemodynamic monitoring:** Systems like non-onvasive cardiac output monitoring, PiCCO (Pulse Contour Cardiac Output), transesophageal echocardiography or Swan-Ganz-Catheter (pulmonary artery catheter) may be used whenever the patient or the complexity of the surgery requires additional monitoring of volume status and the hearts function.

- **Arterial blood gas tests** measure the amounts of arterial gases, such as oxygen and carbon dioxide. This test requires that a small volume of blood be drawn from an artery with a syringe and a thin needle or from an arterial catheter. Further parameters like the level of bicarbonate and concentrations of lactate, several electrolytes, Hb, HbO_2, carboxyhemoglobin and methemoglobin are also obtained.

1.3. Heart Rhythms

As already mentioned in subsection 1.1.2 and subsection 1.2.3, the heart pumps blood by a periodical sequence of contraction and relaxation of its chambers and atria. This is caused by the autorhythmicity of the electric conduction system of the heart. Different diseases and structural abnormalities can cause problems in this system and can lead to so called cardiac arrhythmia. In the following paragraphs some common occurring heart rhythms are explained.

1.3.1. Sinus rhythm

As mentioned in subsubsection 1.1.2.3, a normal heart beat is initiated in the SA node and the depolarization then spreads to the rest of the heart via the atrial myocardium and the AV node. In terms of ECG, this is characterized by a periodical sequence of P waves, QRS complexes and T waves. An examples of a normal sinus rhythm is shown in Figure 11a.

Because of activation of the ANS (sympathetic/parasympathetic system) the heart rate slows down or speeds up in order to adapt to the bodies current demand of blood flow (cardiac output). Furthermore, stress and pain can make the heart rate speed up because of sympathetic activation.

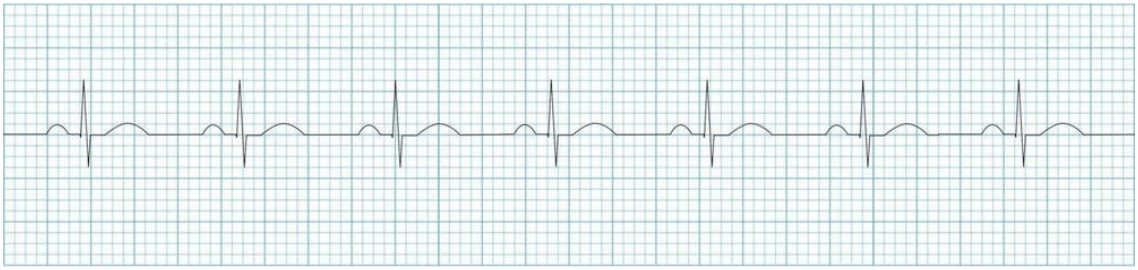

(a)

(b)

Figure 11.: (a) Example of a normal sinus rhythm [18] and (b) Sinus arrhythmia [19]: the interval between heart beats changes according to the respiratory activity.

1.3.1.1. Respiratory sinus arrhythmia

Figure 11b shows a so called sinus arrhythmia, an arrhythmia caused by intermittent vagus nerve activation because of changing intrathoracal pressure during respiration. This arrhythmia is a normal finding and especially present in young and athletic persons. It occurs due to an increased filling of the right side of the heart during inspiration. Because of this higher pressure in the right heart, the left ventricle is compressed and consequently a decrease in stroke volume occurs. The autonomous nerval system makes up for the smaller stroke volume by increasing the heart rate temporarily.

1.3.2. Cardiac arrhythmia

When the impulse formation (originating in the atria) or impulse propagation to the ventricle (see subsubsection 1.1.2.3) is disturbed, so called cardiac arrhythmia occur. Cardiac arrhythmia are irregularities in the heartbeat (including when the heartbeat is too fast or too slow) that may or may not cause symptoms and can be associated with serious adverse medical events including increased mortality. In the following sections some of the most important cardiac arrhythmias are explained.

1.3.2.1. Atrial fibrillation

Atrial fibrillation (as shown in Figure 12a) is the most common sustained arrhythmia. As of 2014, atrial fibrillation affected about 2 to 3% of the population of Europe and

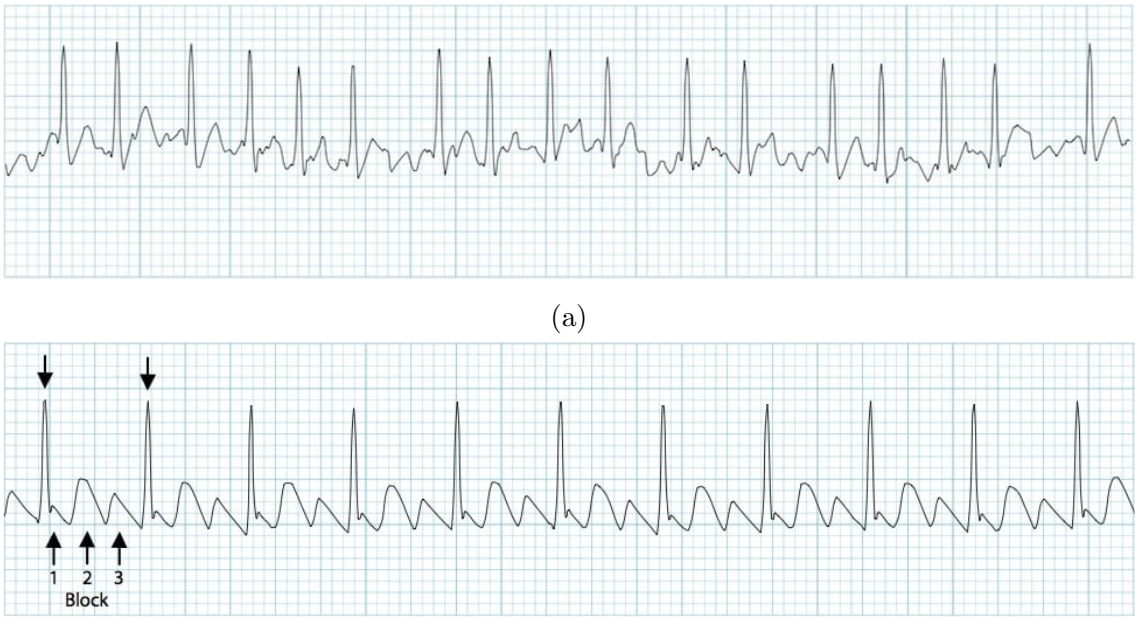

(a)

(b)

Figure 12.: (a) Atrial Fibrillation with irregular heart beat [21] and (b) Atrial flutter with a 3:1 block [22].

North America [20]. It is a type of supra-ventricular tachycardia and is characterized by disorganized atrial electrical activity and contraction. It features an irregular rhythm with no P waves and a variable ventricular rate.

1.3.2.2. Atrial flutter

Atrial flutter (as shown in Figure 12b) is a form of supraventricular tachycardia caused by a re-entry circuit within the right atrium. Ventricular rate is determined by the AV conduction ratio (degree of AV block). The most common AV ratio is 2:1, resulting in a ventricular rate of 150 bpm. Higher-degree blocks can occur resulting in lower rates of ventricular conduction, e.g. 3:1 or 4:1 block.

1.3.2.3. Ventricular tachycardia (VT)

A VT is a broad complex tachycardia originating from the ventricles most commonly with a heart rate faster than 120 beats per minute. There are several different forms of VT - the most common is monomorphic VT (see figure Figure 13a). Although a few seconds may not result in problems, longer periods are dangerous as they may result in ventricular fibrillation or cardiac arrest. VT can occur due to coronary heart disease,

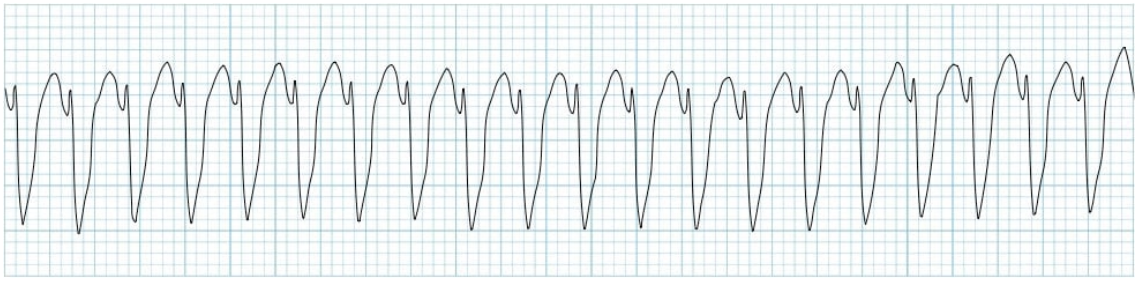

(a)

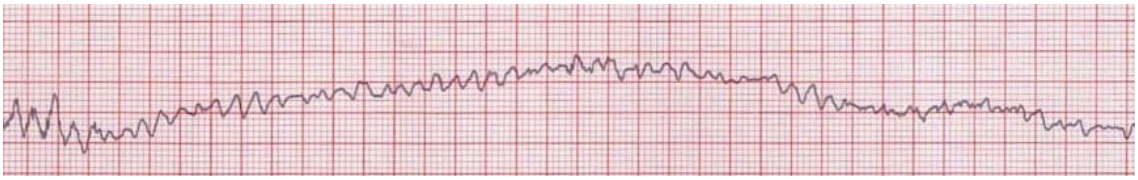

(b)

Figure 13.: (a) Monomorphic VT [23] and (b) Ventricular fibrillation: Chaotic irregular deflections without identifiable P-QRS-T waves [24].

aortic stenosis, cardiomyopathy, electrolyte problems, or a heart attack.

1.3.2.4. Ventricular Fibrillation

Ventricular fibrillation features chaotic irregular deflections of varying amplitude and therefore the heart is no longer an effective pump and is reduced to a quivering. This rhythm is invariably fatal unless advanced life support is rapidly instituted. The primary goal is to convert this rhythm via defibrillation.

1.3.2.5. Atrioventricular block (AV block)

An AV block is a disease of the electrical conduction system of the heart at which the signal propagation between the atria and ventricles through the AV node and the His bundle is disturbed. Depending on the type of AV block, the transmission of electrical impulses from the atria to the ventricles can either be slowed down (AV block grade I) or the the impairment results in a failure to conduct an impulse, which causes a skipped beat (AV block grade II). In AV blocks grade III the transmission of electrical impulses from the atria to the ventricles can even be blocked completely. When the impulse is completely blocked in the AV node, an accessory pacemaker in the lower chambers will typically activate the ventricles resulting in a slow heart rate and two independent rhythms of atria and ventricles can be noted on the ECG. Examples of AV blocks are

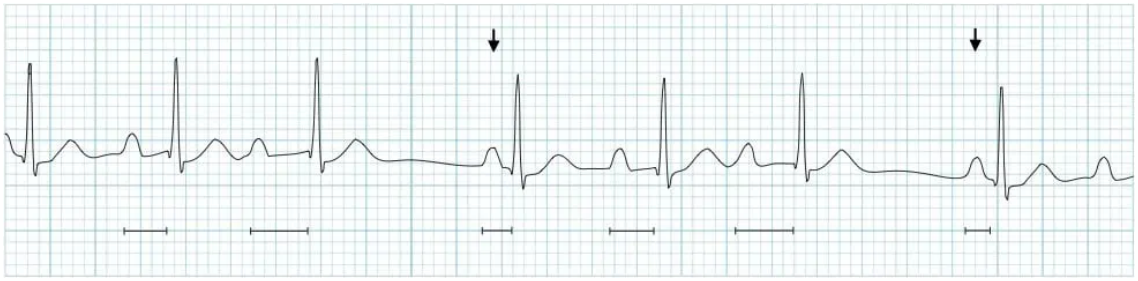

(a)

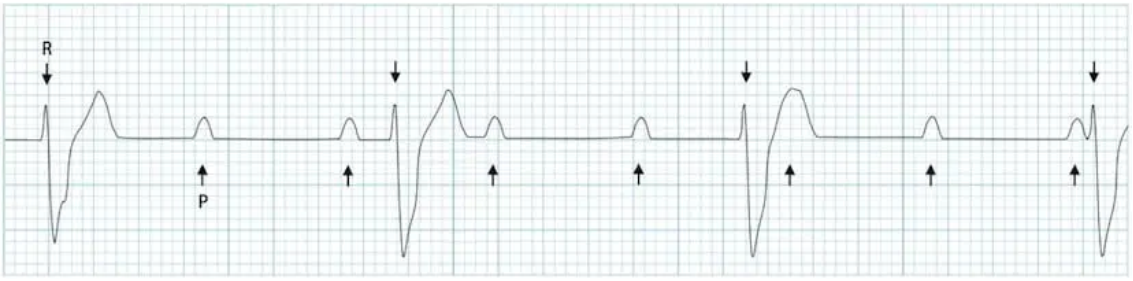

(b)

Figure 14.: (a) 2nd degree AV blockType 1 (Mobitz I/Wenckebach): progressive prolongation of the PR interval followed by a blocked P wave (dropped QRS complex) [25] and (b) AV block 3rd degree (complete heart block): two independent rhythms of atria and ventricles can be noted [26].

given in Figure 14.

1.3.2.6. Ectopic beats

An ectopic beat is a heart rhythm disorder corresponding to a premature contraction of one of the chambers of the heart. These beats arise from fibers or group of fibers outside the region in the heart muscle ordinarily responsible for impulse formation.

Atrial ectopic A premature atrial complex (also called atrial ectopic, supra-ventricular ectopic or atrial extrasystole) is a premature beat arising from ectopic pacemaking tissue within the atria. There is an abnormal P wave, usually followed by a normal QRS complex. A post-extrasystolic pause may be present with a longer-than-normal interval before the next sinus beat arrives. An example is given in Figure 15a.

Ventricular extrasystole A premature ventricular complex (also called ventricular ectopics, ventricular extrasystoles) is a premature beat arising from an ectopic focus within

(a)

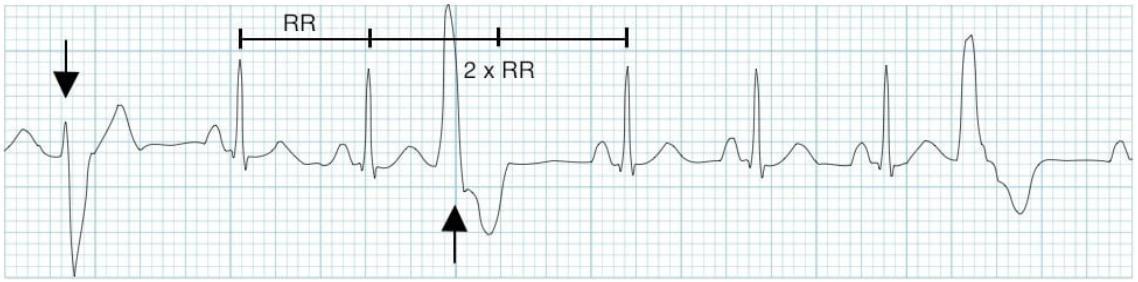

(b)

(c)

Figure 15.: (a)Premature atrial complexes [27], (b) Multifocal Premature Ventricular Complex [28] and (c) triplet or non-sustained VT [28].

the ventricles. They typically occur earlier (premature) than would be expected for the next sinus impulse and feature a broad QRS complex (longer than 120 ms) with abnormal morphology. They are also usually followed by a full compensatory pause. Examples are given in Figure 15b and Figure 15c.

Bigeminy rhythm A bigeminy is a rhythm with single ectopic beat, following each regular (sinus) heartbeat. A bigeminy rhythm can either be of supra-ventricular or ventricular origin. Ventricular bigeminy rhythms are usually followed by a full compensatory pause and supra-ventricular ones are not because they also reset the SA node. Two examples are given in Figure 16a and Figure 16b.

Trigeminy rhythm Like the bigeminy rhythm if every third beat is aberrant (ectopic) it is called trigeminal rhythm (see Figure 16c). As with bigeminy rhythms the trigemini

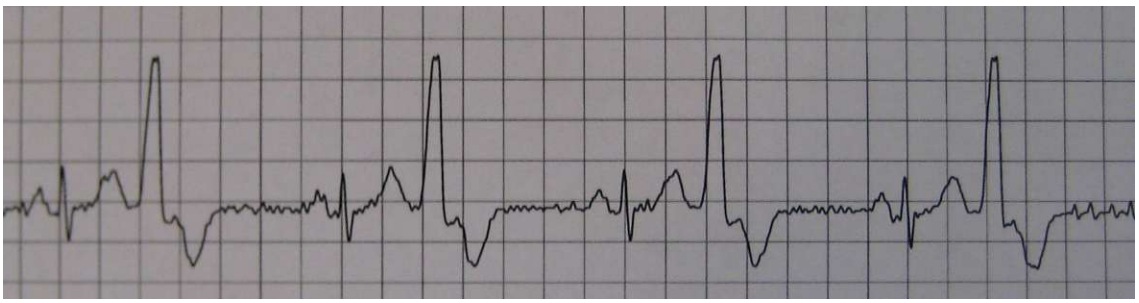

(a)

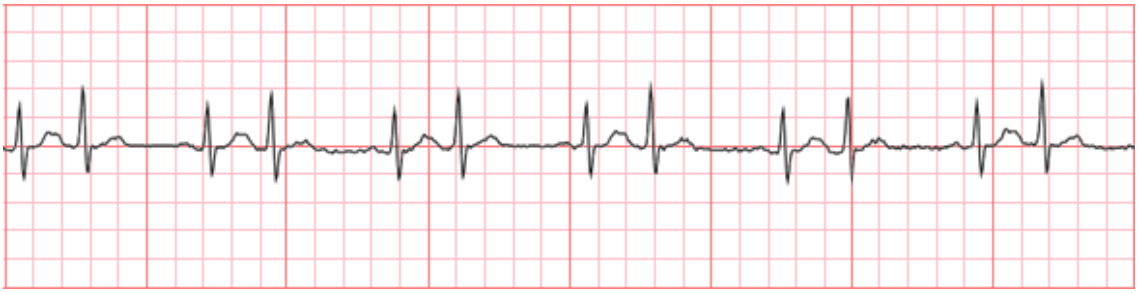

(b)

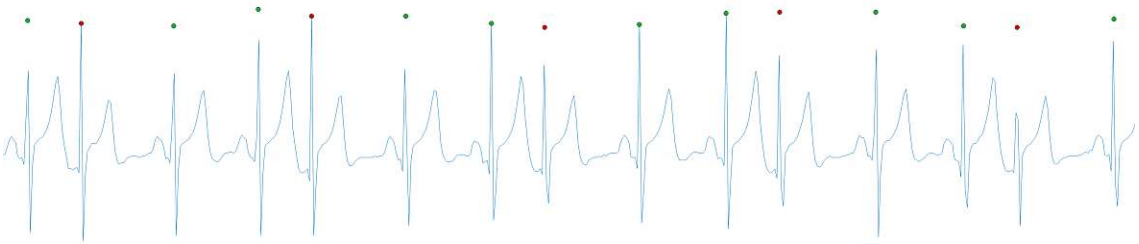

(c)

Figure 16.: Examples of (a) ventricular bigeminy [29] and (b) supraventricular bigeminy [30]. In contrast to supraventricular beats, the ventricular beats feature a broad QRS complex (longer than 120 ms) with abnormal morphology. (c) shows an example of a supraventricular trigeminy rhythm.

can be of ventricular and supraventricular origin.

1.4. Heart rate variability (HRV)

HRV is the beat to beat variation in either heart rate or the time difference between two successive heart beats (R peaks). This variation originates in changes of the intrinsic activity of the heart's primary pacemaker (SA node) [31]. The SA node is influenced

by the balance between sympathetic and parasympathetic tone and thereby the ANS controls the final heart rate and the HRV [32].

Stimuli decreasing the HRV can be, for example, mental or physical stress, cardiac or non-cardiac diseases or pharmacological treatment [31]. A normal level of HRV is associated with health and self-regulatory capacity or resilience [32].

1.4.1. Measurement

HRV reflects fluctuations in the atrioventricular conduction speed superimposed on the P-wave to P-wave interval (see also subsubsection 1.1.2.3 and subsubsection 1.1.2.6). Therefore in theory, it would be ideal to use P-P intervals for HRV analysis. It has been shown that beat-to-beat changes in RR intervals reflect the variability of the SA node quite accurately [33]. Therefore, as the accurate determination of P wave peak is quite difficult (the amplitude of the P wave is quite small compared to noise in the signal), the R-R intervals are typically used for the HRV calculation.

1.4.1.1. Time-domain HRV analysis

In the time-domain analysis HRV parameters are derived from direct measurements of the N-N (normal-to-normal) R-R intervals, or from the differences between N-N intervals.

One main limitation of time domain methods is their lack of discrimination between effects of sympathetic and parasympathetic autonomic branches [33]. Furthermore, the length of recording significantly influences the overall variability values. Therefore, it is emphasized that time-domain HRV parameters obtained from periods of different durations should not be directly compared [34].

Standard deviation of normal to normal heartbeat intervals (SDNN) The simplest and most widely used HRV parameter is the SDNN (in ms) calculated over a long-term period (typical durations are 24h). The SDNN is believed to reflect overall HRV [32]. The value of the SDNN can be calculated using Equation 4, where NN is the time distance between two consecutive normal (sinus) heart beats and n is the absolute number of heart beats in the signal.

$$SDNN = \sqrt{\frac{1}{n-1}\sum_{i=1}^{n}(NN_i - NN_{mean})^2} \tag{4}$$

$$NN_{mean} = \frac{1}{N} \sum_{i=1}^{n} NN_i \tag{5}$$

Standard deviation of the average normal-to-normal intervals (SDANN) Another similar metric is the SDANN of 5 min segments. This value is calculated by splitting up the signal in 5 min segments. In this way, multiple values are calculated for one patient.

Root mean square of successive heartbeat interval differences (RMSSD) The RMSSD is also given in ms. To compute this value, first each successive time difference between heartbeats is calculated. Then, each of the values is squared and the result is averaged before the square root of the total is obtained [32] (see Equation 6). The RMSSD reflects especially the high-frequency (vagal) modulation of heart rate and is influenced by respiratory sinus arrhythmia.

$$RMSSD = \sqrt{\frac{1}{n-1} \sum_{i=1}^{n} (NN_{i+1} - NN_i)^2} \tag{6}$$

Percentage of successive normal to normal heartbeat intervals differing by more than 50ms (pNN50) The pNN50 represents the percentage of adjacent normal heartbeats that have a difference in their duration (RR intervals) greater than 50 milliseconds. It is used as an indicator of parasympathetic (vagal) activity and can provide insights into cardiac autonomic function. Higher pNN50 values suggest greater variability in heart rate and stronger parasympathetic influence on the heart.

1.4.1.2. Frequency-domain HRV analysis

Spectral analysis provides information on how the power of HRV is distributed as a function of frequency. Thereby, the entire R-R intervals modulation (HRV) is separated into its components that operate within different frequency ranges. The most frequently used approach to compute spectral indices is based on fast Fourier transformation [32].

The total power of R-R interval variability is thus typically split up into four spectral bands, low frequency (LF), high frequency (HF), very low frequency (VLF) and ultra low frequency (ULF) [32]:

ULF Band The ULF band (smaller than 0.003 Hz) represents very low oscillations and requires a recording period of at least 24 h. There is no consensus regarding the

mechanisms that generate ULF power, but it might reflect very slow-acting biological processes like circadian and neuroendocrine rhythms [32].

VLF Band The VLF Band (0.003-0.03 Hz) requires a recording period of at least 5 min and predicts the risk of adverse outcomes (the VLF band is stronger associated with all-cause mortality than the LF or HF band) [32]. The VLF power represents several factors influencing the heart such as thermoregulation, inflammation, the renin-angiotensin system, and endothelial factors. It is also considered as a measure of parasympathetic activity [32].

LF Band The LF band (0.04-0.15 Hz) is generated by baroreceptor reflexes as well as parasympathetic and sympathetic activity [32].

HF Band The HF band (0.15-0.4 Hz) reflects parasympathetic activity and is also called the respiratory band because it corresponds to the heart rate variations related to breathing (respiratory sinus arrhythmia, see also subsection 1.3.1) [32].

LF/HF Ratio Sympathovagal balance is frequently described by LF/HF ratio as the parasympathetic and sympathetic activity contribute to LF power but only the parasympathetic activity primarily contributes to HF power [32]. Because the interaction between sympathetic and parasympathetic system are complex and non-linear, the description of the LF/HF ratio as sympathovagal is controversial [32].

1.4.2. Influence on HRV

Various physiological and pathological factors may influence sympathovagal status and consequently the heart rate and its variability.

1.4.2.1. External factors

Sampling Frequency A too low sampling rate of the ECG produces digitization noise and introduces errors in HRV measures. In most cases sampling rate of 200 Hz is enough and higher sampling rates do not give better results [33]. If the overall variability of RR interval is very low, HRV analysis may require a higher sampling rate than 200 Hz (corresponding to a temporal resolution of 5 ms), since changes in the length of RR intervals cannot be detected below that resolution [33].

Removal of Artefacts Artefacts can significantly distort both time- and frequency-domain measurements. Missed beats produce greater increases than extra beats since deviation from a missed beat equals the mean heart period versus half the mean heart period for extra beats. When artefacts are present it is necessary to select an artefact-free epoch or remove periods with artefacts from the signal [33].

Respiration As already mentioned in subsection 1.3.1, the heart rate is influenced by the breathing frequency (respiratory sinus arrhythmia). Thus the HRV depends on the breathing frequency and to a lesser degree also on the breathing volume [33]. Another influencing factor on HRV metrics is controlled respiration at a constant rate as it influences the the function of the ANS by inducing stress [33].

Period Length The length of the recorded signal significantly affects both HRV time-domain and frequency-domain measurements [35]. Normally longer recordings are associated with increased HRV, therefore the direct comparison of metrics like SDNN is not allowed when they are calculated from epochs of different length [32].

1.4.2.2. Autonomic blockade

Drugs that influence the ANS are often used during general anesthesia or in intensive care to influence the cardiovascular system (blood pressure, heart rate). In a study, the influence of atropine sulfate and propranolol hydrochloride on the HRV of dogs was investigated [36]:

Atropine When the parasympathetic system was inhibited using the cholinergic (muscarinic receptor) antagonist atropine sulfate, a significant increase in heart rate was observed. Atropine treatment further provoked significant reductions in R-R interval variability and HRV. After correction for prevailing heart rate, corrected R-R interval and corrected HRV were still significantly reduced by atropine treatment [36].

β-adrenergic receptor antagonists The inhibition of the sympathetic system using the non-selective β-adrenergic receptor antagonist propranolol resulted in reductions of the heart rate, but neither R-R interval nor HRV before heart rate correction were altered. After correction for heart rate reduction, a significant reduction in corrected R-R interval variability could be measured [36].

1.4.2.3. Subject Variables

The general health as well as the age and gender of a person are considered as a major determinant of HRV values. A constant decline in HRV parameters is observed through the life course and women generally have higher mean heart rate and lower SDNN values, but higher HF values compared to men [32].

Diabetic patients show a reduction in HRV compared to healthy patients. This might be an expression of (diabetic) autonomic neuropathy [37].

A decrease in HRV also occurs in patients after myocardial infarction and is associated with increased mortality [38]. A shift towards increased sympathetic activity and loss of vagal protection may also contribute to enhanced arrhythmogenesis and subsequently sudden death. Decreased HRV parameters can also be observed in patients with nonischemic cardiomyopathy and in those with heart failure [38].

In general, HRV is useful in predicting morbidities from common mental and physical disorders (e.g., stress, depression, inflammation, chronic pain,...), which increase sympathetic activity and produces autonomic imbalance [32]. Therefore poor HRV parameters show a dysfunction of the ANS and are a denominator of poor health. HRV can also be seen as a risk factor for serious health issues such as cancer survivorship, cardiovascular diseases and overall mortality [32].

1.5. Metadata

1.5.1. General patient information

The patient data typically include a patient ID, the name, age, sex as well as the height and weight of the patient. Furthermore, all of the diagnosis (previous and current medical conditions) and the type of operation to be carried out are important.

1.5.1.1. Body mass index (BMI)

The BMI value is calculated from the mass (weight) and height of a person using the Equation 7. Using the BMI value a person can be categorized as underweight (under $18.5\,\mathrm{kg\,m^{-2}}$), normal weight ($18.5\,\mathrm{kg\,m^{-2}}$ to $24.9\,\mathrm{kg\,m^{-2}}$), overweight ($25\,\mathrm{kg\,m^{-2}}$ to $29.9\,\mathrm{kg\,m^{-2}}$), and obese ($30\,\mathrm{kg\,m^{-2}}$ or more) [39].

$$BMI = \frac{mass_{kg}}{height_m^2} \tag{7}$$

1.5.2. General risk factors

The general preoperative risk assessment includes:

- Smoking
- Obesity
- Physical inactivity
- Whether the patient has or had one of the following medical conditions:
  - Arterial hypertension
  - Elevated cholesterol levels
  - Diabetes mellitus
  - Transient ischemic attack or stroke
  - Acute coronary syndrome: myocardial infarction or unstable angina pectoris
  - Atrial fibrillation
- Whether father or mother of the patient had a heart attack before the age of 60 years
- If the procedure is an emergency surgery

1.5.3. Scores

Internationally standardized scores help to further evaluate the perioperative risk and to quantify the health status of the patient.

1.5.3.1. American Society of Anesthesiologists (ASA) score

The ASA score is a physical status classification system for assessing the fitness of patients before surgery [40]. There are six categories: ASA I: Healthy person, ASA II: Mild systemic disease, ASA III: Severe systemic disease, ASA IV: Severe systemic disease that is a constant threat to life, ASA V: A moribund person who is not expected to survive without the operation and ASA VI: A declared brain-dead person whose organs are being removed for donor purposes [41].

1.5.3.2. New York Heart Association (NYHA) classification

The NYHA score is a system for classifying the extent of heart failure. It places patients in one of four categories: NYHA I: No limitation of physical activity, NYHA II: Slight limitation of physical activity. Comfortable at rest, NYHA III: Marked limitation of physical activity. Comfortable at rest, NYHA IV: Unable to carry on any physical activity without discomfort. Symptoms of heart failure at rest. If any physical activity is undertaken, discomfort increases [42].

1.5.3.3. Metabolic equivalent (MET)

Another method to quantify the functional status of a patient is the maximum achieved MET. For example, a person functioning at maximum 1 MET is limited to simple activities such as eating, dressing, and using the toilet. A person achieving 4 METs can climb stairs, walk up a hill, etc. [43].

1.5.3.4. Revised Cardiac Risk Index (RCRI)

The RCRI is a tool used to estimate a patient's risk of perioperative cardiac complications [44]. It includes binary coded values for high-risk type of surgery, ischemic heart disease, history of congestive heart failure, history of cerebrovascular disease, insulin therapy for diabetes and preoperative serum creatinine $>2.0\,\mathrm{mg\,dl^{-1}}$. The rates of major cardiac complications during surgery correlate with the number of points in the RCRI [44].

1.5.3.5. National Surgical Quality Improvement Program (NSQIP) Risk Factors

The NSQIP risk factors provide risk predictions for the first 30-days after surgery. They include the age, creatinine, ASA classification, functional status/level of self-care and the procedure site [45].

1.5.4. Blood tests

1.5.4.1. B-type natriuretic peptide (BNP)

The BNP is a hormone secreted by cardiomyocytes in the heart ventricles in response to stretching caused by increased ventricular blood volume. High levels help to suspect a diagnosis of heart failure while normal levels help to rule out chronic heart failure.

1.5.4.2. Creatinine

Creatinine is produced by muscle metabolism and is eliminated from the blood almost entirely by glomerular filtration. Because the production rate varies little in a given individual (only depends on the muscle mass), the plasma concentration is relatively constant [9]. Therefore, the creatinine can be used as an indicator (but not direct measure) of renal function.

1.5.4.3. C-reactive protein (CRP)

There are numerous causes of an elevated CRP. These include acute and chronic conditions, and these can be infectious or non-infectious in etiology. However, markedly elevated levels of CRP are most often associated with an infectious cause [46].

1.5.4.4. Troponin

Whenever there is a damage to cardiac muscle cells (e.g., necrosis or cell death) there is troponin released into the blood stream. For example, this is the case when there is a mismatch between oxygen supply and oxygen demand of the myocytes when blood flow is blocked in the coronary vessels (e.g. myocardial infarction). Furthermore, the troponin can also be elevated in inflammation of the heart [47].

1.5.4.5. Cholesterol

The primary source of cholesterol and its derivatives is from animal-based food and it is vitally crucial for cell membranes and a lot of metabolic processes in the body. On the other hand to high cholesterol levels are a predictor of the risk of developing atherosclerotic cardiovascular diseases (coronary artery disease, stroke,...) [48]

2. Methods

The primary goal of this work was to perform heart beat detection on a large ECG dataset and to further obtain HRV information from these patients. It is necessary to do these steps in a fully automated manner in order to analyze huge datasets of ECG data from many different patients. In the following sections the necessary steps to achieve this objective are explained in detail.

All of the analysis of the previously recorded ECG signals was done using a common personal computer. The actual algorithms were developed and tested using the scientific computing environment MATLAB [49] as it is perfectly suited for matrix and vector manipulations. It allows for rapid development of signal processing algorithms and visualization of the data. Furthermore there are already lots of existing libraries and tools for ECG signal processing one can use integrated into MATLAB. For statistical evaluation the statistical software suite IBM SPSS Statistics [50] was used.

2.1. Data acquisition

The patient data used in this work was provided by the Department of Anaesthesia, Intensive Care Medicine and Pain Medicine of the Medical University of Vienna [51]. The recordings were performed with the Vital-signs REal-time Analysis for Clinical Translation (VREACT) system, developed in a previous project by Jakub Matta [52] and Fatih Kartal [53]. To accomplish that, informed consent forms were signed and an approval from the ethic committee was obtained (NCT02761031, [54])

The dataset consists of biosignals (ECG, blood pressure, SpO_2) which were recorded from patients in general anesthesia during different surgical procedure and the following period in the post anesthesia care unit. Corresponding to the biosignals, there is an anonymized patient list that includes some metadata about the patient as well as some information about the surgical procedure carried out.

2.1.1. Metadata

The anonymized list of patients was provided as a Microsoft Excel Workbook file[1] and includes the following general patient information and details about the procedure:

- Patient ID
- Age and sex
- Body height and weight
- BMI of the patient (see subsubsection 1.5.1.1)
- Surgery date
- Type of operation
- Diagnosis
  - Including pre-existing diseases
- Start and end time of the surgery
- The time in the post anesthesia care unit

The Excel file further includes some preoperative findings and classification of the patient. Unfortunately, this information is incomplete for some of the patients.

- ASA, NYHA and MET classification (see subsection 1.5.3)
- Preoperative ECG, chest X-ray and echocardiography findings (not available for all of the patients)
- Preoperative blood test results (BNP, Troponin, Creatinine, Cholesterin, CRP (see subsection 1.5.4)), it should be noted that not every value is available for all of the patients.
- General Risk Assessment score (sum of the risk factors mentioned in subsection 1.5.2)
- RCRI (see subsection 1.5.3)

[1] Microsoft, *Excel Workbook .xlsx*. [Online]. Available: `https://support.microsoft.com/en-us/office/file-formats-that-are-supported-in-excel-0943ff2c-6014-4e8d-aaea-b83d51d46247` (visited on 07/09/2022).

- NSQIP Risk Factors (see subsection 1.5.3)
- Use of Glycopyrroniumbromid (Robinul) an anticholinergic drug (see subsubsection 1.1.1.2, it is only stated whether drug is given but not the time the drug was given.)

2.1.2. Recorded biosignals

For every patient/surgery there are several biosignals measured. These signals are stored as wave and time vectors and also start and end dates are given:

- ECG: only Lead II (see subsection 1.2.3), all other leads are just empty vectors (sampling frequency 200 Hz).
- Blood pressure: measured either non-invasively or invasively (sampling frequency 1 Hz, non-invasive blood pressure is not measured that often. When non-invasive blood pressure measurement is used the same values are stored multiple times in the vectors), three vectors are given:
  - Systolic blood pressure
  - Medium pressure
  - Diastolic blood pressure
- PPG (sampling frequency 100 Hz)
- Pulse oximetry: SpO_2 in % (sampling frequency 1 Hz).
- Heart rate: derived either from the ECG, the PPG or the arterial blood pressure curve (if measured) and calculated by the monitor device itself. The used signal source depends on the monitor settings.

Since the purpose of this work was to perform a HRV analysis, only the ECG signal was further processed in all later steps, although the other signals were still stored in the output file for completeness.

2.1.3. Output format

The fist step of this work was to extract the data from the different input files and generate one file per patient containing all the metadata and biosignals. This file later

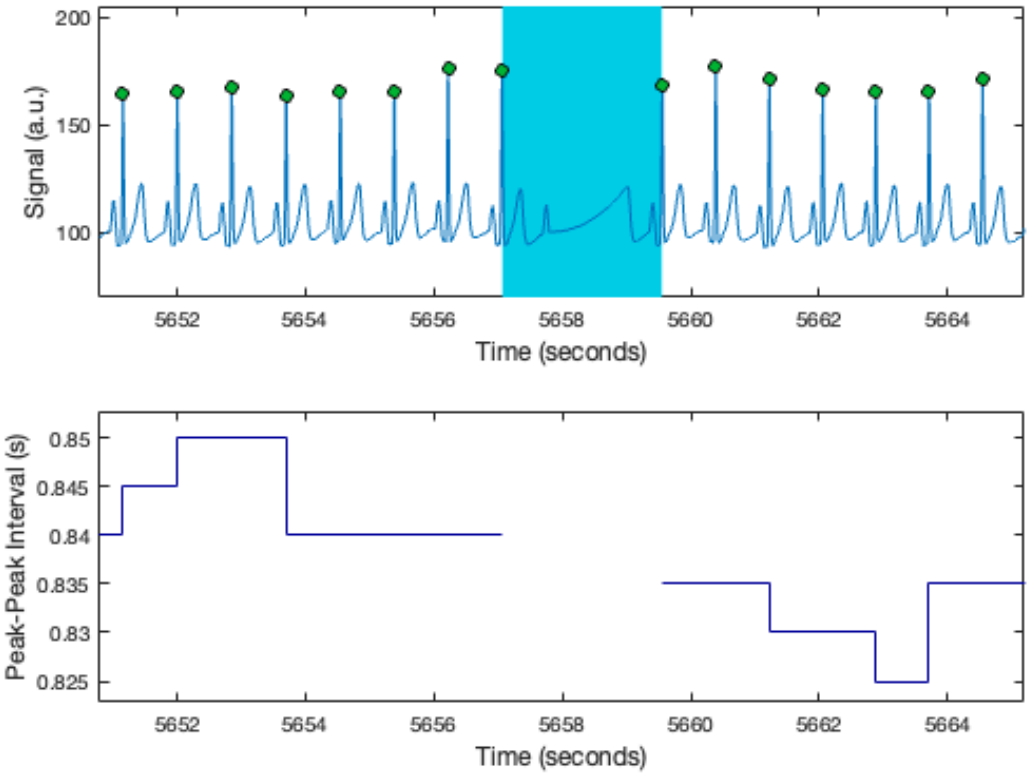

Figure 17.: Section of the annotated ECG of a patient as well as the peak-to-peak intervals. Marked in blue is an artefact area.

also stored all the derived data for this patient (annotated heart beats, artefact areas in the ECG, HRV data,...). When the data was fully extracted and merged from the different source (input) files, for each of the patients one MATLAB structure array[2] was generated that contains all of the metadata and biosignals from that patient. The hierarchy of this output structure is shown in Figure 18.

In the desired output directory there was a folder created for every patient and the MATLAB structure was saved in that folder. Furthermore, a zoomable MATLAB figure of the ECG and the derived data (position of the detected QRS complex, artefact areas, peak to peak interval) was stored in the patient folder to make it easier to quickly examine the data. As an example, a small zoomed in section of such a signal is shown in Figure 17.

[2]Data type that groups related data using data containers called fields, see `https://mathworks.com/help/matlab/ref/struct.html`

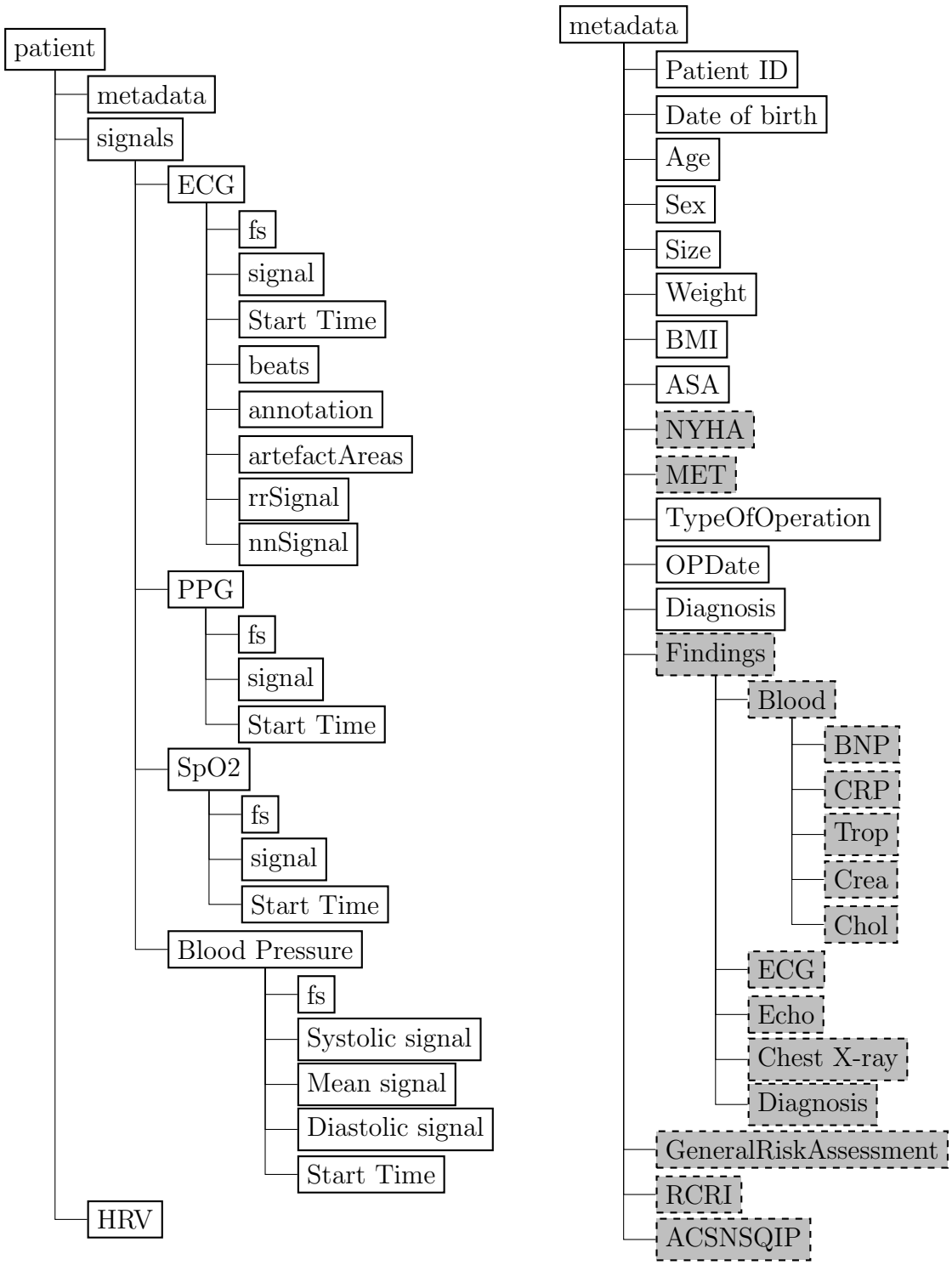

Figure 18.: Hierarchy of the output structure. Gray boxes represent optional information that is not available for all patients.

2.2. Beat annotation

When the signals and metadata are extracted from the input files the next step is to further investigate the ECG signals and detect the correct position of every heart beat (QRS complexes). The steps necessary for that purpose are explained in the following sections.

2.2.1. ECG preprocessing

As already mentioned in subsubsection 1.2.3.3, there are different types of artefacts that can distort an ECG signal. The ECG signals used in this work were recorded under conditions associated with considerable amounts of noise and artefacts caused by, for example, muscle activity, artificial ventilation, cauterization and changes in body position.

To optimize the outcome of all following steps (especially correct QRS detection and thereby HRV analysis) it is necessary to first detect and eliminate those distortions as good as possible. Unfortunately, the literature research has shown that there is no universal "one fits all" method to reliably eliminate all artefacts [1].

One possible way to reduce distortions is filtering the signal. Another way to obtain a better starting position for all further signal processing is searching and marking the artefact areas as invalid sections of the signal. In this work, both approaches were done before performing further signal processing steps.

2.2.1.1. Signal filtering

The ECG signals used in this work are sampled at 200 Hz and are already pre-filtered by the recording device itself. For that reason, some typical artefacts like 50 Hz line-frequency interference are already mostly filtered out.

The process of signal filtering was therefore not needed to address those signal distortions but signal filtering was used to remove the baseline offset of the signal and any changes in the constant component if present. This is necessary because in the next step artefact areas will be detected using the absolute value of the signal.

As shown in Figure 19, the present ECG signals feature different amounts of offset from the X-axis at different time instances. To remove this offset a high-pass filter with a relatively low cutoff frequency was used. The cut-off frequency of the filter should obviously be chosen so that the relevant information in the ECG signal remains

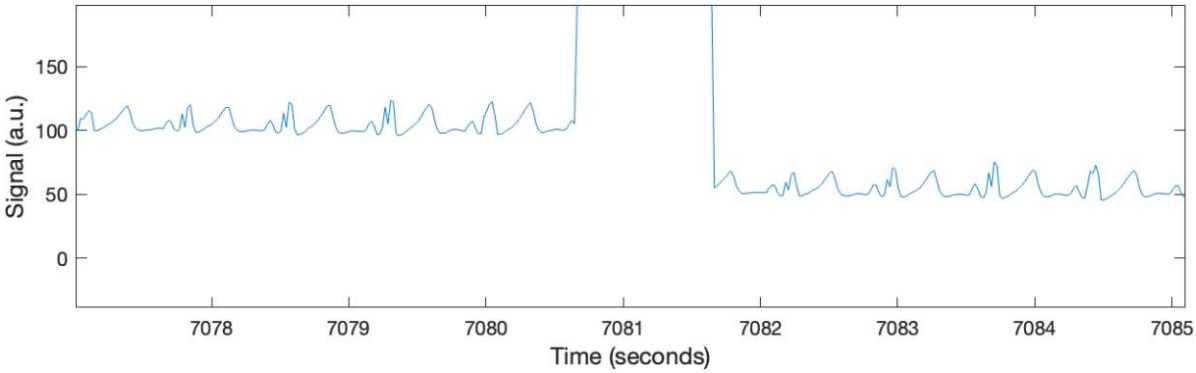

Figure 19.: Different baseline offsets in an ECG signal from the dataset.

undistorted while as much as possible of the offset is removed. Because the main goals of this work were to determine the position of QRS complexes as precisely as possible, distorting other parts of the ECG with the used high-pass filter was not a problem (for example, the elevation of depression of the ST segment; the spectral composition of the ECG parts is shown in Figure 9).

Therefore, it is reasonable to use a cut-off frequency slightly lower than the lowest expected heart rates during bradycardia (about $30\,\mathrm{min}^{-1}$ to $40\,\mathrm{min}^{-1}$)[1]. For that reason, a cut-off frequency F_c of 0.5 Hz was chosen.

In order to be able to later compare the position of the automatically detected QRS complex with a manually annotated position the exact position of the QRS complex must not be changed by the filter. Therefore a filter with zero phase-shift (zero-phase filter) was needed. This was achieved by using the MATLAB function `filtfilt`, that performs zero-phase digital filtering by processing the input data in both the forward and reverse directions. Using this function the transfer function equals the squared magnitude of the original filter transfer function and the order of the specified filter is doubled.

In a grid search (see section 2.3), different filter techniques and filter parameters were compared and the best filter for the present data was chosen. A fifth order Chebyshev type II filter was designed with the MATLAB filter designer and used to filter all the ECGs before further signal processing. The magnitude response and phase response of the used filter are shown in Figure 20.

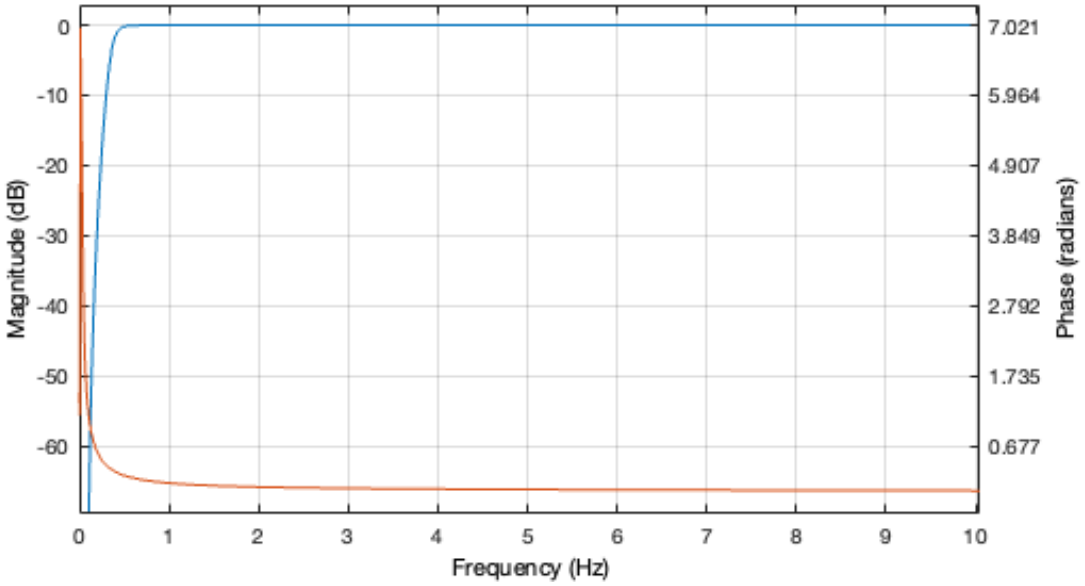

Figure 20.: Magnitude Response of the filter.

2.2.1.2. Artefact Detection

Different approaches had been tried to detect artefacts in the signal. By using a grid search (see section 2.3), the best method for the used dataset was determined. As artefacts in the ECG signal typically have a higher amplitude than the rest of the signal an artefact detection method based on the root mean square value (RMS) of the signal was used. Figure 21 shows an ECG signal with a typical artefact area as well as the trend of the RMS value.

After the signal is filtered with the high-pass filter mentioned in subsubsection 2.2.1.1, the root mean square value (RMS) of the signal was calculated using the formula given in Equation 8. The RMS value calculation was done piecewise for overlapping sections with a specified length of $windowDuration = 0.5seconds$. Hence, when the sampling rate is 200 Hz the window length of those sections is 100 samples.

$$x_{RMS} = \sqrt{\frac{1}{N}\sum_{n=0}^{N}|x_n|^2} \tag{8}$$

As a next step, the standard deviation and the mean value of this local RMS values were calculated. If the local RMS value is greater than the mean RMS value plus the threshold factor $findArtefactsFactorThreshold1$ times the standard deviation of the

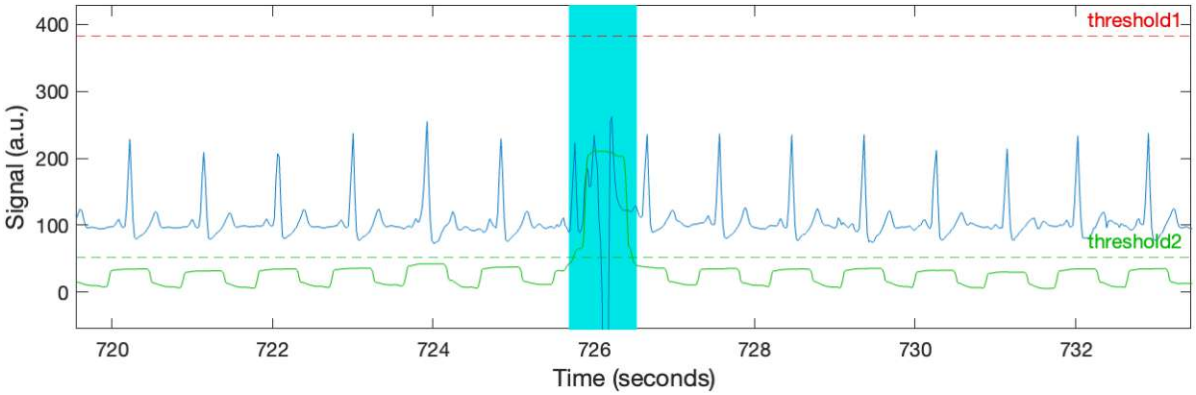

Figure 21.: Typical artefact in the ECG signal in the turquoise rectangle. The RMS value of the signal is shown in green and the threshold values are also shown with two dashed lines.

RMS value, the section is considered to be an artefact. The used code of the algorithm is shown in the appendix (Listing 1).

If there are a lot of artefacts in the ECG signal and artefacts have a large amplitude, the standard deviation of the RMS values will consequently be large. As this would result in some smaller artefact areas to not be detected, the artefact identification steps are then repeated a second time. In this second iteration, the already detected artefact areas are ignored when calculating the local RMS value. This will result in smaller standard deviation and mean values of the RMS value and thereby even relatively smaller artefacts can be detected. In this second iteration the threshold factor $findArtefactsFactorThreshold2$ is used. The factors $findArtefactsFactorThreshold1$ and $findArtefactsFactorThreshold2$ were determined via the grid search (see section 2.3).

To store the position of the detected artefact areas, the start and end indices of the artefact areas are then saved in a vector. In this vector all the odd entries (1,3,5,...) consequently correspond to the start of an artefact area and the even entries correspond to the ends.

2.2.2. QRS Detection

The presence of a QRS complex and its occurrence time is basic information required in all types of ECG signal processing. Therefore, the precise detection of QRS complexes is the next crucial step in order to calculate the beat to beat intervals and consequently perform the HRV analysis.

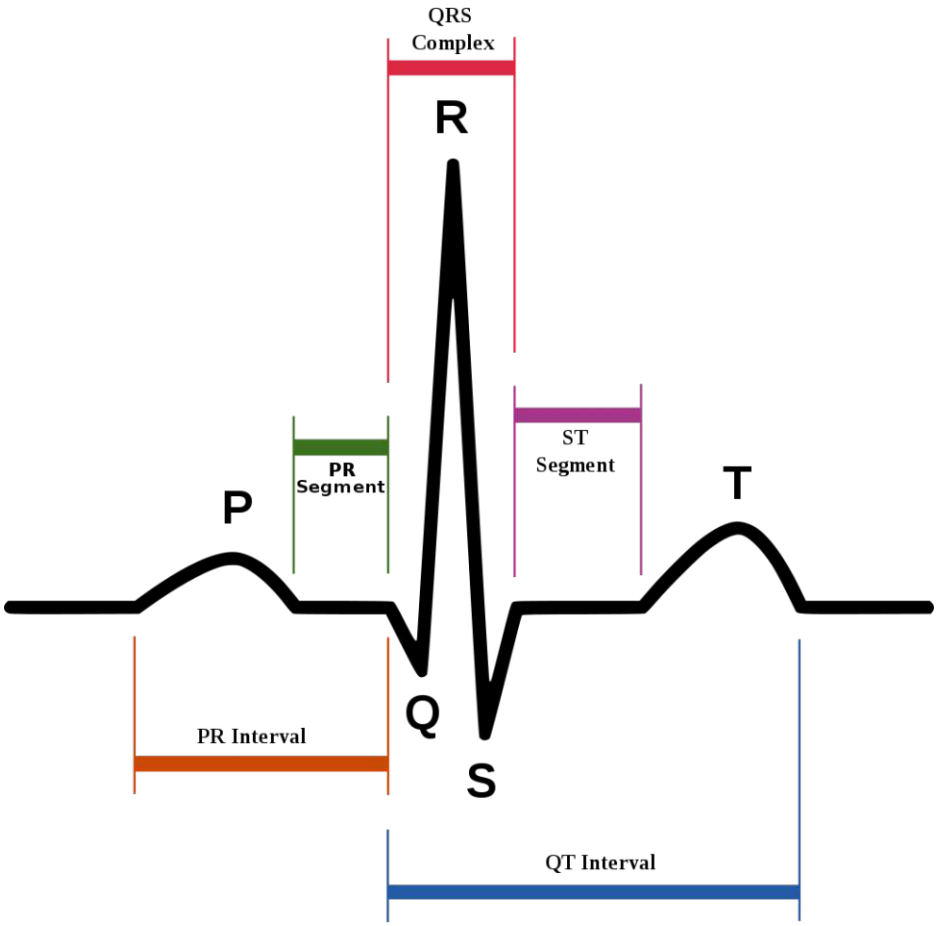

Figure 22.: Schematic diagram of a normal sinus rhythm as seen on an ECG [56].

The R peaks are the most distinctive feature in ECG signals due to their high amplitude and steep slope. This is why they are relatively easy to detect (see subsection 1.2.3 and Figure 22).

Literature research has shown many different approaches to detect the QRS complexes. In this work, a proprietary algorithm provided by the Austrian Institute of Technology (AIT) was used [57]. This algorithm detects R peaks based on the amplitude, the first derivative and local statistic characteristics of the signal. Furthermore, classification to distinguish premature ventricular contractions (ectopic beats) from normal heartbeats is performed by this algorithm [57].

In the original publication from the developers a sensitivity of 98.2% and a positive predictive value (PPV) of 98.7% (see subsection 2.2.4) were achieved in the verification of the detection rate of the algorithm [57]. This was done using ECGs from the four different ECG databases (QT Database, AF Termination Challenge Database, MIT-BIH

Arrhythmia Database, Fantasia Database).

It was found that the AIT algorithm alone does not achieve such a good performance with the data used in this work (see section 3.2). Especially the PPV is not good enough in order to achieve significant results from the HRV analysis performed later upon the annotated heart beat signal. Therefore, additional measures needed to be done in order to increase the performance of the heart beat annotation. Those methods are explained in the following sections.

2.2.3. ECG postprocessing

In order to further improve the annotation of heart beats different algorithms have been applied. These steps are especially important to obtain a good quality beat to beat interval signal (exact position and right annotation of the heart beats) as input to perform the HRV analysis upon. Furthermore some obviously wrong beat to beat interval (outlier) values are marked as artefacts to not confound the result of the HRV analysis.

Most but not all of these improvement measures are based on investigating the beat to beat intervals of the QRS complexes already detected with the AIT algorithm (see subsection 2.2.2). Therefore these algorithms use the beat to beat interval signal as their primary input. This interval signal can be calculated using two different methods that are explained in detail in Table 4. In both signals whenever there is an artefact area the beat to beat interval duration is given as `NaN` in the vector before and after the artefact area.

Vector name	Calculation method
nnSignal	Interval durations are calculated only from one normal heartbeat to another. When there is an ectopic beat the interval duration is given as `NaN` in the vector before and after an ectopic beat
rrSignal	Interval durations are calculated between all heart beats (ectopic and normal beats)

Table 4.: Beat to beat interval calculation methods. In both vectors the duration of the intervals is given in seconds.

By using the grid search (explained in section 2.3) it was also investigated which of this two beat to beat duration signals (all beat intervals (ectopic and normal) or only

the normal heart beats) should be used as the input for the post-processing algorithms in order to achieve the best performance metrics.

The **additional post-processing algorithms** are applied to the beat to beat interval data in the following order:

1. **Enlarge the artefact areas**
2. **Detect single artefact**
3. **Detect artefacts before and after artefact areas**
4. **Remove longer breaks**
5. **Detect ectopic beats and bigeminy rhythm**

All of these algorithms are implemented as individual MATLAB functions and are being called from the main program whereby all the needed input parameters (rrSignal or nnSignal, annotations) are also passed to the algorithms. Furthermore the beat to beat interval signal is recalculated and reassessed between each of theses steps. The code for the individual functions is given in the Appendix A.

2.2.3.1. Falsely annotated beats in proximity to artefact areas

Empirically it was found that there are an exceptionally high number of incorrectly detected heart beats in close proximity to already detected artefact areas (see also Figure 23). The reason for this is that a artefact often consists of parts with higher amplitude and some parts with lower amplitude, but only the high amplitude part can be detected with the artefact detection algorithm using the root mean square value of the signal (see subsubsection 2.2.1.2).

Enlarge the artefact areas As a first step all of the artefact areas were enlarged in both directions by a certain amount of samples (*minDistance*). The MATLAB code of the used algorithm is shown in the appendix (Listing 2). The beats found in these enlarged areas are then deleted. The optimal amount of samples to enlarge the artefacts and get the best result was determined via the grid search (see section 2.3). It was found that this method gives a better result than adjusting the threshold values of the artefact detection algorithm.

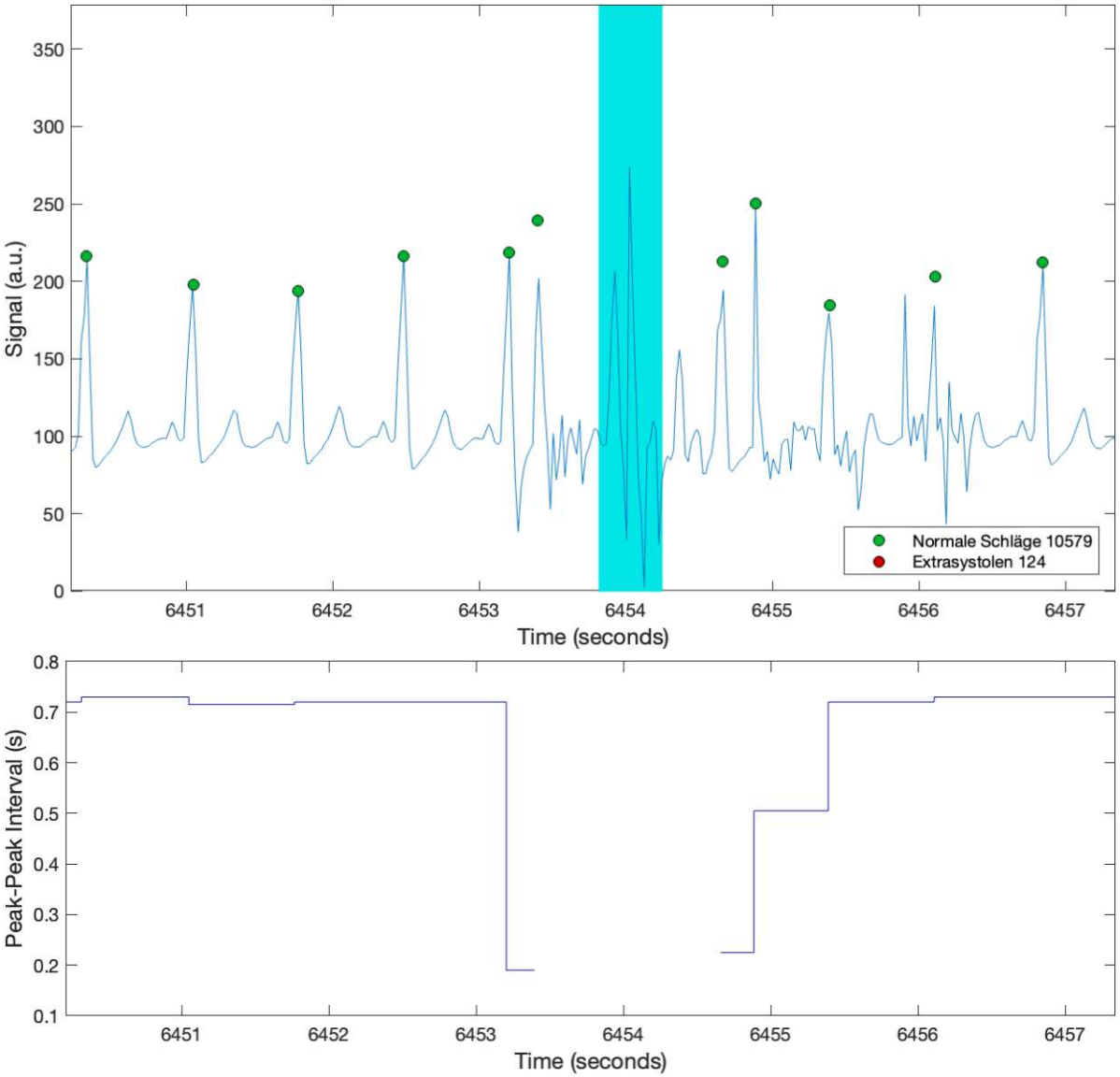

Figure 23.: Typical artefacts in the ECG signal after already detected artefact areas. The beat to beat intervals of the incorrectly detected beats vary tremendously from the correct beats.

Detect artefacts before and after artefact areas After enlarging the artefact areas as described in the previous section, there were still some incorrectly detected heart beats next to the artefact areas. Therefore, another method was used to further decrease the number of those incorrectly detected heart beats. In Figure 23, one can see that the beat to beat intervals after the artefact areas were significantly shorter than the normal (baseline) beat to beat intervals.

The used method to identify those falsely detected beats works in the following way: First the local mean value and standard deviation of beat to beat intervals are calculated and then the individual intervals next to the artefact areas are closer investigated. If the beat to beat interval of the three closest beats next to the artefact area is exceptionally short or long (when comparing them to the local mean value of the beat to beat intervals), these beats are then marked as artefacts.

This means if the beat to beat interval directly before or after artefact areas is smaller or larger than the local mean interval minus or plus a factor ($beforeAferFactor1$) times the variance of the beat to beat interval, this beat is considered to be an artefact. For the next two beats another factor ($beforeAferFactor23$) is used. Again, the MATLAB code of this algorithm is shown in the appendix (Listing 3) and the exact limits/thresholds for this algorithm were determined via the grid search (see section 2.3).

2.2.3.2. Detect single artefacts from abnormal beat to beat interval

Sometimes the QRS detection algorithm detects and annotates some artefacts as normal beats, when they are most certainly artefacts. An example of such error is shown in Figure 24. The peak pictured in this example is probably just an artefact and not an ectopic beat, because there is no post-extrasystolic pause and the morphology of the peak does not correspond to a normal QRS complex. These mistakes occur mostly isolated one at a time and as a consequence are called single artefacts.

These single artefacts can be detected by investigating the beat to beat interval signal. In the given example, the interval before and after the mistakenly detected peak greatly differ from the other (normal) intervals as they are much shorter. The two intervals combined are approximately the same length as a normal interval and can thereby be distinguished from most of the ectopic beats which have a post-extrasystolic pause (of approximately a normal beat to beat interval length).

By calculating a local mean beat to beat interval and comparing the sum of two consecutive intervals with this mean value the incorrectly detected peaks can be identified. If the sum of two consecutive intervals is smaller than the threshold factor $singleArtefactFactor$ times the local mean beat to beat interval, the beat in between the two intervals is considered to be an artefact. In the appendix (Listing 4), the used code is displayed. The threshold factor was determined using the grid search (see section 2.3) and $singleArtefactFactor = 1.3$ has shown to give good results.

This approach is necessary because when comparing only one interval with the mean interval it would not be clear whether the peak before or after the abnormal interval

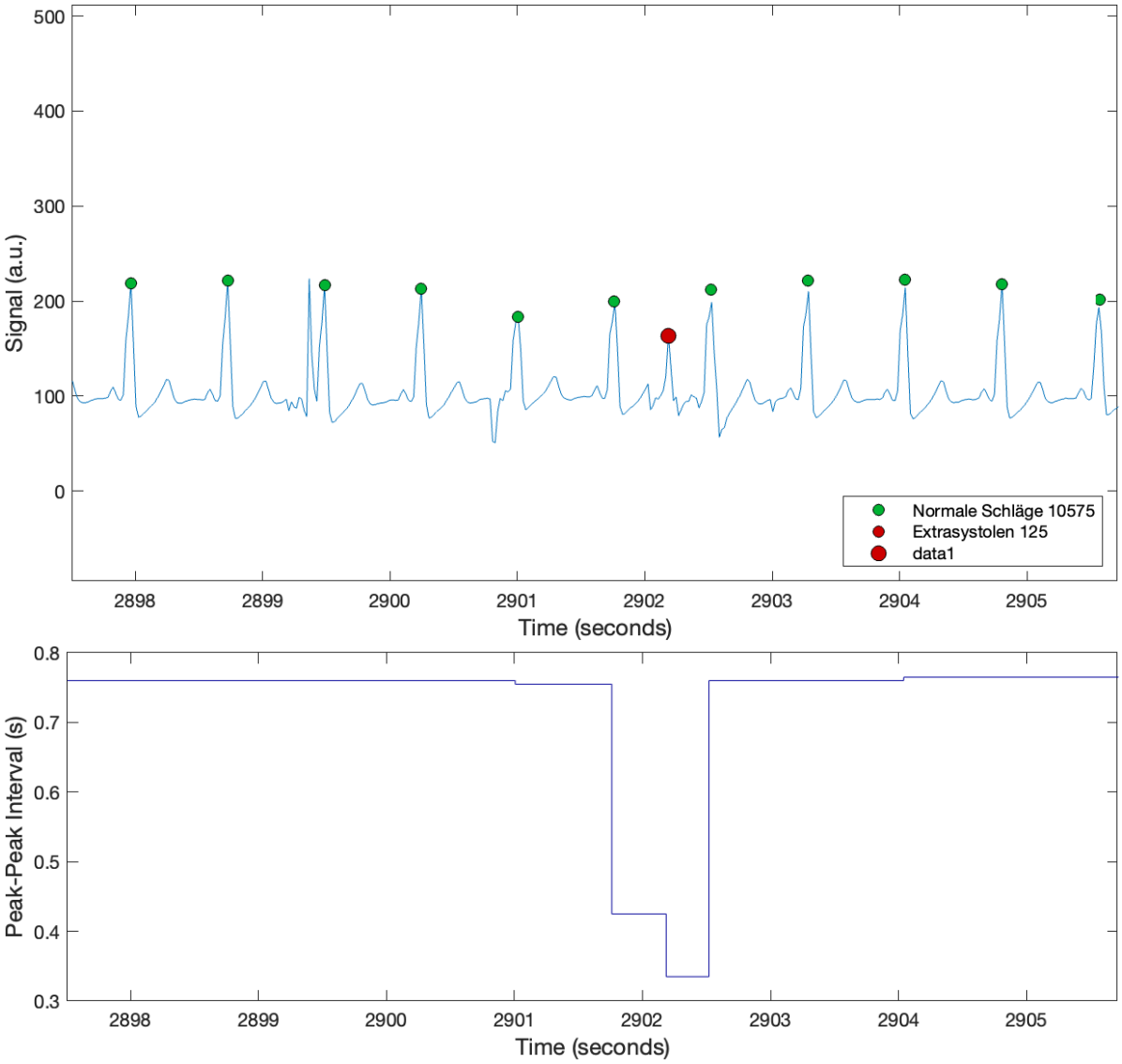

Figure 24.: Typical single artefact. The beat to beat intervals before and after the incorrectly detected beat are much shorter than the normal intervals.

length is incorrect. Furthermore, also ectopic beats with a post-extrasystolic pause would be marked as artefact when they really schould be annotated as ectopic beat.

2.2.3.3. Remove longer breaks

In a normal ECG signal, there is a maximum believable gap in beat to beat intervals. If this break is too long, the most common cause is that the data is either incomplete or the signal has been incorrectly derived from the patient (removal of ECG electrodes).

When there is no problem with the acquisition of the ECG such breaks would only

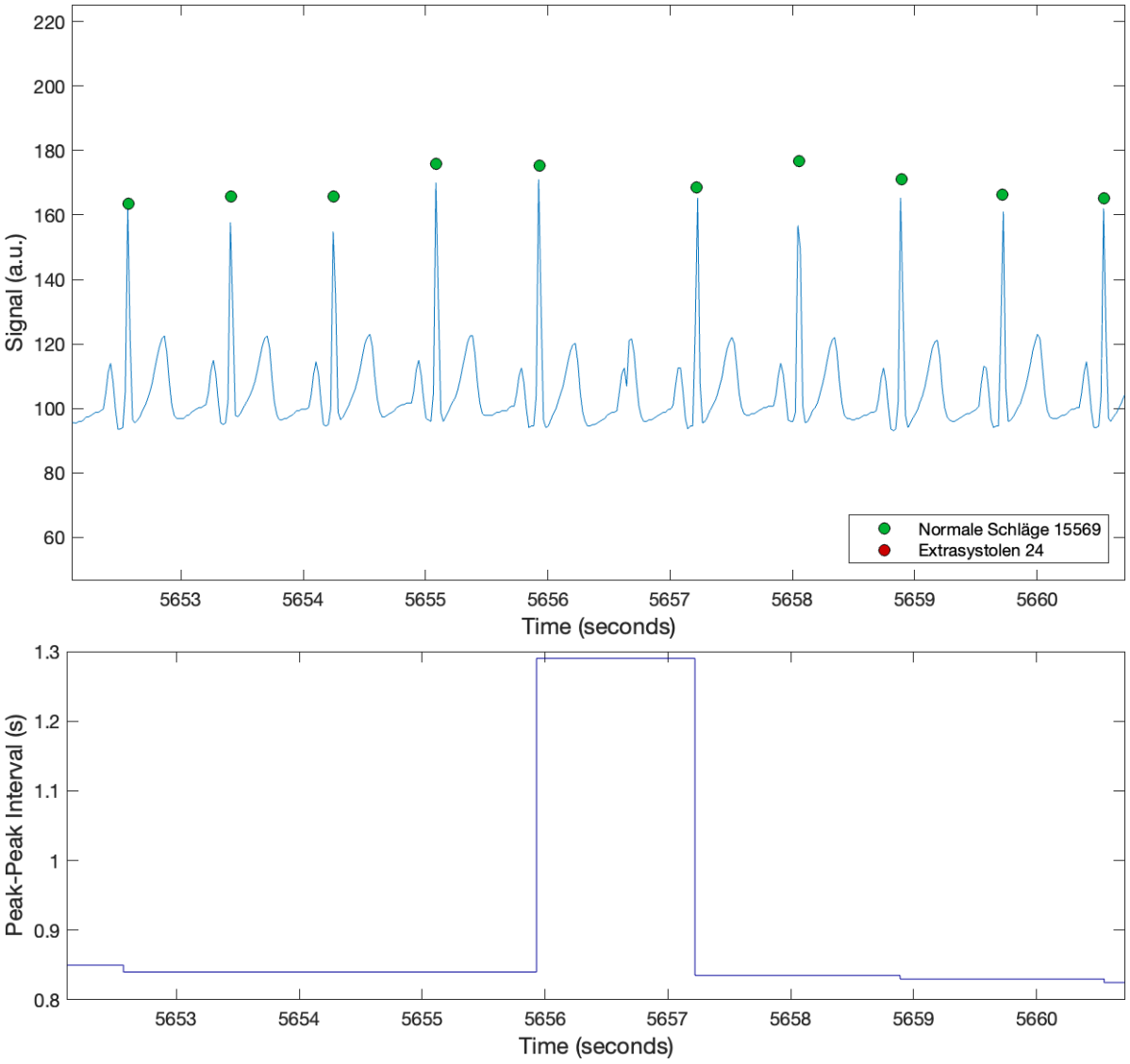

Figure 25.: Gap in the ECG signal with a too long beat to beat interval.

arise from serious pathologies (e.g. AV block, SA node dysfunction, intoxication) or even that the patient is in a condition not compatible with life. These conditions are quite rare during a normal procedure and by means of the ECG they are hard to differ from artefacts. Thereby, those breaks are all marked as artefacts.

The MATLAB code of the algorithm to remove longer breaks is shown in the appendix (Listing 5) and limit ($maxBreakLength$) for the maximum break duration for this method were once again determined via the grid search. All gaps longer than this defined time are marked as artefact area (see Figure 25). As shown in section 2.3, a maximum duration of 1.55 sec gave the best results. This is especially feasible as this

corresponds to a minimum heart rate of $39\,\mathrm{min}^{-1}$.

Another option is to use an individual limit for every patient based on the (local) mean heart rate of the patient. The maximum break length is then calculated by multiplying the mean heart rate with the threshold $maxBreakFactor$. This gives better results with patients who have a very low intrinsic heart rate (e.g. very athletic patients).

The algorithm works by annotating the major part of the longer interval between two normal beats as artefact areas, as the two adjoining beat annotations should remain preserved.

2.2.3.4. Detect ectopic beats and bigeminy rhythms

Another improvement to the original QRS detection algorithm (see subsection 2.2.2) was made by implementing an additional algorithm for detecting ectopic beats and bigeminy rhythms (see subsubsection 1.3.2.6, Figure 15 and Figure 16). The detection of isolated ectopic beats is done by finding two consecutive segments in the beat to beat interval signal with the following properties:

1. A shorter than normal beat to beat interval, followed by:

2. A longer than normal beat to beat interval (post-extrasystolic pause).

This typical features and the associated beat to beat intervals of an supraventricular ectopic beat are shown in the ECG in Figure 26.

Analogously to the ectopic beats, bigeminy rhythms can be detected when the beat to beat intervals are alternating between shorter and longer than normal. Furthermore also trigeminy rhythms can be detect using this method. The crucial step for this algorithm is to define the threshold values when the signal or beat to beat interval is considered to be abnormal (e.g. too short and too long before an ectopic beat).

The algorithm is based on calculating a local mean value of the beat to beat interval and then comparing the individual intervals with this mean value. If the interval before the beat is shorter than a predefined factor (called $withBreakThreshold1$) and the interval after the beat is longer than a predefined factor (called $withBreakThreshold2$) multiplied with the mean value of the beat to beat intervals, the beat is considered to be ectopic. For the bigeminy rhythm two thresholds ($bigeminyThreshold1$ and $bigeminyThreshold2$) in order to account for the alternating beat to beat intervals are used. The MATLAB code of the algorithm is shown in the appendix (Listing 6) and the best suited factors (window length, $withBreakThreshold1$, $withBreakThreshold2$,

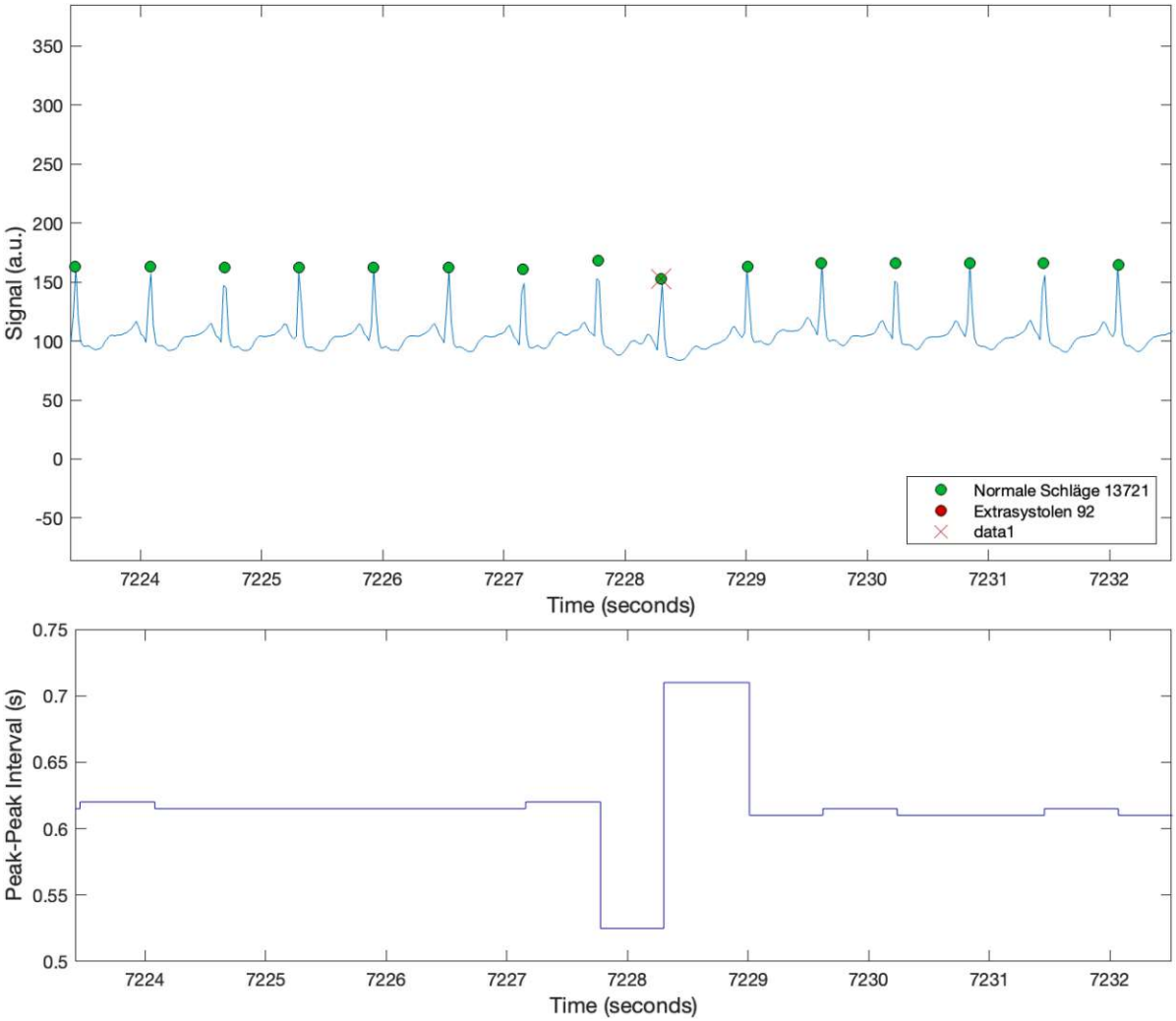

Figure 26.: Isolated atrial ectopic beat marked in red. The beat to beat interval before is shorter and the interval after the ectopic beat is longer than the normal intervals.

*bigeminyThreshold*1 and *bigeminyThreshold*2), were determined via the grid search (see section 2.3).

2.2.4. Verification

During the development process, the QRS complex annotation results of the developed algorithms were continuously verified against manually annotated ECG signals. The manual annotation was done by medical experts upon a part of the ECG database whereby all the QRS complexes were identified and classified as normal (sinus) beats or

ectopic beats.

The result of the manual annotation was then defined as established truth. It was then investigated how well the results of the automatic annotation algorithms can meet the manual ones. This was done by comparing the position of the QRS complexes as well as the correct classification of heart beats.

In order to statistically compare the quality of automatic heart beat (QRS complex) detection it was necessary to compute some metrics that resemble the quality of the output of the algorithms. The following two parameters are recommended by the American National Standards Institute for the evaluation of the detection rate [58]:

- **Sensitivity or true positive rate**
- **Precision or positive predictive value (PPV)**

These two parameters are calculated using the Equation 9 and Equation 10. A true positive (TP) means a real heart beat correctly identified as heart beat. A false negative (FN) means a heartbeat not identified as such (either not detected or annotated as extrasystole). Furthermore a false positive (FP) means that there is a heart beat annotated when in reality there is no such beat (e.g. an artefact).

$$Sensitivity = \frac{\text{number of true positives}}{\text{number of true positives} + \text{number of false negatives}} = \frac{TP}{TP + FN} \quad (9)$$

$$PPV = \frac{\text{number of true positives}}{\text{number of true positives} + \text{number of false positives}} = \frac{TP}{TP + FP} \quad (10)$$

Therefore, the PPV or precision is the number of properly detected normal beats divided by the number of all positive results, including those not identified correctly. The sensitivity is the number of properly detected normal beats divided by the number of all beats that should have been identified as normal.

F_1 score The main statistical parameter to measure the algorithm's accuracy used in this work is the so-called F_1 score.

The F_1 score is the harmonic mean of the precision and sensitivity and can be calculated using the Equation 11.

$$F_1 = 2 * \frac{\text{sensitivity} * \text{PPV}}{\text{sensitivity} + \text{PPV}} = \frac{TP}{TP + \frac{1}{2}(FP + FN)} \quad (11)$$

Another statistical parameter is the accuracy, which measures the fraction of all instances that are correctly categorized. It can be calculated for binary classification and multi-class classification by using the Equation 12.

$$Accuracy = \frac{TP + TN}{TP + TN + FP + FN} = \frac{\text{correct classifications}}{\text{all classifications}} \tag{12}$$

For every annotated ECG, these metrics were separately calculated for normal (sinus) beats as well as for the ectopic beats.

What is more, the beat detection results of the additionally developed ECG pre- and postprocessing algorithms (see subsection 2.2.1 and subsection 2.2.3) were compared to the results of the original AIT QRS complex detection algorithm [57] mentioned in subsection 2.2.2. The results of these calculations are presented in section 4.2.

2.3. Optimization of the algorithms

For the newly developed signal processing algorithms mentioned in subsection 2.2.1 and subsection 2.2.3, there are lots of different threshold values and settings that can be adjusted. A crucial step of this work was to determine whether different threshold values and settings have a positive effect on the resulting beat detection quality (measured using the the performance metrics explained in subsection 2.2.4).

The goal was to find the ideal combination of parameters to achieve the best performance metrics. Of course this is a complicated problem because by increasing the sensitivity, the PPV often goes down (and vice versa). This is why, the F_1 score of normal (sinus) heart beat was tried to be optimized and it was attempted to achieve a good balance between sensitivity and PPV.

Furthermore, for the following HRV analysis it is important to have as little as possible extreme outlying values in the beat to beat interval signal, hence the option achieving a higher PPV was chosen to have as little as possible wrong beats detected as normal ones.

To solve this optimization problem a so-called **grid search** was used. A grid search is an algorithm which helps to select the best parameters for an optimization problem from a list of parameter options. Thereby the trial-and-error method to obtain the parameters at which the algorithms give the best accuracy is automized by applying all

of the parameter options combinations to the problem in multiple iterations.

In MATLAB the grid search was implemented using a for-loop for every input threshold parameter and every option of the signal processing algorithms. This means that there are many nested for-loops in the grid search and all combinations of input parameter values were computed.

For every iteration, the performance matrices of the beat detection were calculated (see subsection 2.2.4) and stored in an `.csv`[3] file for statistical analysis.

A list of parameters optimized by the grid search is given in Table 5. The result of the grid search and the best parameters are presented in section 3.3.

The main problem of this optimization problem was the amount of parameters. This is why the grid search needed a lot of iterations and therefore a lot of time to machine all the ECGs. Thus, in a first step the value range was run-through coarsely and in a second step the values were limited to a smaller range and the grid search was run-through with smaller gaps.

As already mentioned above, the goal was to further investigate the HRV and therefore the main focus was the correct detection of normal (sinus) beats. The goal of the grid search was to achieve the highest possible F_1 score of the normal beats. By using the statistical software suite IBM SPSS Statistics [50] the results of the grid search were analyzed and the best suited threshold values to meet this goal were selected.

[3]Comma separated values format, see `https://datatracker.ietf.org/doc/html/rfc4180`

Function	Parameter	Value range
Artefact Detection	Filter	Different highpass filter and no filter option
	$windowDuration$	0.5 sec to 2 sec
	$findArtefactsFactorThreshold1$	1 to 22
	$findArtefactsFactorThreshold2$	1 to 9
Enlarge Artefacts	$minDistance$	0 to 50 samples
Detect single artefacts	Beat to beat interval signal	NN or RR signal
	$singleArtefactWindowLength$	10 to 50 beats
	$singleArtefactFactor$	1.1 to 1.5
	Iterations	0 to 3
Artefacts before and after artefact areas	Beat to beat interval signal	NN or RR signal
	$beforeAfterWindowLength$	5 to 50 samples
	$beforeAfterFactor1$	1.1 to 4
	$beforeAfterFactor23$	1.1 to 4
Remove longer breaks	Threshold method	Adaptive or fixed
	$maxBreakWindow$	5 to 90 samples
	$maxBreakFactor$	1.2 to 3
Find ectopic beats	$ectopicWindowLength$	50 to 6000 beats
	$withBreakThreshold1$	0.7 to 0.95
	$withBreakThreshold2$	1 to 1.175
	$bigeminyThreshold1$	0.5 to 1
	$bigeminyThreshold2$	1.05 to 1.6

Table 5.: Grid search parameters and the search range.

2.4. Heart rate variability

The HRV parameters were calculated in the time domaine by using an adapted version of the already pre-existing `Calculate_HRV_Time_Domain` MATLAB function developed by Stefan Kampusch (Institute of Biomedical Electronics, Vienna University of Technology [59]).

The calculated HRV parameters are explained in section 1.4 and in Table 6 an overview of the calculated parameters is given. These parameters were calculated for the whole dataset and for standard 5 minute data-segments. When calculating the HRV parameters (standard deviation, mean, RMSSD, pNN50) for 5 min intervals, an 80% overlap of windows was used.

HRV Parameter	
POS	vector of time instances for calculated HRV values in seconds
MNN	mean normal to normal interval in ms
SDNN	standard deviation of normal to normal intervals over the whole dataset in ms
RMSSD	root mean square of successive differences, square root of the mean of the sum of the square of successive RR intervals over the whole dataset in ms
pNN50	percentage of successive normal to normal intervals of the whole dataset differing by more than 50 ms
std5min	standard deviation of normal to normal intervals over 5 minute data-segments in ms
mean5min	mean of normal to normal intervals over 5 minute data-segments in ms
rmssd5min	root mean square of successive differences over 5 minute data-segments in ms
pNN505min	percentage of successive normal to normal intervals of 5 minute data-segments differing by more than 50 ms
SDANN	standard deviation of 5 minute average normal to normal intervals over the whole dataset in ms
SDNNindex	index giving the mean of all 5 minute standard deviations in ms
nnsum5min	sum of NN intervals in window

Table 6.: Output parameters of the `Calculate_HRV_Time_Domain` function.

3. Results

3.1. Data acquisition

The dataset includes a total of 88 patients but there were only 76 patients that included a valid ECG. The performed surgeries range from small hernia repairs and biopsies to kidney transplants and laparotomies. The duration of the datasets ranges from only a few minutes to several hours depending on the procedure/surgery carried out.

Type of operation	**Number of datasets**
Small proctological interventions	6
Kidney transplants	9
Gastric bypass	4
Cholecystectomy (laparoscopic or open)	8
Intestinal surgery (hemicolectomy, Hartmann operation, laparoscopic-assisted ileocolic resection)	6
Hepatectomy (partial resection)	1
Colostomy reversal	1
Hernia repair (laparoscopic or open)	10
Nephrectomy	2
Thyroid gland surgeries	10
Laparotomy	5
Nissen fundoplication	2
Tonsillectomy	3
Mastectomy	1
Other (sentinel node procedures, vascular access port or dialysis catheter implantation, changing of wound dressing)	6
Surgery type or diagnosis not given	11

Table 7.: Different surgery types and their respective numbers in the dataset.

Diagnosis	Number of Patients
Hypertension	9
Diabetes melitus II	7
Chronic kidney disease	4
Depression	4
Gastroesophageal reflux disease	4
S.p. Kidney transplantation	3
Cardiac arrhythmia	3
Hepatitis C	3
Nicotine	3
Adipositas	3
Hypercholesterolemia	3
COPD	2
Asthma	2
Inflammatory bowel disease	2
Diverticulitis	1
Prostate cancer/Colon cancer/Kidney cancer	2/2/1
Thrombosis/Pulmonary embolism	2
Epilepsy	2
Thyroid disease	2
Pancreas cancer/Pancreatitis	1/1
S.p. Nephrectomy	1
S.p. Liver transplantation	1
S.p. Cardiopulmonary resuscitation	1
Sepsis	1
S.p. Percutaneous aortic valve replacement	1
HIV	1
Ileus	1
Coronary artery disease	1

Table 8.: Previous medical diagnosis

In Table 7, an overview of the type and the number of the surgeries is given. Furthermore, the pre-existing medical diagnosis of the patients are given in Table 8. It is evident that the surgery type and the preexisting medical diagnoses of the patient have

great influence on the vital signs of the patients and therefore the later computed HRV parameters might not be directly comparable (see also subsubsection 1.4.2.3).

3.2. Beat annotation

The precision of the beat annotation was measured by comparing the results of the different algorithms to the same ECGs manually annotated by medical experts and thereby having an absolute truth as a reference (see subsection 2.2.4).

3.2.1. Normal (Sinus) Beats

A mean F_1 score of 0.9792 for the detection of normal (sinus) heartbeats was achieved using only the original peak detection algorithm from the AIT [57] (see subsection 2.2.2). With the additionally developed artefact detection and post processing explained in subsection 2.2.1 and subsection 2.2.3, a higher mean F_1 score of 0.9813 was achieved. A comparison of the mean performance metrics for the detection and annotation of normal (sinus) heart beats is given in Table 9.

	mean F_1 score	mean PPV	mean sensitivity
original QRS Detection	0.9792	0.9792	0.9793
additional Algorithms	0.9813	0.9889	0.9738

Table 9.: Mean values of the original QRS detection and the additional artefact area detection and post-processing algorithms. All of the performance metrics given relate to the detection of normal sinus heart beats and not ectopic beats.

All in all, the F_1 scores were improved by 0.21% using the additional artefact detection and post processing algorithms when compared to the original algorithms. A box-plot comparing the F_1 scores of the two methods is shown in Figure 27. Especially the PPV of the normal (sinus) beats was improved by over 1% using the additional artefact detection and post processing algorithms. This means there are significantly less errors annotated as normal heart beats by the additional algorithms, which makes the beat to beat signal more valid compared to the original algorithms. On the other hand, the sensitivity achieved using only the original peak detection method was about 0.55% higher than the sensitivity achieved with the additional artefact detection and post processing.

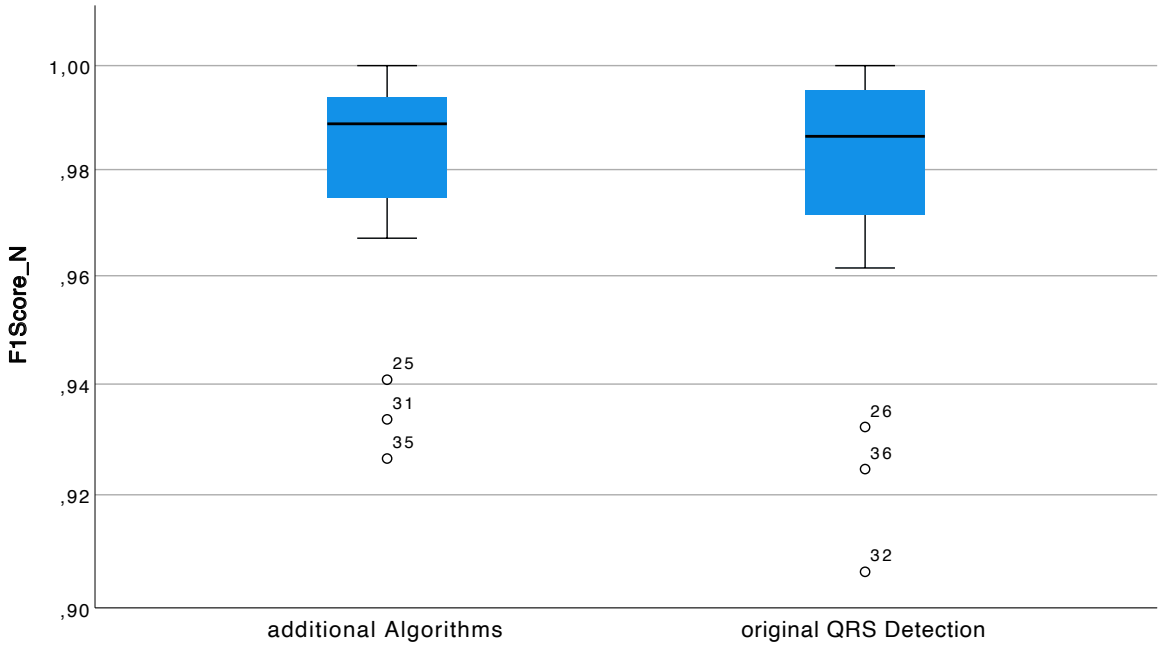

Figure 27.: The F_1 score of normal (sinus) heartbeats results from the original QRS detection algorithm and from the additional artefact area detection and post-processing algorithms.

3.2.2. Ectopic Beats

In addition to the changes mentioned in the previous section concerning the normal (sinus) beats, also the F_1 score, the sensitivity as well as the PPV for the detection of ectopic beats have been greatly improved by using the additional artefact detection and ECG post processing explained in subsection 2.2.1 and subsection 2.2.3 compared to the original QRS detection method from the AIT [57].

	mean F_1 score	mean PPV	mean sensitivity
original QRS Detection	0.0732	0.0277	0.1503
additional Algorithms	0.2470	0.2027	0.4655

Table 10.: Mean values of the original QRS detection and the additional artefact area detection and post-processing algorithms. All of the performance metrics given relate to the detection of ectopic (extrasystole) heart beats and not normal (sinus) beats.

A comparison of the mean performance metrics from the two different approaches can

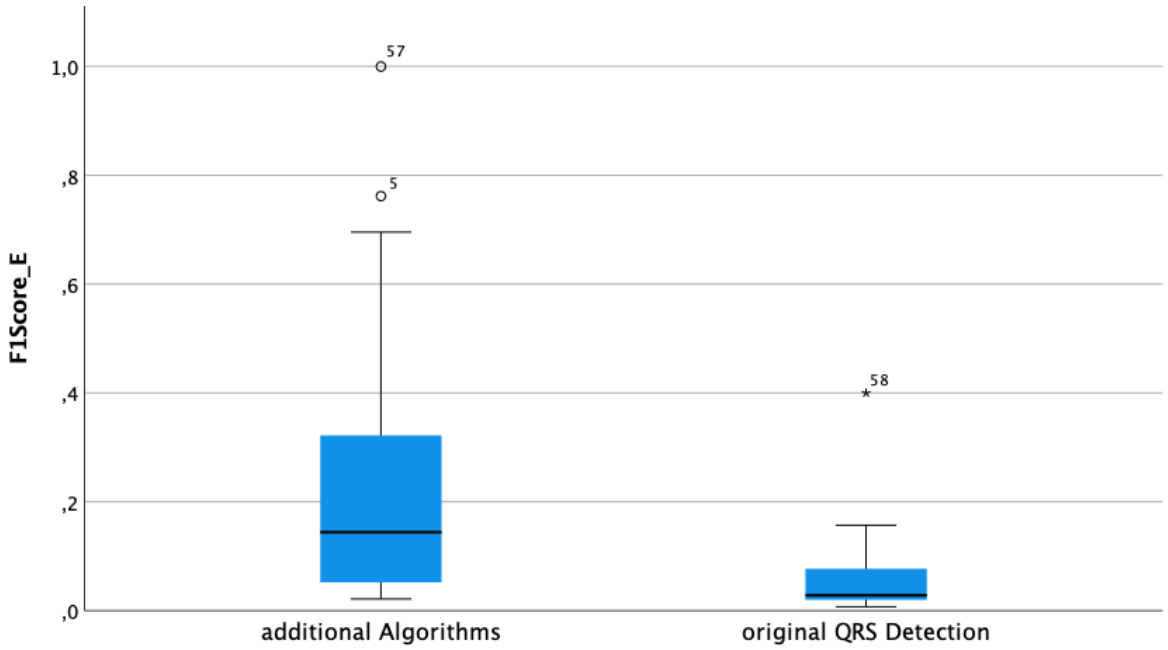

Figure 28.: The F_1 score of ectopic heartbeats results from the original QRS detection algorithm and from the additional artefact area detection and post-processing algorithms.

be seen in Table 10 and a box-plot comparing the F_1 score of the two methods is shown in Figure 28.

The PPV of ectopic beats was improved by over 17% using the additional artefact detection and post processing. Furthermore the sensitivity achieved using only the original peak detection method was about 30% lower than the sensitivity achieved with the additional artefact detection and post processing. This results in an overall improvement of the F_1 scores for the detection of ectopic beats of about 17%.

3.3. Optimization of the algorithms

The artefact detection and ECG post processing algorithms explained in subsection 2.2.1 and subsection 2.2.3 feature different threshold parameters. By using a grid search (see section 2.3) the optimal values of those threshold parameters were determined in order to get the accuracy of the QRS complex detection to the highest possible level and thereby gain the maximum quality beat to beat interval signal.

As already explained in subsection 2.2.4, all of the threshold values have been opti-

mized to achieve a maximal F_1 score for normal (sinus) heart beats. Therefore, all of the performance metrics given in this section relate to the detection of normal sinus heart beats and not ectopic beats, as those are the relevant input for the subsequent HRV analysis. In the following sections, the results of this optimization process are shown.

3.3.1. Artefact detection

For the detection of artefact areas the algorithm based on the root mean square (RMS) value of the signal, as described in subsubsection 2.2.1.2, was used. The needed threshold values ($findArtefactsFactorThreshold1$ and $findArtefactsFactorThreshold2$) for this algorithm are also explained there and the MATLAB code is given in the appendix (Listing 1). The determination of the best threshold factors for this algorithm proved to be quite difficult as two threshold values needed to be found for the two iterations of the algorithm.

The trend of the F_1 score resulting from different combinations of threshold values is shown in Figure 29. It can be seen that there is kind of a plateau of the F_1 score when using $findArtefactsFactorThreshold1$ of approximately 14 and a $findArtefactsFactorThreshold2$ greater than 3.

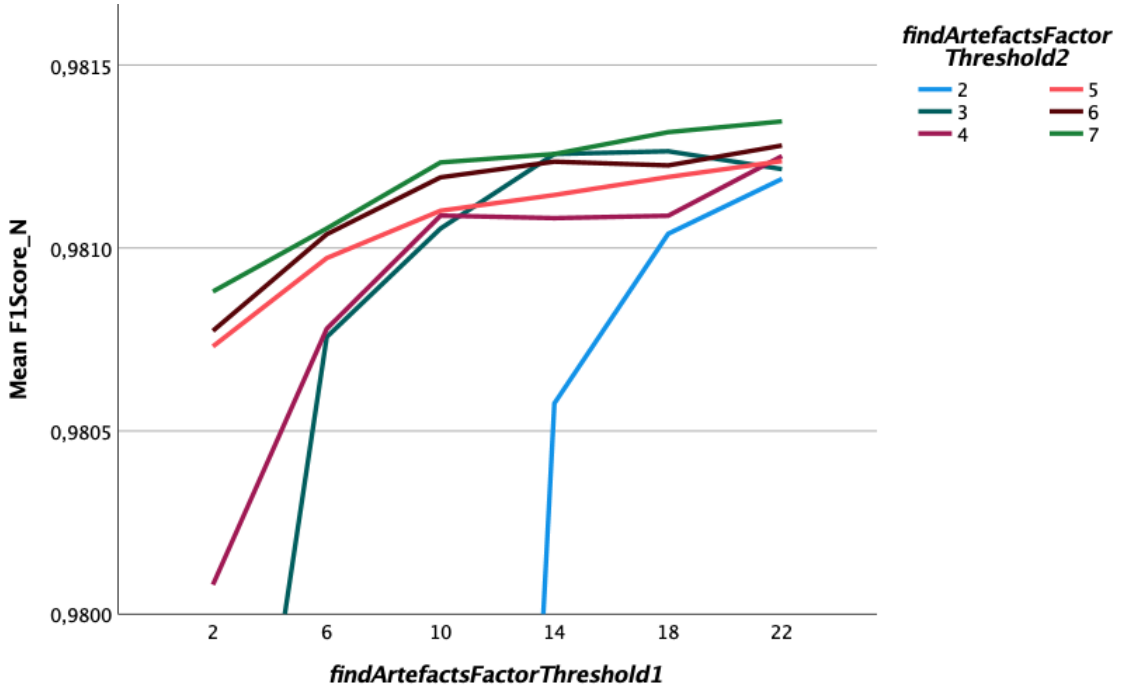

Figure 29.: The trend of the F_1 score for different combinations of threshold values.

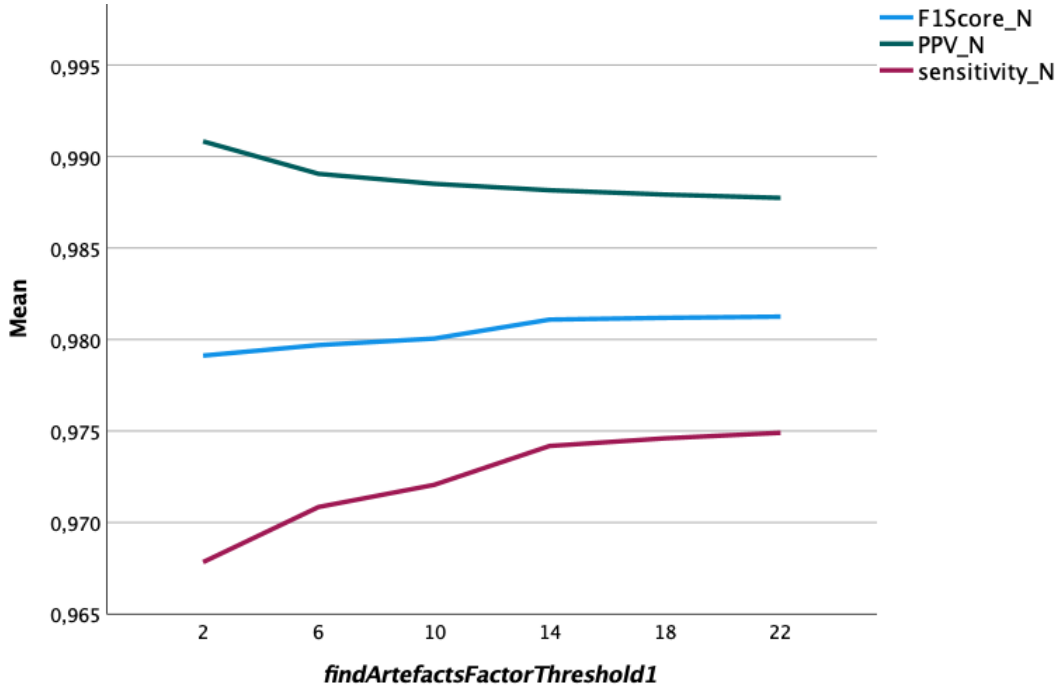

(a)

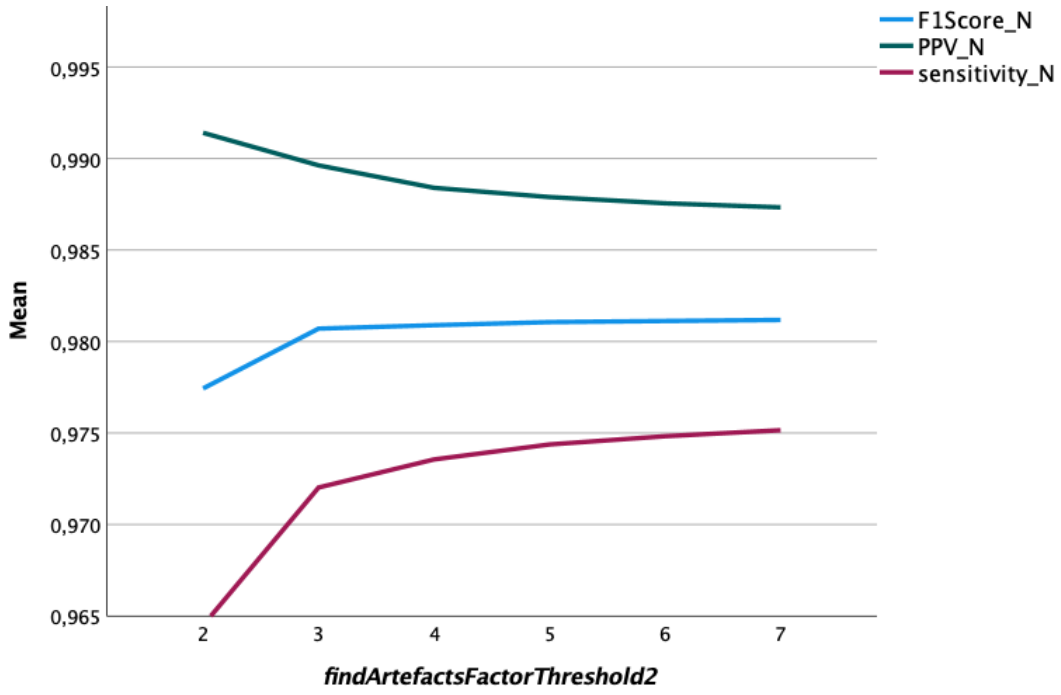

(b)

Figure 30.: F_1 score (blue), PPV (green) and Sensitivity (red) of the peak detection algorithm, for different values of (a) $findArtefactsFactorThreshold1$ and (b) $findArtefactsFactorThreshold2$.

As it can be seen in Figure 30a and Figure 30b, there is a negative correlation between higher threshold factors and the PPV and positive correlation between higher threshold values and the sensitivity. It can be seen that the F_1 score maintains a constant value when reaching the plateau while the PPV values still decrease when using higher $findArtefactsFactorThreshold2$ and $findArtefactsFactorThreshold1$ values. Therefore, the ideal threshold values were then defined to result in a good balance between the F_1 score (and sensitivity) and PPVs.

Both combinations - first a high threshold then a low and first a low and then a high - gave good results for the PPV value but only a combination of a higher $findArtefactsFactorThreshold1$ value and a lower $findArtefactsFactorThreshold2$ gave good results for the F_1 score. An optimum (good compromise between PPV and F_1 score) was found by using a $findArtefactsFactorThreshold1$ of 14 and a $findArtefactsFactorThreshold2$ of 3, which gives a good balance between sensitivity and PPVs.

Furthermore, the usage of different window lengths for the artefact area detection algorithm was investigated in the grid search. The results showed a preference for $windowDuration = 0.5seconds$. The F_1 scores resulting from different signal filtering methods showed no advantages from one filter over the others. Therefore, the computing time was used to determine which filter should be used.

3.3.2. Minimum distance from artefact area to beats

The algorithm and the needed threshold value ($minDistance$) of the used algorithm to enlarge the artefact areas are given in section 2.2.3.1 and the MATLAB code is shown in the appendix (Listing 2). The F_1 score resulting from different $minDistance$ values of the minimum distance from heart beats to artefact areas is relatively constant over a certain period (see Figure 31a). It can be seen that this interval spreads from about 10 to 25 samples of minimum distance from heart beats to artefact areas.

Thus, the sensitivity and the PPV resulting from different $minDistance$ values was further investigated. In Figure 31b the trend of this performance parameters is shown. It can be seen that there is a steep rise and respectively fall of the performance parameters for $minDistance$ threshold values from 1 to 14. By defining the threshold value as $minDistance = 12$ samples a good balance could be achieved as this results in a relatively high PPV and an acceptable sensitivity value.

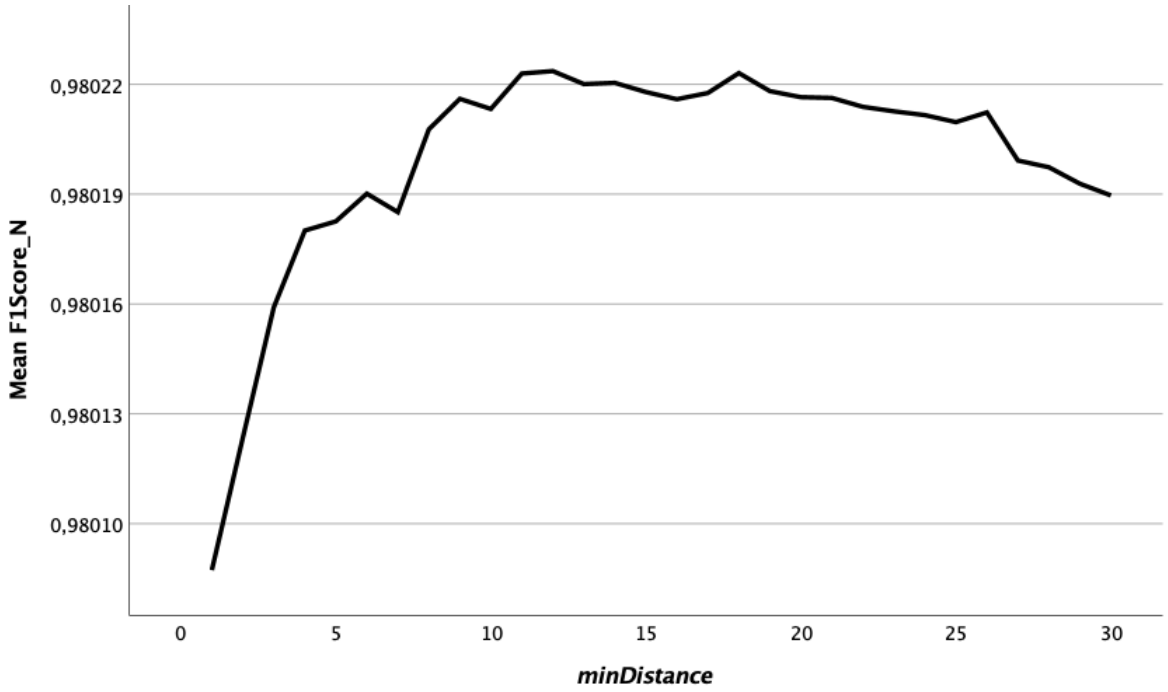

(a)

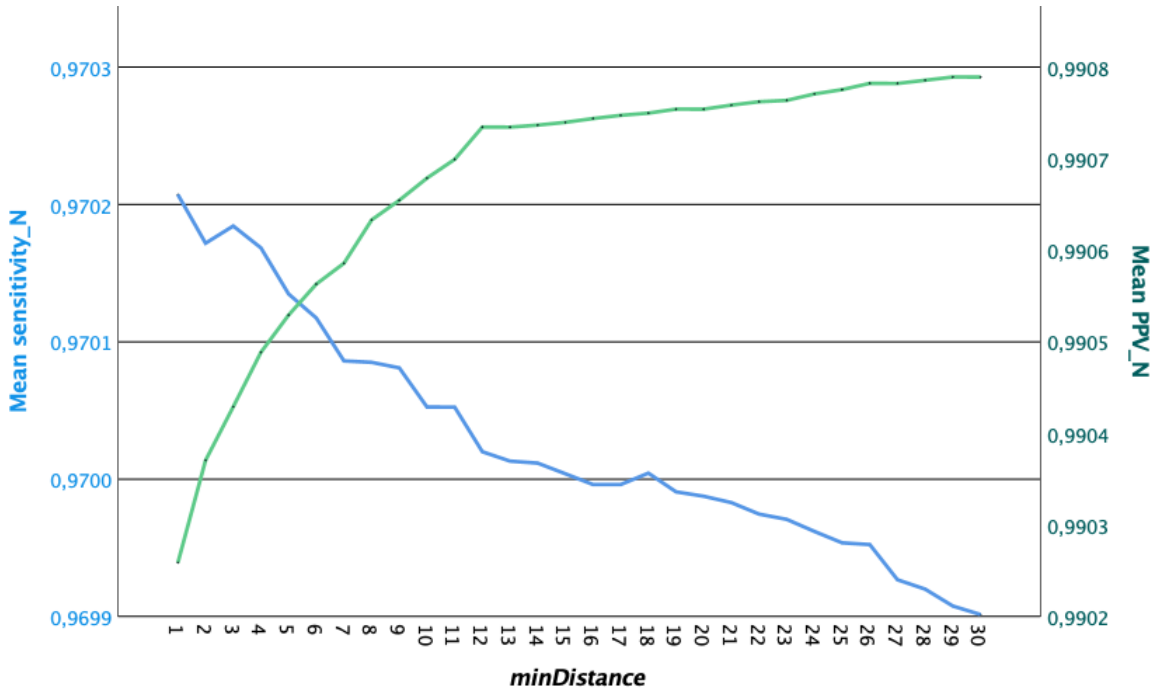

(b)

Figure 31.: Mean (a) F_1 score and (b) sensitivity (blue) and PPV (green) resulting from different *minDistance* values.

3.3.3. Detect single artefacts

The algorithm used to find single artefacts as well as the needed threshold parameter $singleArtefactFactor$ are described in subsubsection 2.2.3.2 and the MATLAB code is shown in the appendix (Listing 4). The trend of the F_1 score resulting from different values of $singleArtefactFactor$ are shown in Figure 32. The maximum F_1 score was achieved by using a threshold value of $singleArtefactFactor = 1.3$. This means a peak is considered to be an artefact if the sum of the beat to beat interval before and after the (mistakenly) detected peak is shorter than 1.3 times the local mean beat to beat interval.

For this algorithm, the best results were achieved when using the original beat to beat interval (sinus and ectopic beats) and not a normal (sinus) beat to normal beat signal as an input (see Table 11).

input signal	mean F_1 score
original beat to beat intervals	0.97942
normal beat to normal beat intervals	0.97937

Table 11.: The mean F_1 score resulting from the original (sinus and ectopic) beat to beat signal is marginally higher than the one resulting from only the normal (sinus) heart beats.

It was further tried whether the algorithm gives better results if it was applied multiple times (thereby the local mean beat to beat interval would change for the next iteration, as there are already some beats eliminated). As shown in Table 12, the best results were achieved with only one iteration.

Number of iterations	mean F_1 score
0	0.97936
1	0.97988
2	0.99749
3	0.97887

Table 12.: The mean F_1 score resulting from different number of iterations the algorithm is is applied to the ECG.

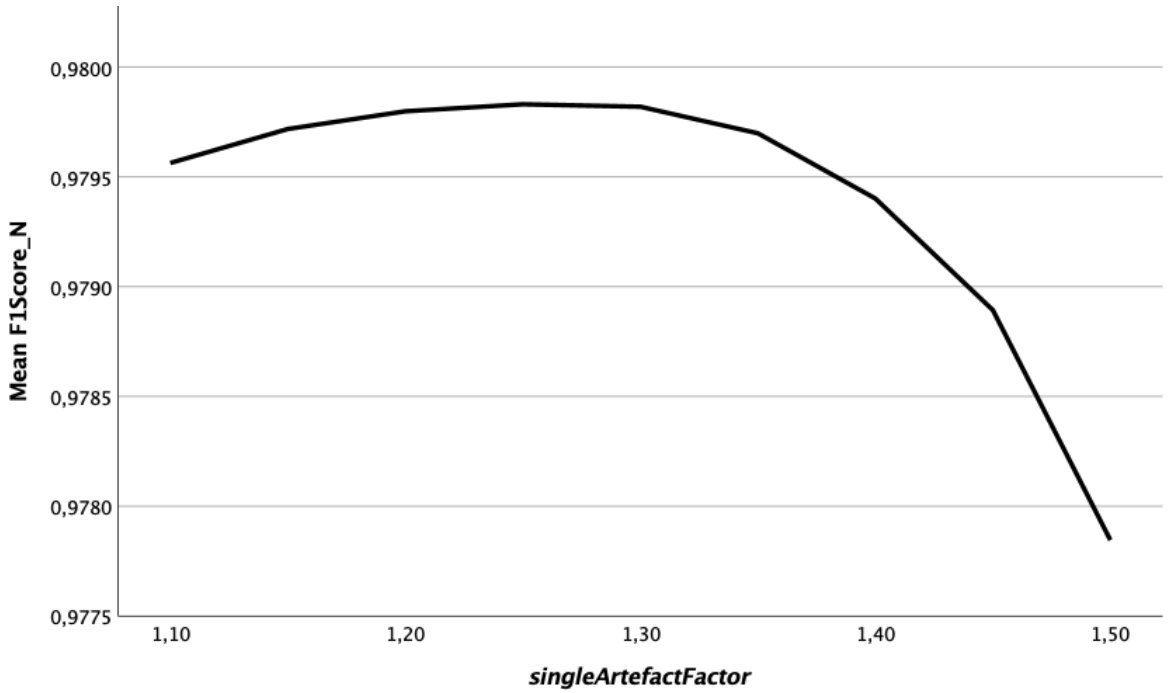

Figure 32.: Mean F_1 scores resulting from (a) different $singleArtefactFactor$ values

3.3.4. Remove longer breaks

With the fixed (non adaptive) method described in subsubsection 2.2.3.3 the best F_1 score was achieved when the maximum beat to beat interval was set to $maxBreakLength = 1.55$ seconds. This corresponds to a minimum heart rate of $39\,\mathrm{min}^{-1}$.

By using an adaptive maximum break length based on the local mean beat to beat interval, the resulting F_1 score was further increased. The F_1 scores resulting from both algorithms are compared in Table 13.

Method	mean F_1 score
fixed maximum break length	0.98036
adaptive maximum break length	0.98042

Table 13.: The mean F_1 score resulting from the fixed and adaptive maximum break length.

In the adaptive method the maximum beat length threshold is given as a factor of the local mean beat to beat interval ($maxBreakFactor$, see subsubsection 2.2.3.3). The trend of the F_1 score resulting from different values of the adaptive maximum break

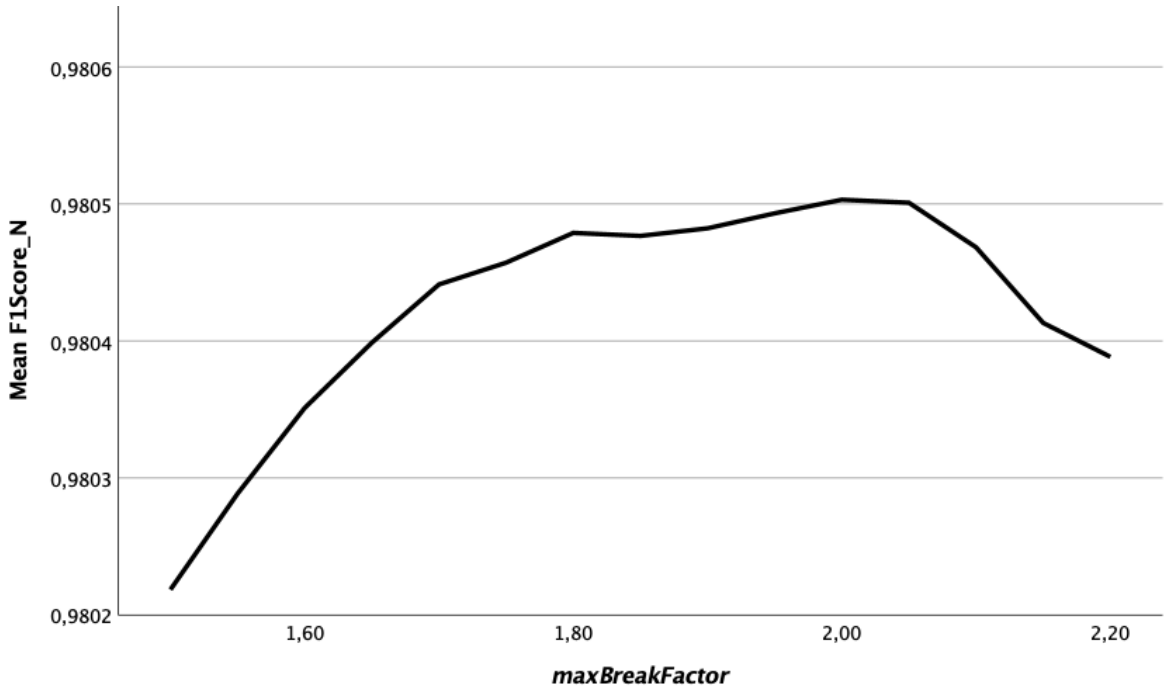

Figure 33.: Mean F_1 scores resulting from different $maxBreakLength$ thresholds.

length threshold $maxBreakFactor$ is shown in Figure 33. It can be seen that the optimum threshold is $maxBreakFactor = 2.0$ times the local mean interval length. The best window length for calculating the local mean interval length is 50 intervals.

3.3.5. Detect artefacts before and after artefact areas

For the detection of incorrectly annotated beats before and after artefact areas, the method described in section 2.2.3.1 was used. Here, also the threshold values $beforeAfterFactor1$ and $beforeAfterFactor23$ used by this algorithm are explained. The Matlab code of the algorithm is shown in the appendix (Listing 3).

The trend of the F_1 score resulting from different threshold values is shown in Figure 34a and Figure 34b. In these figures it can be seen that the ideal values based on the optimization of the F_1 score are $beforeAfterFactor1 = 2.1$ and $beforeAfterFactor23 = 2.5$.

This means if the beat to beat interval directly before or after artefact areas is smaller or larger than the local mean interval minus or plus 2.1 times the variance of the beat to beat interval this beat is considered to be an artefact. For the next two beats before and after the artefact area the threshold is then the local mean interval minus or plus

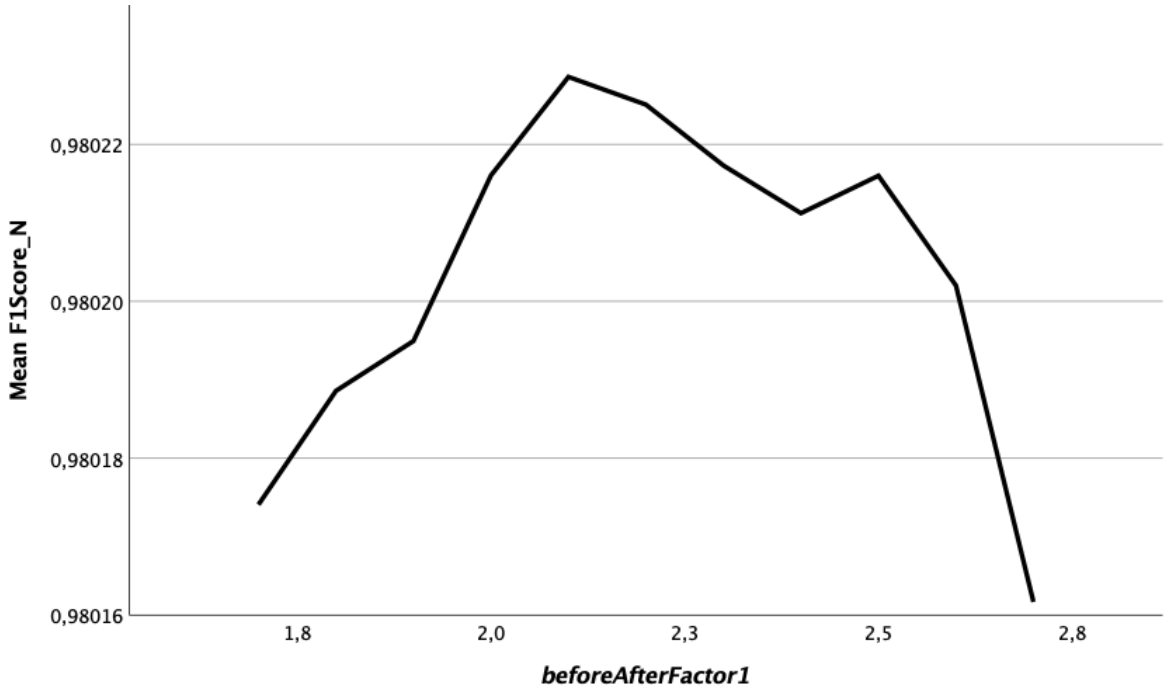

(a)

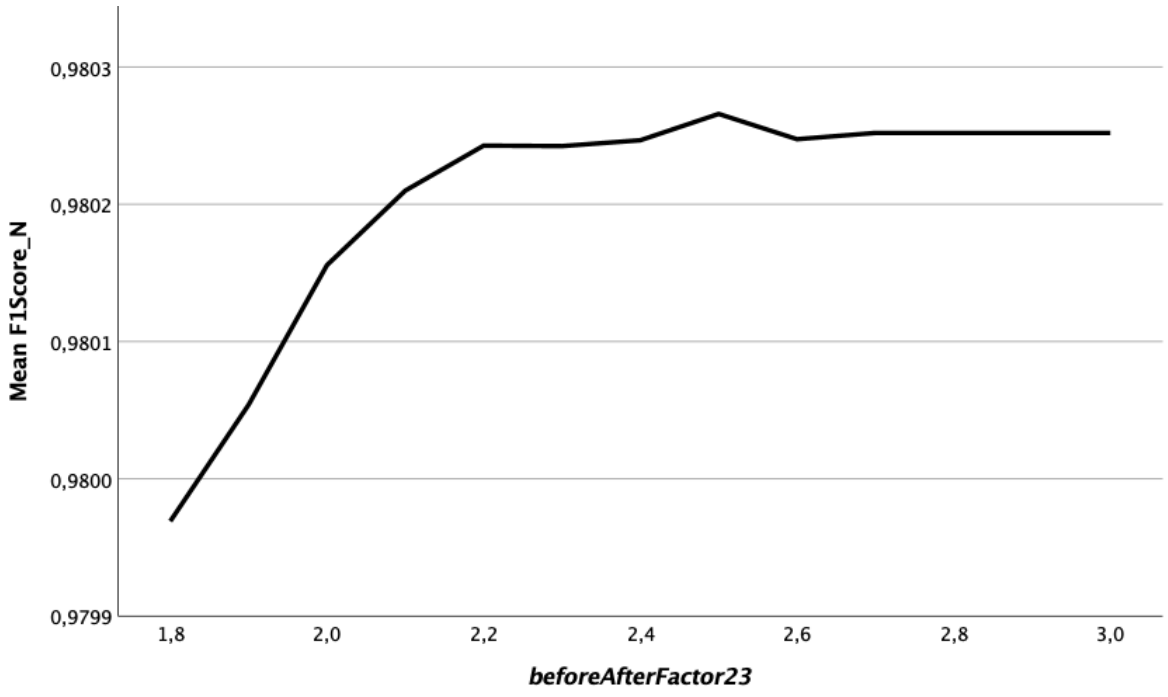

(b)

Figure 34.: Mean F_1 score trend from (a) different $beforeAfterFactor1$ and (b) different $beforeAfterFactor23$ thresholds.

2.5 times the variance of the beat to beat interval.

With this algorithm the optimum F_1 score was achieved by using a window length of 10 heart beats for the calculation of the local mean. Furthermore, it proofed to be better to use the beat to beat interval instead of the normal beat to normal beat interval for the calculation of the mean beat to beat interval time.

3.3.6. Detect ectopic beats

The algorithm as well as the used threshold values used to detect ectopic beats are explained in detail in subsubsection 2.2.3.4 and the corresponding MATLAB code is shown in the appendix (Listing 6). For the detection of ectopic beats with post-extrasystolic pauses, this algorithm uses two threshold values ($withBreakThreshold1$ and $withBreakThreshold2$). The trend of the F_1 score resulting from different values of those thresholds is shown in Figure 35a and Figure 35b. As it can be seen in this figures the optimum threshold values are $withBreakThreshold1 = 0.825$ and $withBreakThreshold2 = 1.05$. This means the beat is considered to be ectopic if the interval before the beat is shorter than $withBreakThreshold1$ times the local mean interval and the interval after the beat is longer than $withBreakThreshold2$ times the local mean.

3.3.7. Detect bigeminy rhythms

For the detection of bigeminy rhythms, the algorithm uses the threshold values $bigeminyThreshold1$ and $bigeminyThreshold2$ (see subsubsection 2.2.3.4). The corresponding MATLAB code is shown in the appendix (Listing 6). The trend of the F_1 score resulting from different values of those thresholds is shown in Figure 36a and Figure 36b. In order to achieve the maximum F_1 score the threshold values $bigeminyThreshold1 = 0.85$ and $bigeminyThreshold2 = 1.45$ were determined using the grid search. Therefore an ECG rhythm is considered to be a bigeminy rhythm if the beat to beat interval alternates between being shorter than the factor $bigeminyThreshold1 = 0.85$ times the local mean beat to beat interval and longer than $bigeminyThreshold2 = 1.45$ times the local mean interval.

For this algorithm and the ectopic beats detection algorithm the best results were achieved by using a window length of 2300 beats.

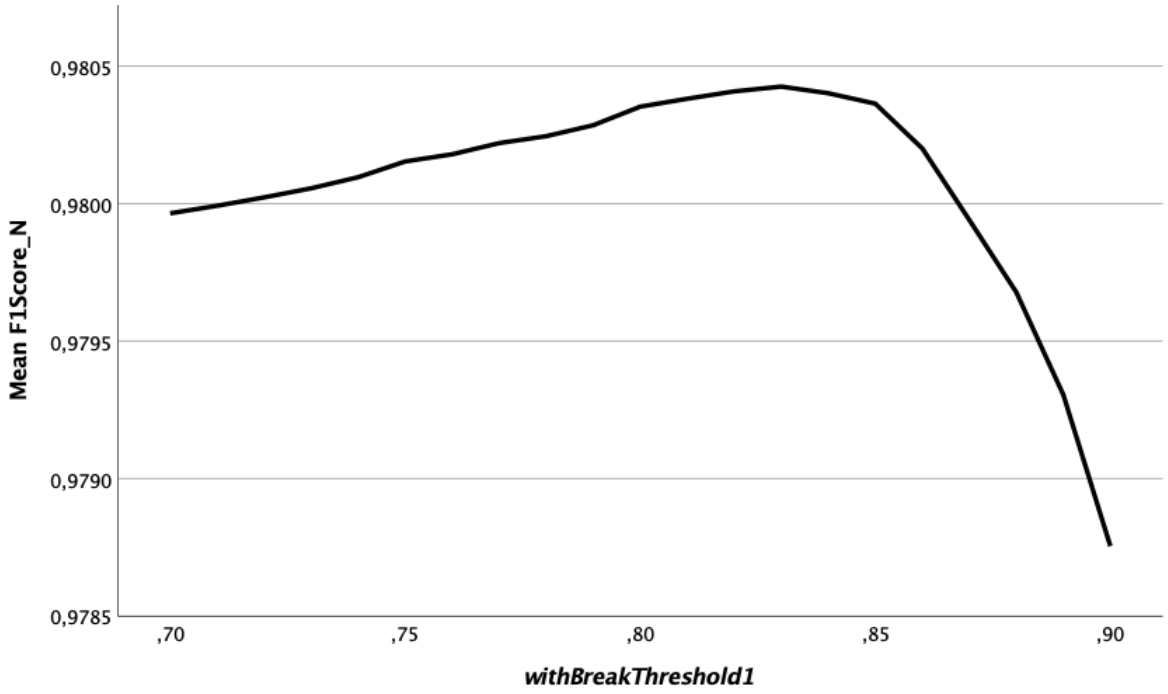

(a)

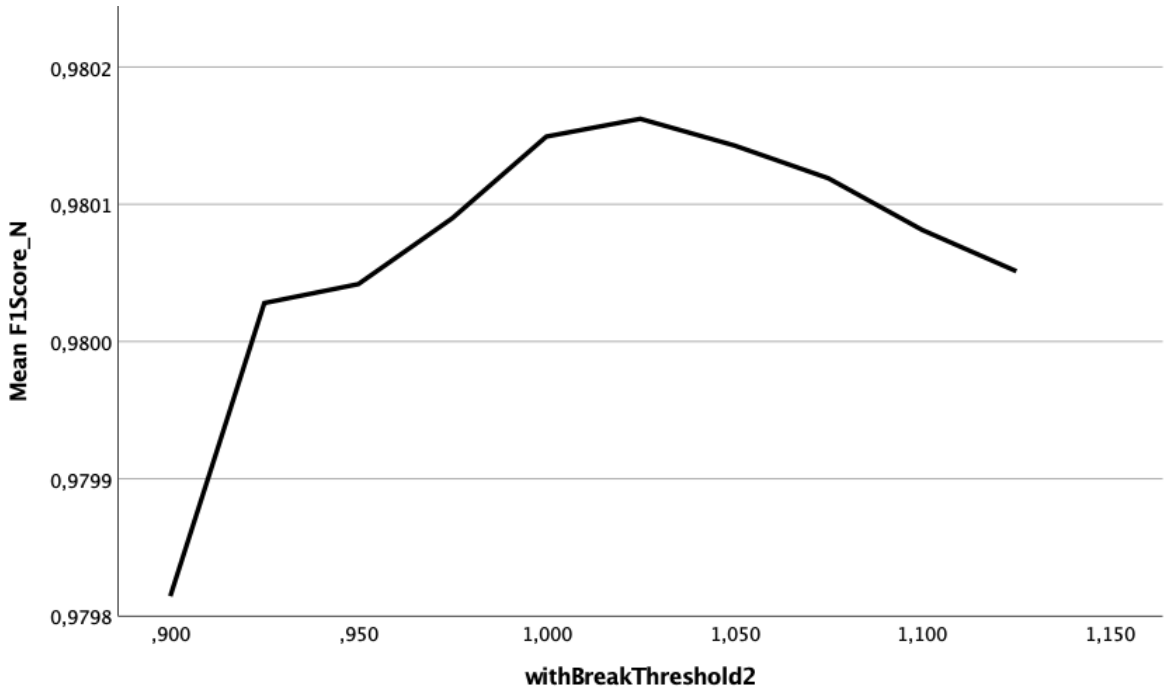

(b)

Figure 35.: Mean F_1 score trend from different (a) *withBreakThreshold*1 and (b) *withBreakThreshold*2 thresholds.

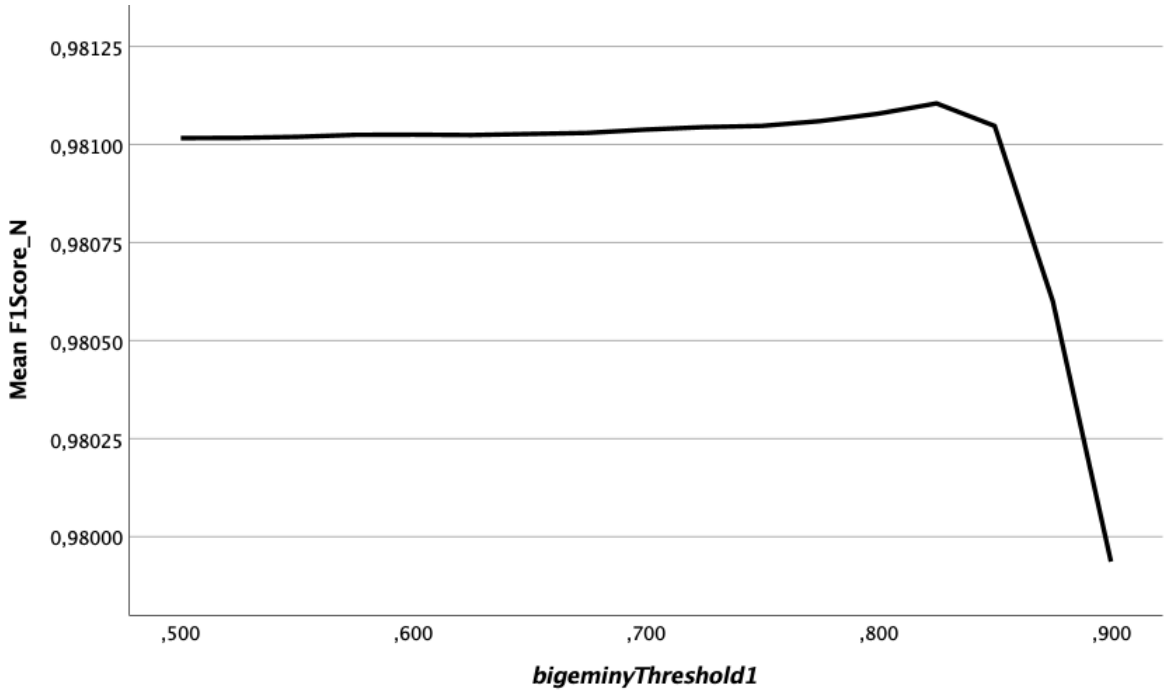

(a)

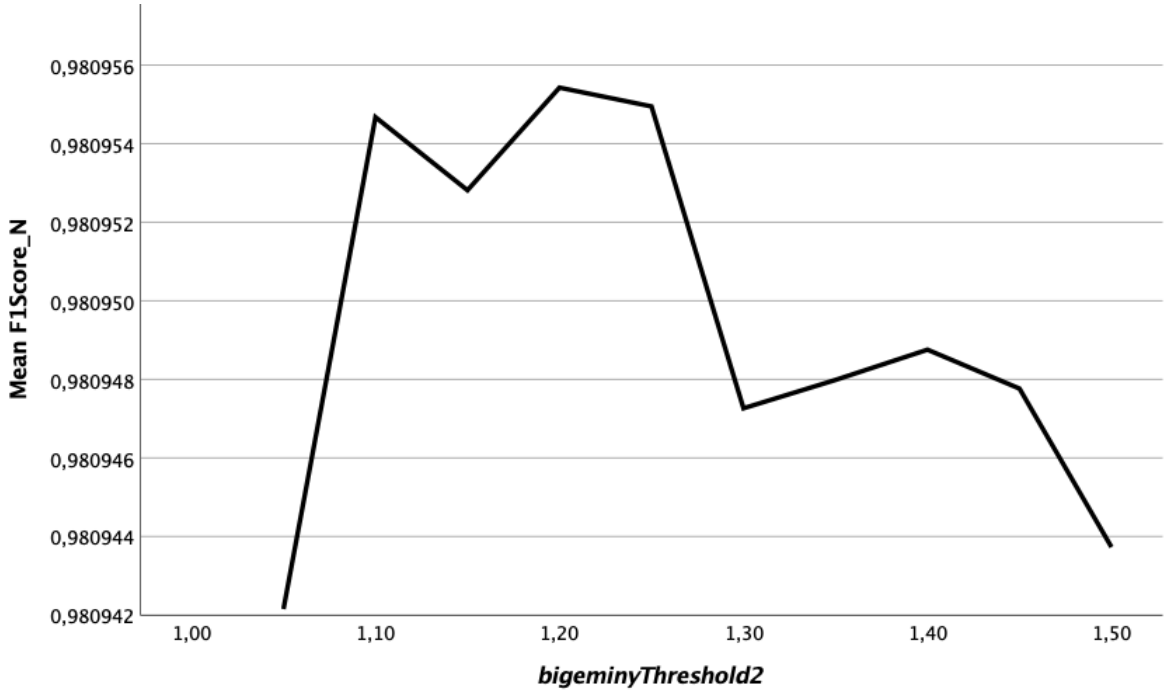

(b)

Figure 36.: Mean F_1 score trend from different (a) *bigeminyThreshold*1 and (b) *bigeminyThreshold*2 thresholds.

3.4. Heart rate variability

When applying the heart rate analysis on the whole dataset, for each of the patients the HRV values as mentioned in section 2.4 were computed. It was then tried to find correlations between the metadata or other biosignals and the HRV parameters of the patients.

For this purpose, either the standard deviation of normal to normal beat intervals over the whole dataset or the trend of the standard deviation of normal to normal beat intervals over 5 minute segments were compared. The results of these statistical evaluations are shown in the following sections.

3.4.1. ASA Score

As already mentioned in subsection 2.1.1, the ASA physical status classification system is a system for assessing the fitness of patients before surgery [40]. In the present dataset there are a total of 18 patients graded ASA I, 28 patients graded ASA II, 22 patients graded ASA III, one patient is graded ASA IV and 7 patients with no given ASA classification.

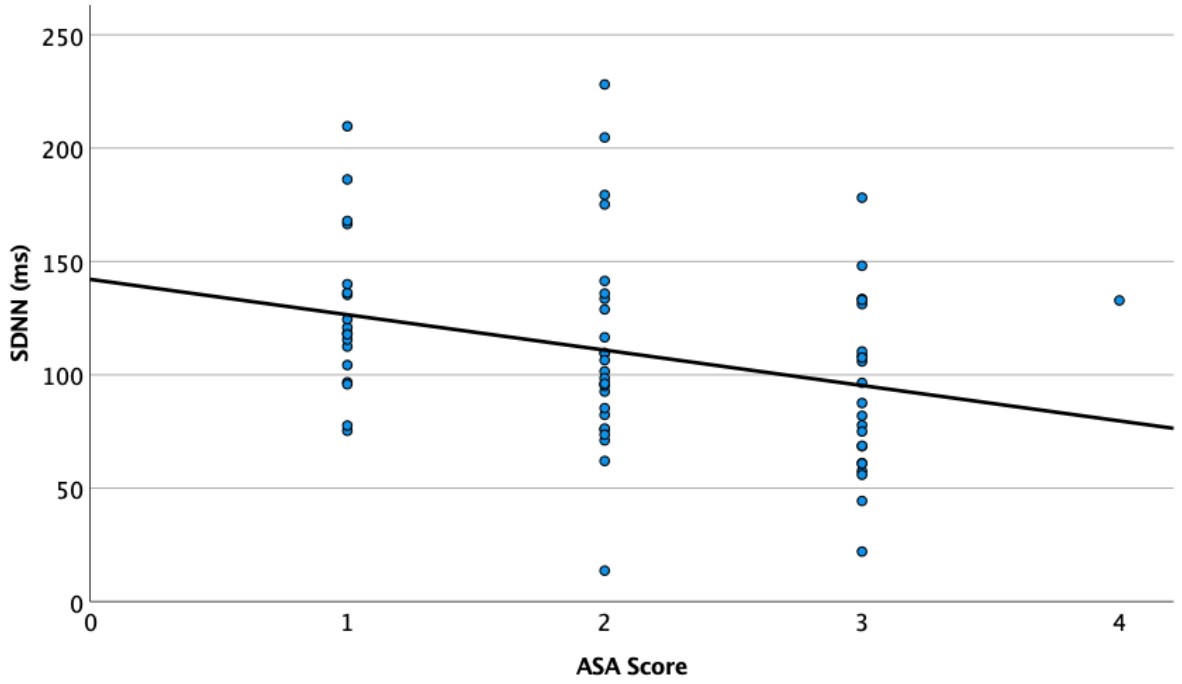

Figure 37.: Linear correlation of the ASA score and the SDNN values (p = 0,045).

Although the relation is not statistically significant, it can be seen in Figure 37 that the patients with higher ASA scores (more ill patients) show lower SDNN values during surgery than those with lower ASA scores.

3.4.1.1. Other Scores

For the given dataset between the SDNN and the other patient scores (see subsection 1.5.3) like the **maximum achieved MET**, the **NYHA Functional Classification**, the **RCRI**, the **NSQIP Risk Factors** or the **General Risk Assessment Score** no clear trend could be detected.

It should be noted that the metadata that includes these scores seems to be incomplete as these scores are missing for almost one third of the patients. Therefore, there might be a correlation if there were enough sufficient data.

3.4.2. CRP value

As also mentioned in subsection 2.1.1, the concentration of CRP in the blood is a measure of the inflammation happening in the body. In Figure 38, it can be seen that patients with higher CRP values show significantly lower SDNN values than those with normal CRP values (smaller than 0.5 mg/dl).

This may support a link between inflammation and autonomic dysfunction [60]. It should be, furthermore, noted that the combination of CRP and HRV predicts death and myocardial infarction with synergism, indicating interaction between inflammatory and ANS with a prognostic significance [61].

3.4.2.1. Other blood tests

When comparing the HRV values of the other blood tests (like **Cholesterol** and **Creatinin**), no clear trend of the HRV parameters was found. Most of the Creatinine values measured are very similar and only a few patients had values higher than the norm. The values **Troponin** and **BNP** are only available for 4, respectively one patient and therefore obviously no correlation was detected between HRV parameters and those values.

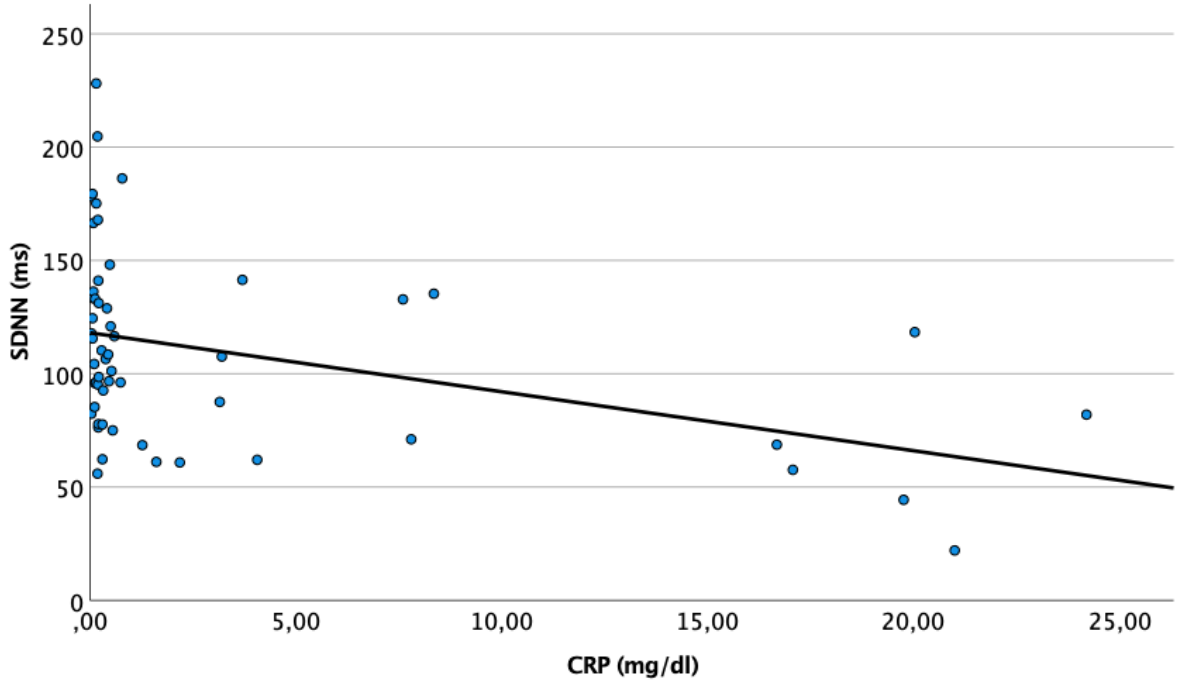

Figure 38.: Correlation between CRP value and SDNN (p = 0,003).

3.4.3. General patient information

In the following sections, the effect of different medical diagnoses and other (body) characteristics on the HRV (SDNN value) is presented.

3.4.3.1. Preexisting medical diagnosis

In the given dataset no correlation between history of ischemic heart disease, history of chronic heart failure or history of cerebrovascular diseases and the HRV could be investigated because these diagnoses are only existing in a very limited number of patients (3, respectively 4 patients).

The given dataset includes 52 non-smokers and 24 smokers, but when comparing the HRV values with this characteristic only a marginal difference could be detected (see Figure 39). As with smoking when dividing the patients in physical active (66 patients) and physically inactive (10 patients), there is only a small difference in SDNN values (see Figure 40).

As it can be observed in Figure 41a, patients with preexisting diabetes (7 patients) show slightly lower SDNN values than those without this medical diagnosis (69 patients). This correlation is even more distinct when comparing the patients who needed preoper-

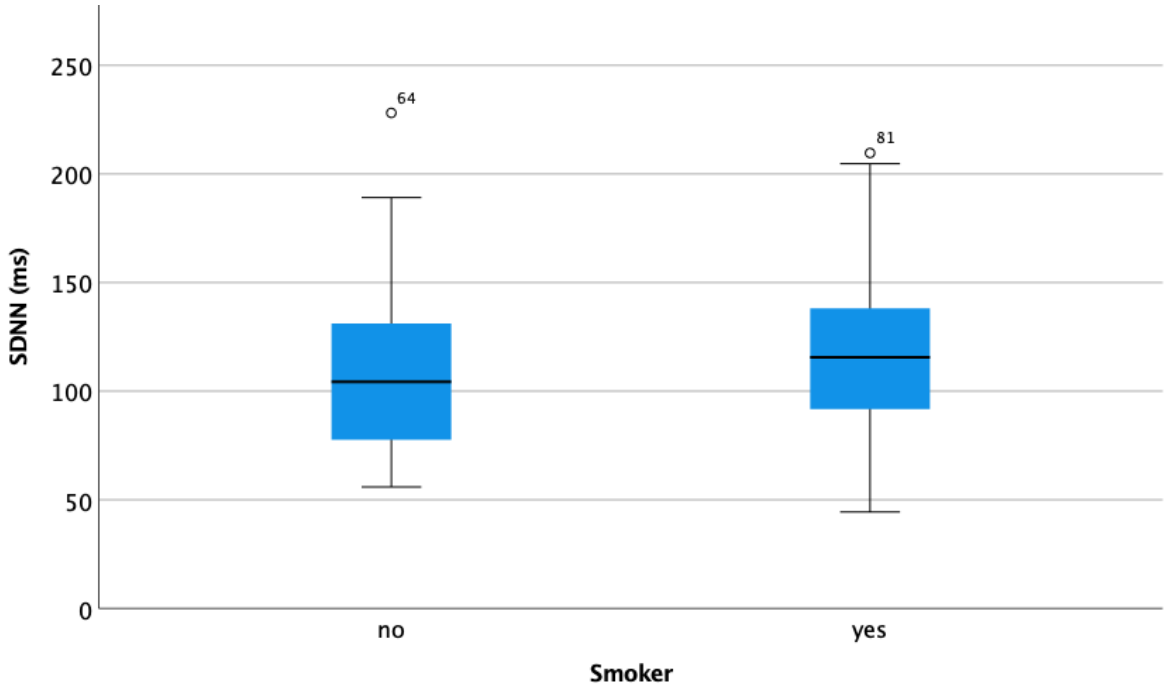

Figure 39.: SDNN values of smoker and nonsmoker.

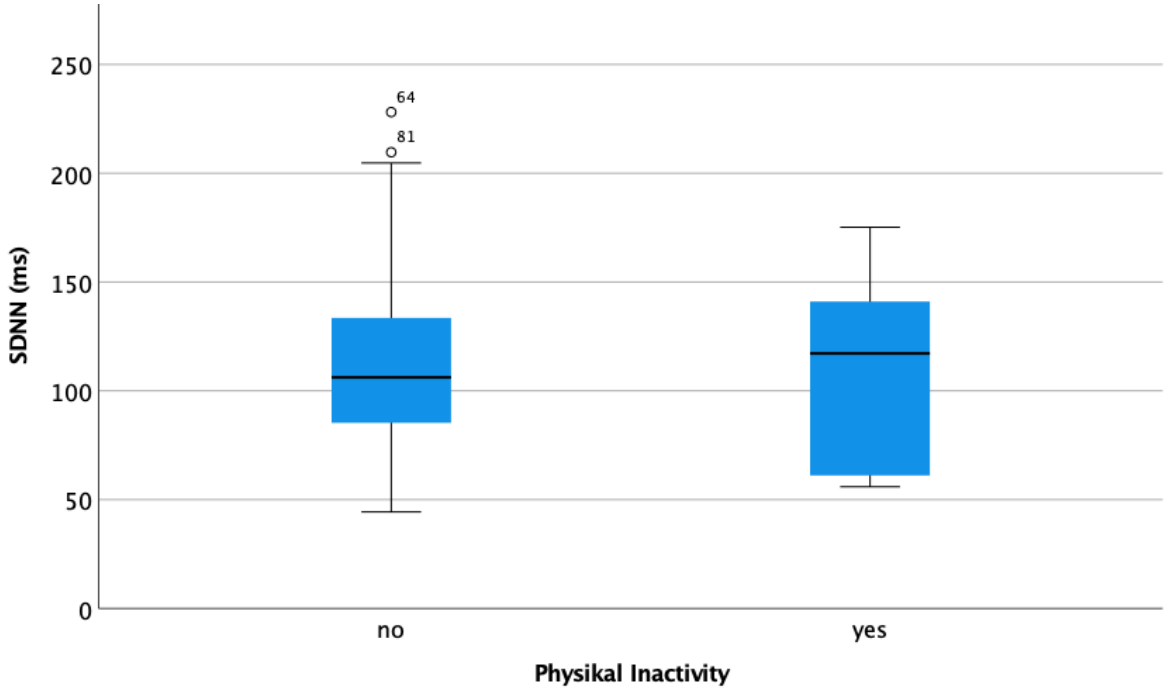

Figure 40.: SDNN values of physical active and inactive patients.

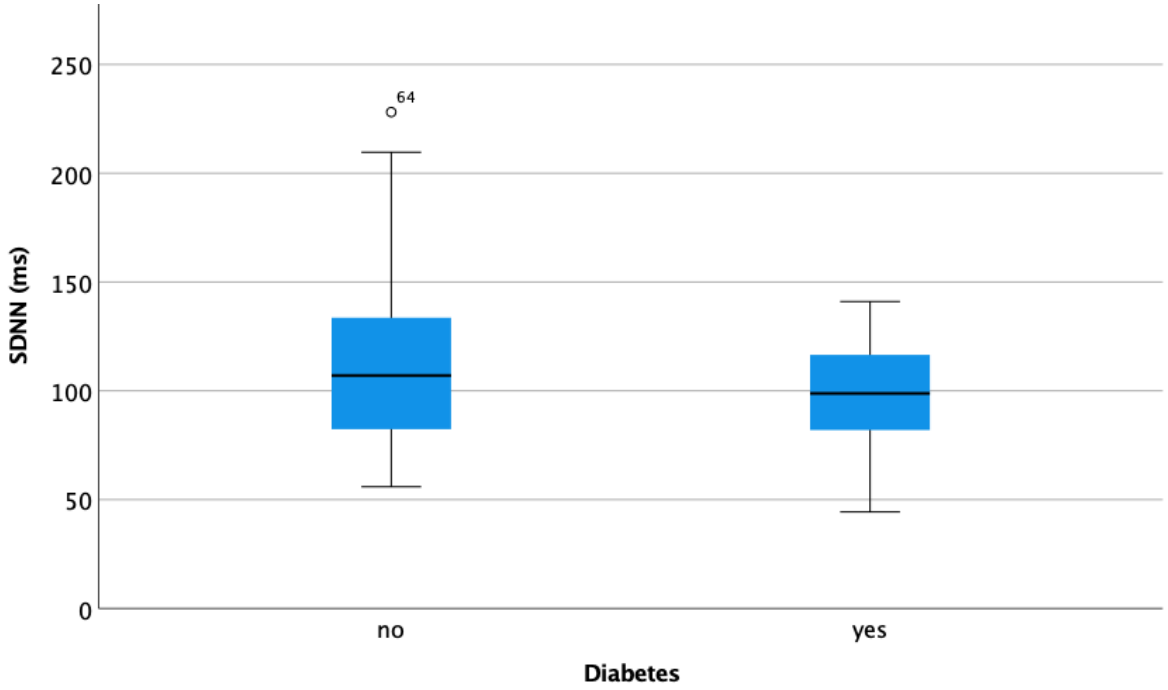

(a)

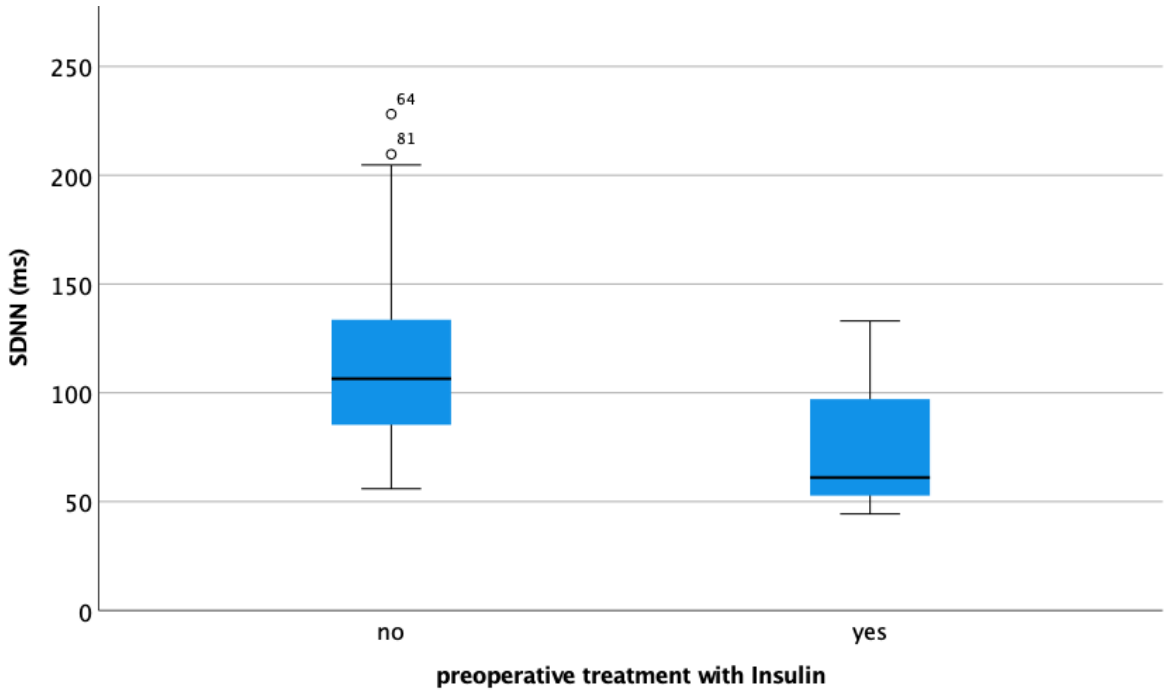

(b)

Figure 41.: SDNN of (a) diabetic and (b) patients with preoperative insulin treatment compared with the rest of the patients.

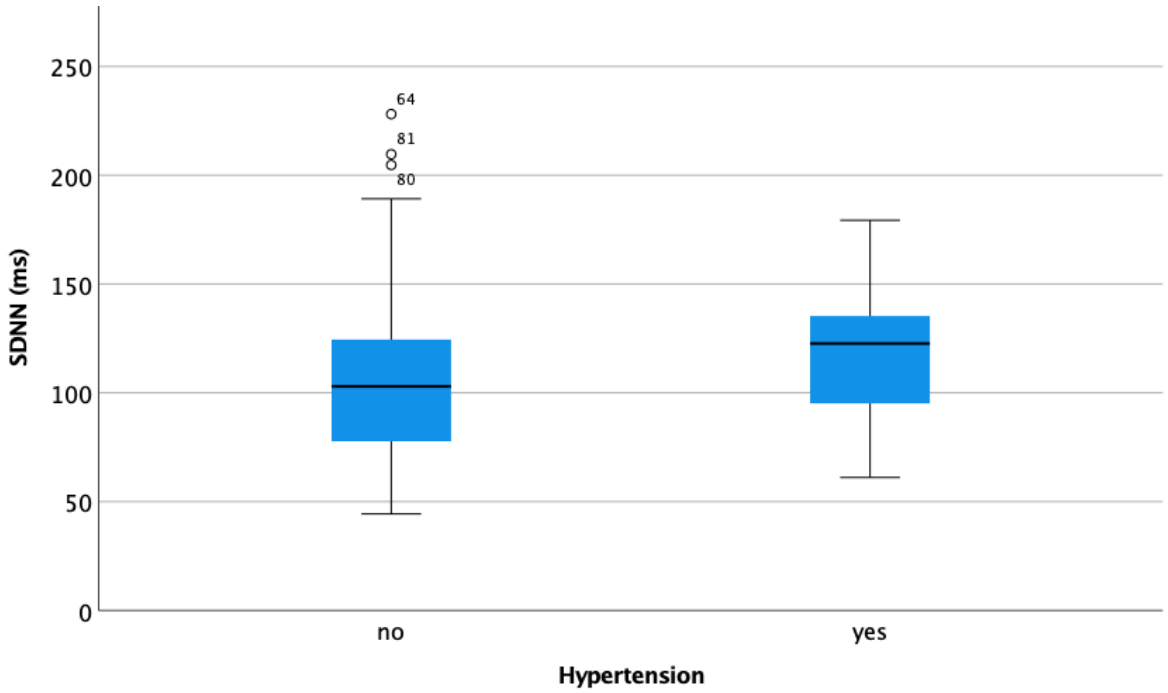

Figure 42.: SDNN values of normotensive patients compared with hypertensive patients.

ative treatment with insulin (3 patients) compared with the rest of the 73 patients (see Figure 41b).

In the given dataset, the SDNN values of patients with hypertension (24 patients) seem to bee higher than those of normotensive patients (52 patients) (see Figure 42).

3.4.3.2. Body mass index

Between the BMI of the patient and the SDNN values there is a very vague quadratic correlation as it can be seen in Figure 43a. The highest SDNN values can be observed in patients with BMI values from $20\,\mathrm{kg\,m^{-2}}$ to $30\,\mathrm{kg\,m^{-2}}$ (mainly normal bodyweight and pre-obese patient). One could think that abnormal (lower and higher) BMI values will result in lower HRV values, but based on the given data, this estimation is rather imprecise.

When the classification obese (BMI $30\,\mathrm{kg\,m^{-2}}$ or more) and non-obese (BMI smaller than $30\,\mathrm{kg\,m^{-2}}$) is used, the correlation with the HRV values seems to be a bit more distinct. In Figure 43b, it can be seen that the obese patients (14 patients) feature a lower SDNN than the non-obese patients (62 patients).

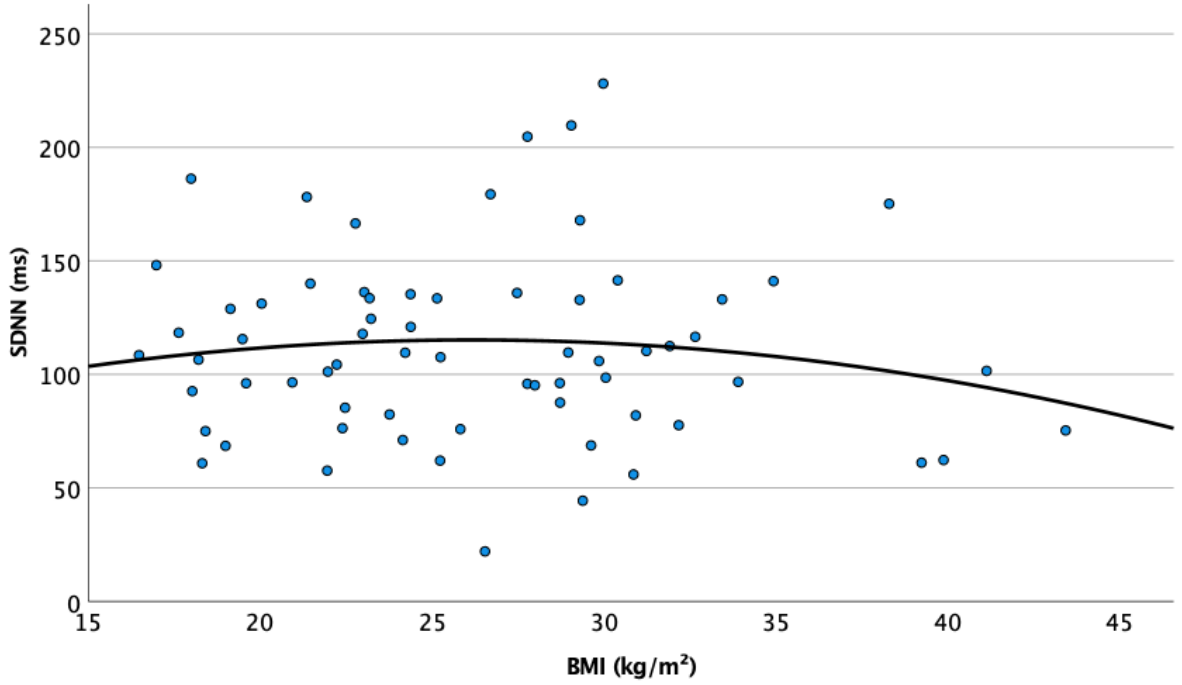

(a)

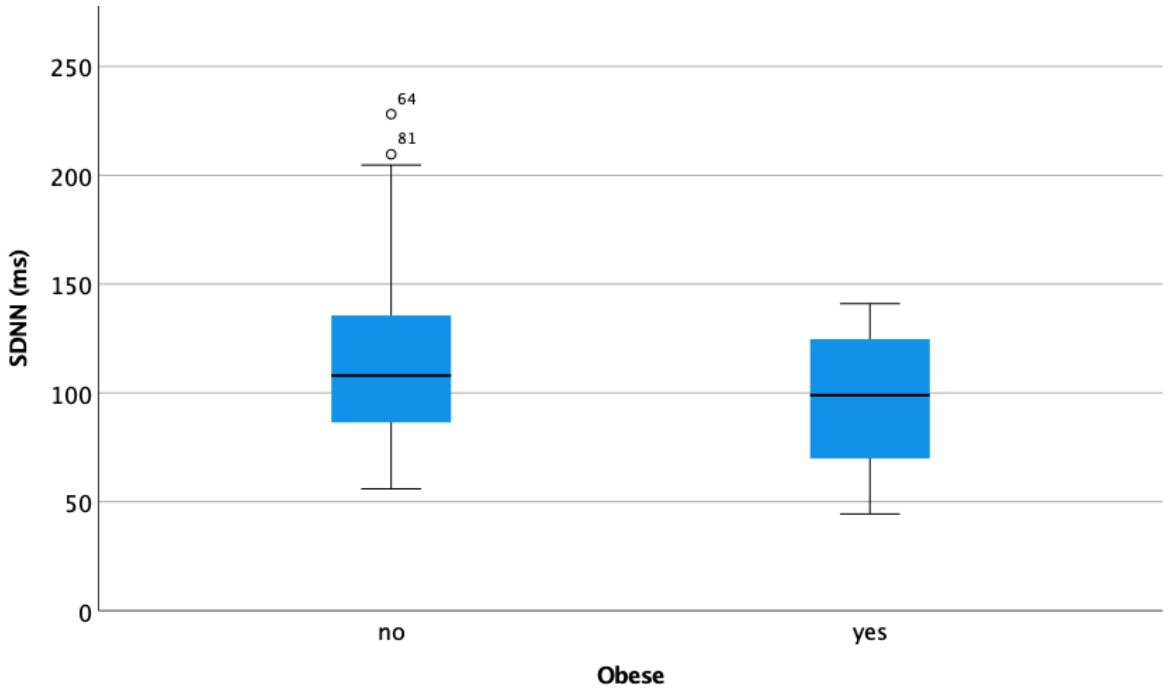

(b)

Figure 43.: (a) Trend of the SDNN values of patients with different BMI values and (b) SDNN values of obese (BMI 30 kg m^{-2} or more) and non obese patients.

3.4.3.3. Age and Size

In the given dataset, no correlation between age respectively sex and the HRV values could be found. The cause of the missing correlation between age and HRV might be the extreme heterogeneous patient collective and types of surgery.

3.4.4. Surgery Duration

In Figure 44 the influence of the surgery duration and thus the influence of the duration of the general anesthesia on the HRV is shown. Figure 45 further shows the relative trend of the HRV in percent relative to the HRV of the first five minutes. It can be seen that there is a sudden drop of the HRV after about 10 min in the ASA I and ASA II patients but this drop is not that distinct in the ASA III patients.

Furthermore, when the absolute values of the standard deviation of normal to normal beat intervals during the surgery time from about 20 min to 60 min are compared an interesting phenomenon can be observed: the HRV values of ASA I and ASA II patients being under general anaesthesia are quite similar to the values of ASA III patients during the same time period.

Although the data does not provide specific time indications, during this time frame, it is likely that all patients will be in deep anesthesia and the surgery will already be underway. From 0 min to approximately 10 min, preoperative preparations are probably still being made or anesthesia is being initiated. After the period of 60 min the HRV data can no longer be compared as some of the surgeries will already be finished and others will continue.

3.4.5. Other biosignals

When the trend of the HRV is compared to other biosignals (for example blood pressure, hypotonic/hypertonic phases, SpO_2, desaturation events) no correlation with the HRV parameters could be found.

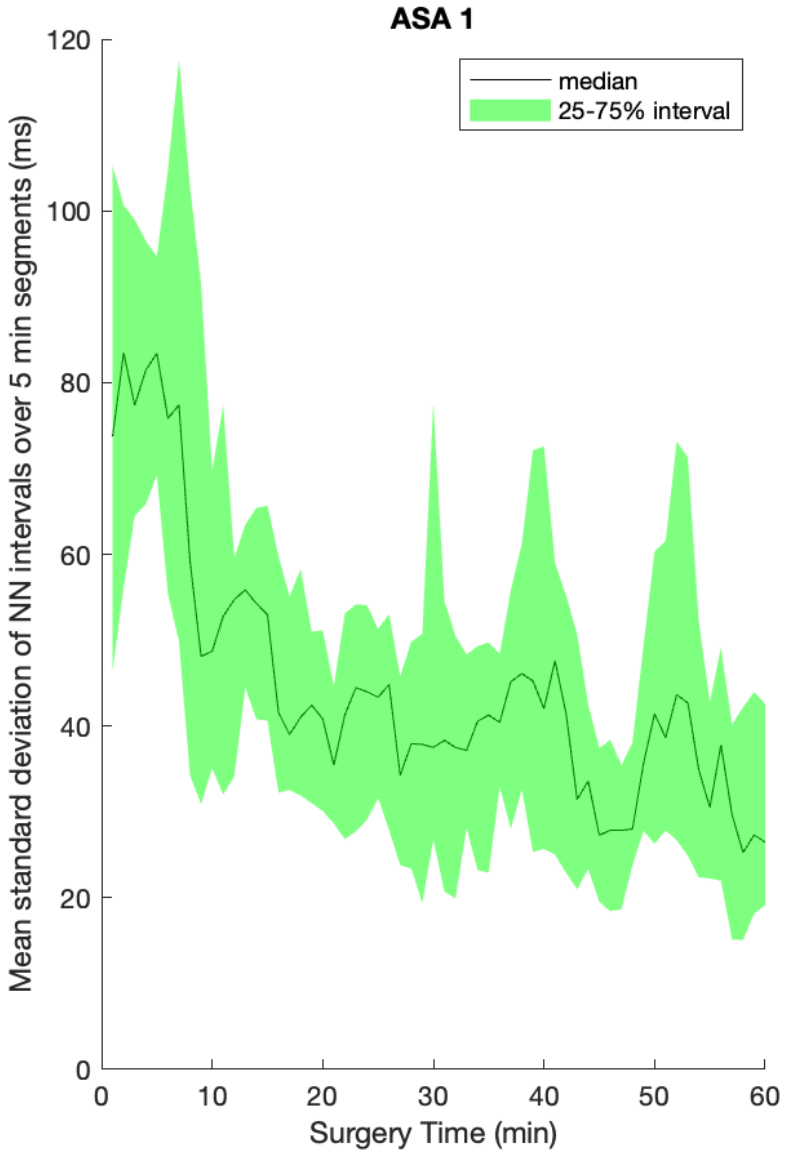

(a)

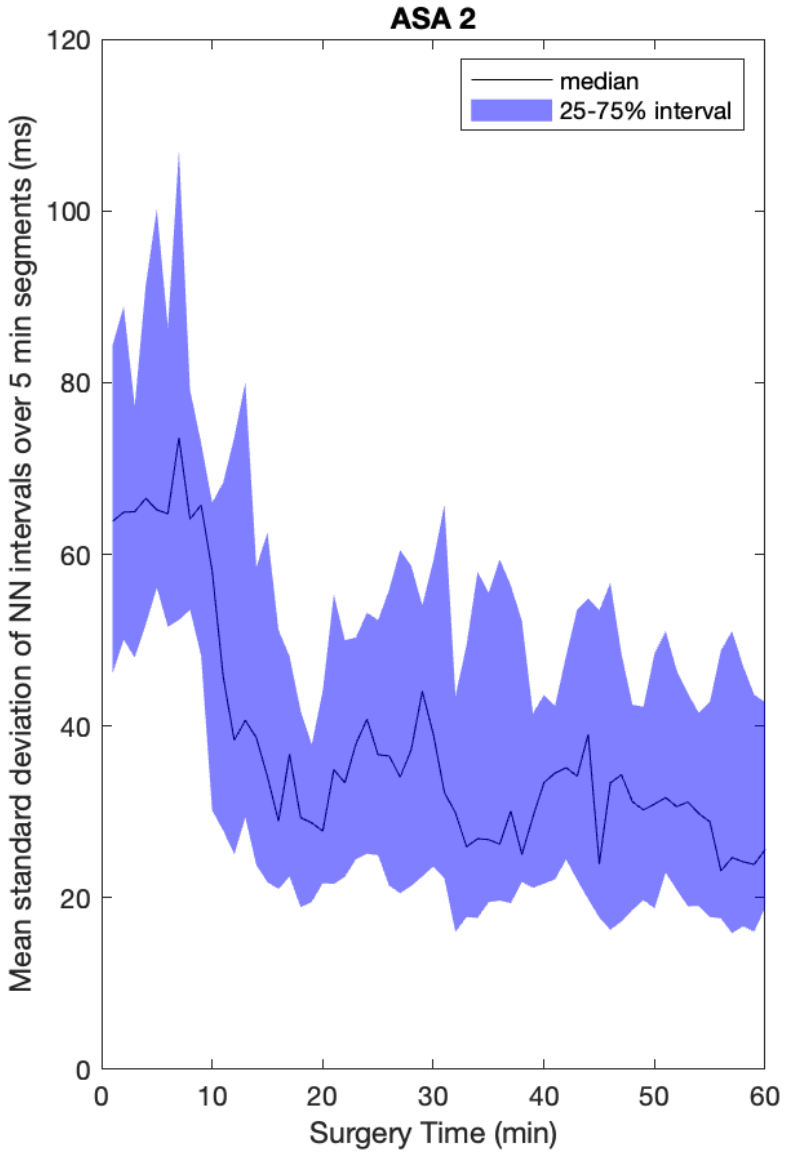

(b)

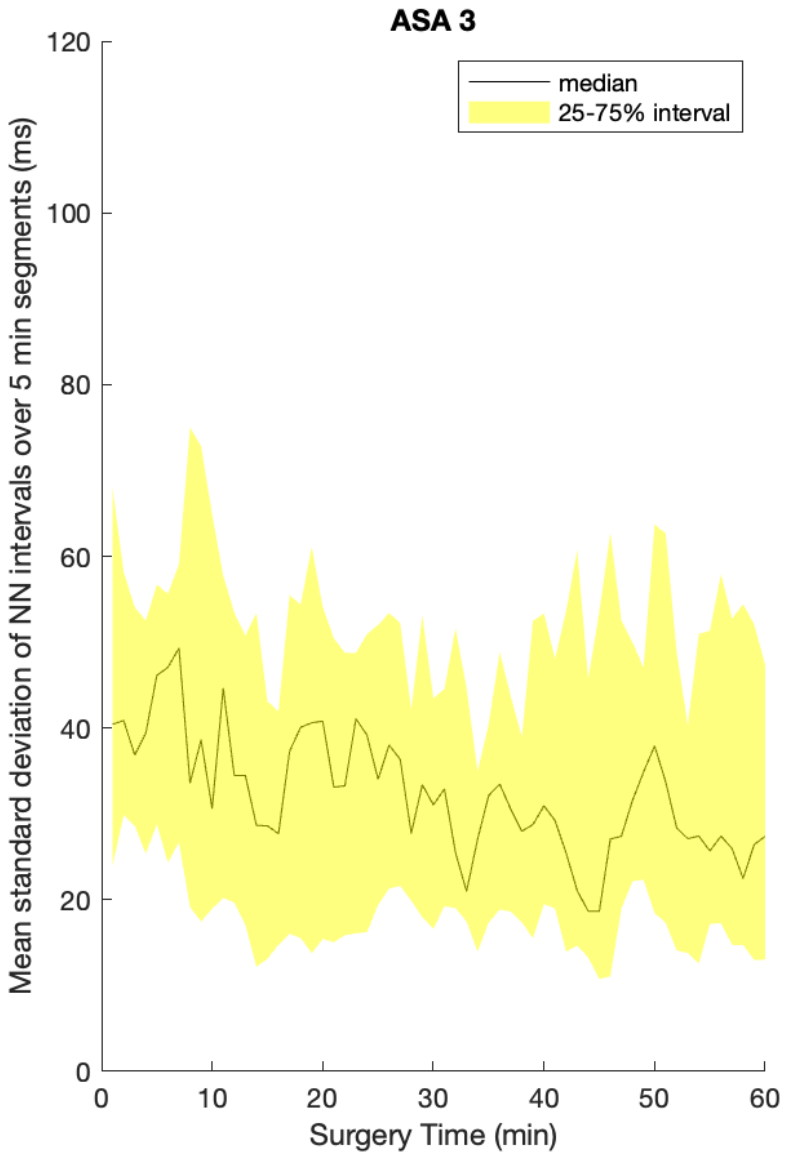

(c)

Figure 44.: Trend of the standard deviation of normal to normal beat intervals over 5 minute segments for the first 60 min in the operating room (start of the recorded ECG) for patients scored (a) ASA 1, (b) ASA 2 and (c) ASA 3.

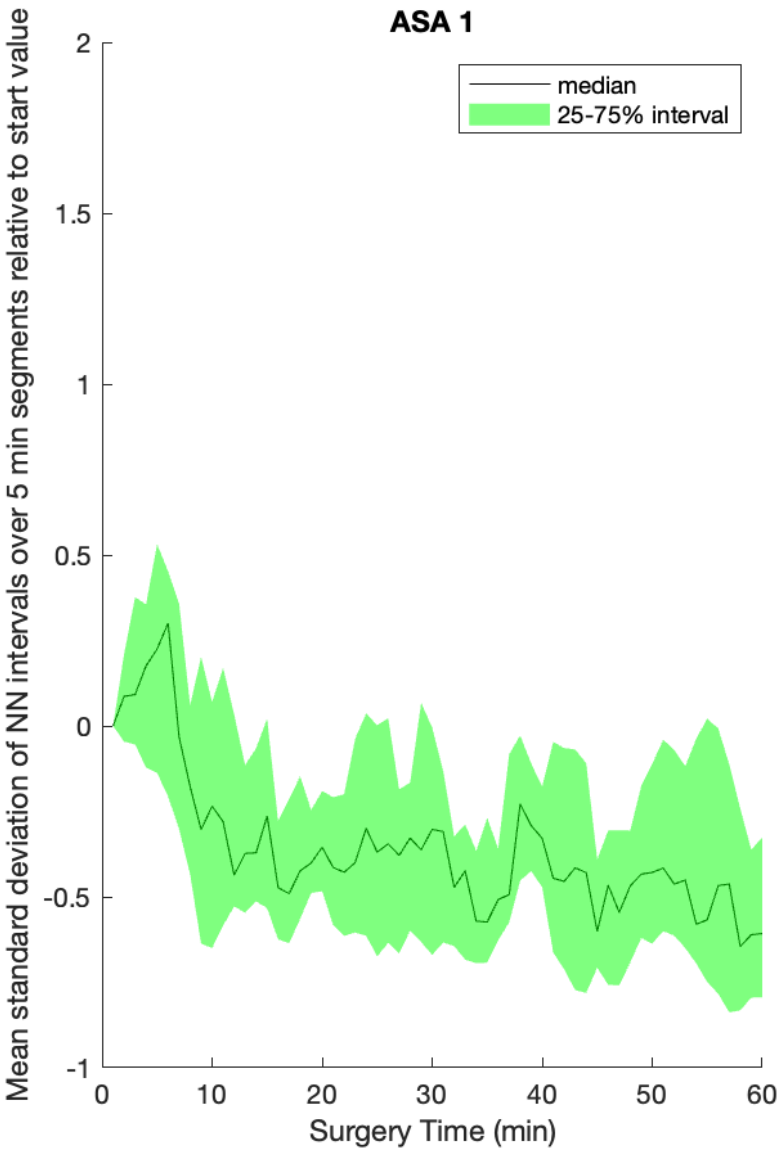

(a)

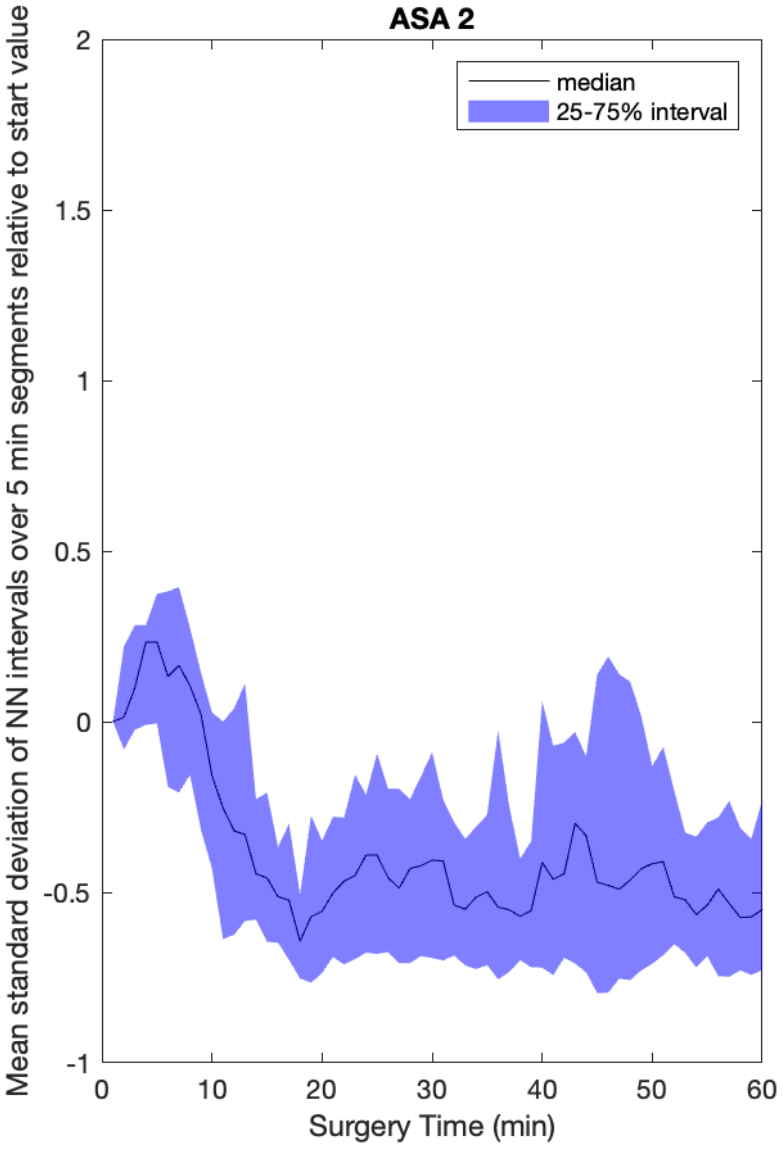

(b)

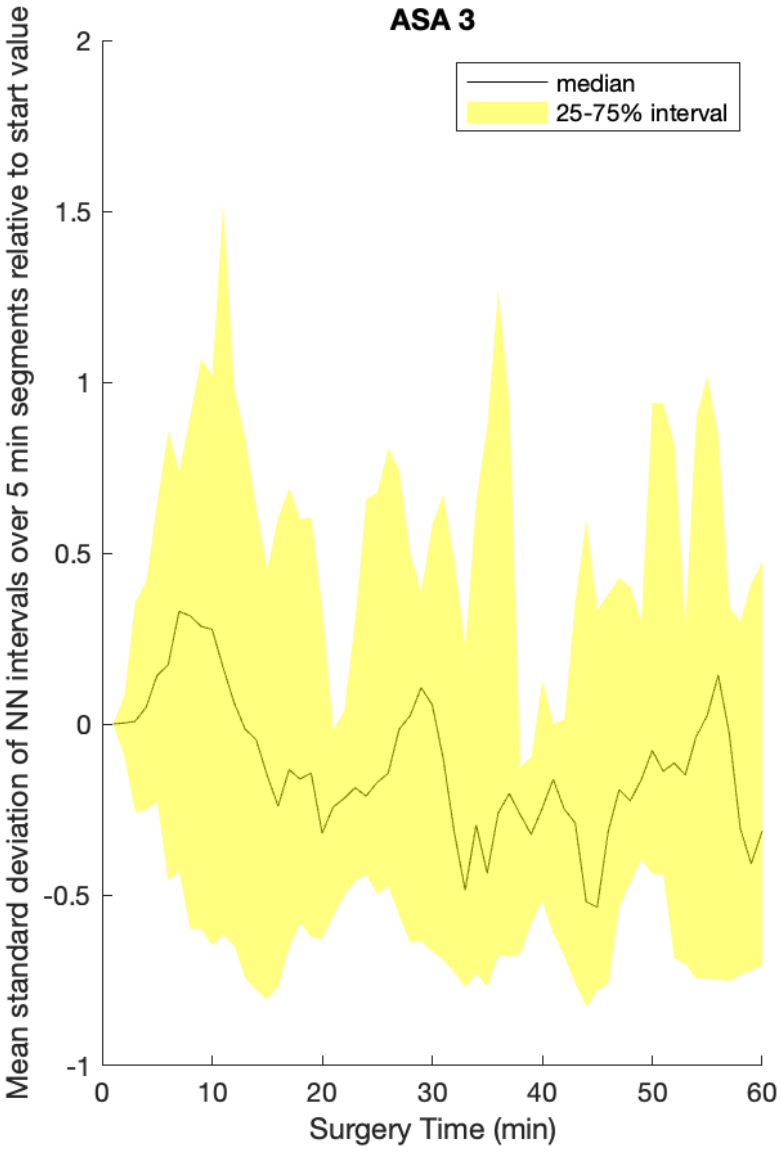

(c)

Figure 45.: Trend of the standard deviation of normal to normal beat intervals over 5 minute segments relative to the initial value for the first 60 min in the operating room (start of the recorded ECG) for patients scored (a) ASA 1, (b) ASA 2 and (c) ASA 3.

4. Discussion

4.1. Data aquisition

The given dataset includes ECG data from over 80 surgical procedures, but unfortunately the metadata is often incomplete. For example, the results of preoperative blood tests and the scores (beside the ASA score) are missing for a significant share of the patients. Furthermore, there is no information available which anesthesia procedures or medication the patients received during the perioperative period. Other outcome parameters like mortality or the need for transferring patients to the ICU are also not included in the dataset.

If this data were available, the statistical evaluation of the HRV parameter might be more significant. Therefore, the given dataset is suitable for testing the quality of the beat annotation or artefact detection but for investigating the effects on HRV parameters further research with other datasets needs to be done.

4.2. Beat annotation

By comparing the performance metrics of the original beat to beat detection algorithms provided by the AIT [57] with the results from the additional algorithms a slightly smaller sensitivity but a higher PPV was achieved for normal sinus beats (see section 3.2). The reduction of the sensitivity happens due to the fact that the methods used to further process the annotation can only delete annotations or convert annotations from normal to ectopic beats but cannot add extra beat annotations.

In summary, the additional artefact detection and post processing algorithms can be seen as a measure to improve the PPV of normal sinus beats and thereby the quality of the normal (sinus) beat to (sinus) beat signal. As a positive side effect the performance metrics (sensitivity, PPV and F_1 score) of the ectopic beats got improved dramatically by correctly converting some annotations from normal to ectopic beats.

4.3. Optimization of the algorithms

As the F_1 score is the harmonic mean of the PPV and sensitivity, all the methods used to improve the F_1 score can also reduce the sensitivity but in doing so an increased PPV is achieved (or vice versa). In this work, all of the algorithms were designed to generate a maximum of true positive beats and a minimum of false positive beats in order to generate a beat to beat signal as precise as possible as an input for the HRV analysis. Thereby it was accepted to miss some beats (have more false negatives) and thus to result in a lower sensitivity.

In detail, the reduced sensitivity can be explained by the fact that the additional algorithms can only delete (or classify as ectopic beats) presumably falsely annotated beats from the original QRS detection algorithms but the algorithms cannot detect additional beats independently. Thereby the F_1 score for the ectopic beats as well as the sensitivity and PPV are increased dramatically as shown in Figure 27 and Figure 28.

This is necessary in order to gain a beat to beat interval signal with as little errors as possible in it to further perform the HRV analysis upon.

4.4. Heart rate variability

Using the HRV analysis some phenomenona that can also be found in literature research could be reproduced. For example, in subsection 3.4.2 it is shown that in the given dataset there is a negative correlation between SDNN and the amount of CRP measured preoperative. This finding is consistent with the reduced (HF and LF) HRV indices found in patients with increased CRP or Interleukin 6 levels [62, 63].

Furthermore, a drop of the HRV after the introduction of general anesthesia can be seen in the results given in subsection 3.4.4. This finding is coherent with the loss of HRV corresponding to the state of general anesthesia found in literature search [64]. Although the clinical implications from this data are uncertain at this time, further investigation could reasonably include a more-complete analysis and more specific meta-data and could therefore bring more insight in this topic. For example there are several obvious limitations as the anesthetic techniques that were used in the patients receiving anesthesia are not known and additionally, because of the uncontrolled nature of this work, the patient population included a heterogeneous mixture of ages, types of surgery and baseline health characteristics.

Therefore, as already mentioned in section 4.1, the quality of the metadata in the

given dataset is not as ideal as it could be and therefore the statistical informative value (for example correlation between the HRV data and the effect of drugs used during general anesthesia) might be further improved by using additional patient information. For example, the artificial ventilation frequency is one of the parameters that might be interesting for the statistical analysis and although this parameter is typically monitored in all general anesthesia procedures the value is not saved in the patient data files.

5. Conclusion

The demonstrated efficacy of the newly developed algorithms offers researchers a powerful tool to gain a comprehensive understanding of big ECG datasets. Furthermore, by comparing the output of the algorithms with manually annotated ECG data it was shown that the algorithms quality is more than adequate. Overall the algorithms achieved a mean PPV of 0.9889 and a mean sensitivity of 0.9738 for detecting normal (sinus) heart beats from the raw ECG data.

From this beat annotation the HRV parameters are then calculated in an automatic manner and all of the patient data (metadata, biosignals and derived data) are stored in a single file in order to simplify further data processing procedures.

In the present ECG dataset from different patients during general anaesthesia it can be concluded that general anesthesia is associated with decreased HRV compared to the baseline HRV at the beginning of the ECG recordings. Furthermore patients with different preexisting medical conditions like diabetes, inflammation or higher ASA classifications also show lower HRV metrics.

Overall the algorithms developed in this work can be used to investigate large ECG datasets as the ones recorded with VREACT as there was also an emphasis on the computational performance of the algorithms. The next step will be a handover of the developed tools to health care professionals in order to receive feedback from end users.

In the future the algorithms can be used to gain more insight in the effects of different surgical procedures and anesthesiological action on the HRV parameters and those information then may be used in clinical practice. In the long run the HRV parameters might also be calculated in real time by the monitoring devices and displayed to the anesthesiologist so that they can react promptly to any changes if necessary.

A. MATLAB Code

To run the following code MATLAB version 2022a or later is required [49].

```
% window length
window = fs*windowDuration;

%% first run
% create the local RMS vector and calculate the local RMS
localRMS1(1:length(signal))=0;

% for the first window/2 samples the rms is calculated only in one side
for i = 1:window/2
    localRMS1(i) = rms(signal(i:i+window));
end
% local rms is calculated from window/2 samples to the right and left
for i=window/2+1:length(signal)-window/2
    localRMS1(i) = rms(signal(i-window/2:i+window/2));
end
% for the last window/2 samples the rms is calculated only in one side
for i = length(signal)-window/2+1:length(signal)
    localRMS1(i) = rms(signal(i-window/2:i));
end

standardDeviation = std(localRMS1);
meanRMS = mean(localRMS1);

% calculate the absolute threshold value
threshold1 = meanRMS+findArtefactsFactorThreshold1*standardDeviation;

%find all the places where the local RMS is higher than the threshhold
noise1 = find(localRMS1> threshold1);

%% secound run with artefacts set to 0
signal(noise1)=0;
```

```
% create the local RMS vector and calculate the local RMS
localRMS2(1:length(signal))=0;

% for the first window/2 samples the rms is calculated only in one side
for i = 1:window/2
    localRMS2(i) = rms(signal(i:i+window));
end
% local rms is calculated from window/2 samples to the right and left
for i=window/2+1:length(signal)-window/2
    localRMS2(i) = rms(signal(i-window/2:i+window/2));
end
% for the last window/2 samples the rms is calculated only in one side
for i = length(signal)-window/2+1:length(signal)
    localRMS2(i) = rms(signal(i-window/2:i));
end

standardDeviation = std(localRMS2);
meanRMS = mean(localRMS2);

% calculate the absolute threshold value
threshold2 = meanRMS+findArtefactsFactorThreshold2*standardDeviation;

%find all the places where the local RMS is higher than the threshhold
noise2 = find(localRMS2> threshold2);

%% combine the artefact areas from run 1 und 2
noise = sort(unique([noise1,noise2]));

% artefactIndex should only store the start and end indices of the
% artefact Areas
if isempty(noise)
    artefactArea = [];
else
    artefactArea= [noise(1), noise((diff(noise)>1)),...
        noise(find(diff(noise)>1)+1),noise(end)];
    artefactArea = sort(artefactArea);
    overlap = [find(diff(artefactArea)==0),find(diff(artefactArea)==0)
       +1];
    artefactArea(overlap) = [];
end
```

Listing 1: MATLAB code of the RMS value based artefact area detection algorithm.

```
%% enlarge the artefact areas to both sides by minDistance samples
if minDistance>0
        artefactArea(1:2:end) = artefactArea(1:2:end)-minDistance;
        artefactArea(2:2:end) = artefactArea(2:2:end)+minDistance;

        if (artefactArea(1)<1)
                artefactArea(1)=1;
        end
        if (artefactArea(end)>length(signal))
                artefactArea(end)=length(signal);
        end
end
```

Listing 2: MATLAB code of the enlarge the artefact areas algorithm.

```
%% detection of artefacts before and after artefact areas

localVariance = movstd(rrSignal,beforeAfterWindowLength,'omitnan');
localMean = movmean(rrSignal,beforeAfterWindowLength,'omitnan');

remove = []; % this vector will store all the beats to be removed
for i=1:2:length(artefactArea)
    before = find(peaks<artefactArea(i),1,'last');
    if before<=length(rrSignal) & before>3
        if ((rrSignal(before-3)<localMean(before)-beforeAfterFactor23*
           localVariance(before))|...
                (rrSignal(before-3)>localMean(before)+
                   beforeAfterFactor23*localVariance(before)))
            remove = [remove, before,before-1,before-2];
        elseif ((rrSignal(before-2)<localMean(before)-
           beforeAfterFactor23*localVariance(before))|...
                (rrSignal(before-2)>localMean(before)+
                   beforeAfterFactor23*localVariance(before)))
            remove = [remove, before, before-1];
        elseif ((rrSignal(before-1)<localMean(before)-
           beforeAfterFactor1*localVariance(before))|...
                (rrSignal(before-1)>localMean(before)+
                   beforeAfterFactor1*localVariance(before)))
            remove = [remove, before];
        end
    end
end
```

```
for i=2:2:length(artefactArea)
    after = find(peaks>artefactArea(i),1,'first');
    if after<=length(rrSignal)-2
        if ((rrSignal(after+2)<localMean(after)-beforeAfterFactor23*
           localVariance(after)) |...
                (rrSignal(after+2)>localMean(after)+beforeAfterFactor23
                   *localVariance(after)))
            remove = [remove, after, after+1,after+2];
        elseif ((rrSignal(after+1)<localMean(after)-beforeAfterFactor23
           *localVariance(after)) |...
                (rrSignal(after+1)>localMean(after)+beforeAfterFactor23
                   *localVariance(after)))
            remove = [remove, after, after+1];
        elseif ((rrSignal(after)<localMean(after)-beforeAfterFactor1*
           localVariance(after)) |...
                (rrSignal(after)>localMean(after)+beforeAfterFactor1*
                   localVariance(after)))
            remove = [remove, after];
        end
    end
end

% wrong beats are annotated as 'A' = artefact
annotation(remove)='A';
```

Listing 3: MATLAB code of the algorithm detecting artefacts before and after artefact areas.

```
%% removing longer breaks from beat to beat interval
localMean = movmean(rrSignal,maxBreakWindow,'omitnan');

newArtefactStart = peaks(rrSignal>localMean*maxBreakFactor)+1;
newArtefactEnd = peaks(find(rrSignal>localMean*maxBreakFactor)+1)-1;

artefactArea = unique(sort([artefactArea,newArtefactStart,
   newArtefactEnd]));
```

Listing 4: MATLAB code of the algorithm removing longer breaks from beat to beat interval.

```
%% detection of single artefacts from beat to beat interval
remove = [];
localMean = movmean(rrSignal,singleArtefactWindowLength,'omitnan');

for i=1:length(rrSignal)-1
    if (rrSignal(i)+rrSignal(i+1)<singleArtefactFactor*localMean(i))
        remove = [remove, i+1];
    end
end

beats = peaks(annotation~='A');
removebeats = beats(remove);
annotation(find(ismember(peaks,removebeats)))='A';
```

Listing 5: MATLAB code of the algorithm detecting single artefacts from the beat to beat interval.

```
%% find ectopic beats and bigeminy rhythm
localMeanNN = movmean(nnSignal,ectopicWindowLength,'omitnan');

for i=1:length(rrSignal)-1
    % ectopic beat with compensatory pause
    if ((rrSignal(i)<withBreakThreshold1*localMeanNN(i)) && (rrSignal(i
       +1)>...
            withBreakThreshold2*localMeanNN(i))&&(annotation(i)=='N'))
        annotation(i+1) = 'E';
    end
end
% Bigeminy
for i=1:length(rrSignal)-2
    if ((rrSignal(i)<bigeminyThreshold1*localMeanNN(i)) && ...
            (rrSignal(i+1)>bigeminyThreshold2*rrSignal(i))&& ...
            (rrSignal(i+2)<bigeminyThreshold1*localMeanNN(i)))
        annotation(i+1) = 'E';
    end
end
```

Listing 6: MATLAB code of the algorithm detecting ectopic beats and bigeminy rhythm.

Bibliography

[1] L. Sörnmo and P. Laguna, *Bioelectrical Signal Processing in Cardiac and Neurological Applications*. Amsterdam ; Boston: Elsevier Academic Press, 2005, 668 pp., ISBN: 978-0-12-437552-9.

[2] J. Schiff, A. Welker, B. Fohr, A. Henn-Beilharz, U. Bothner, H. Van Aken, A. Schleppers, H. Baldering, and W. Heinrichs, "Major incidents and complications in otherwise healthy patients undergoing elective procedures: Results based on 1.37 million anaesthetic procedures," *British Journal of Anaesthesia*, vol. 113, no. 1, pp. 109–121, Jul. 2014, ISSN: 00070912. DOI: 10.1093/bja/aeu094. [Online]. Available: https://linkinghub.elsevier.com/retrieve/pii/S0007091217315519 (visited on 09/07/2022).

[3] D. Sellers, C. Srinivas, and G. Djaiani, "Cardiovascular complications after non-cardiac surgery," *Anaesthesia*, vol. 73 Suppl 1, pp. 34–42, Jan. 2018, ISSN: 1365-2044. DOI: 10.1111/anae.14138. pmid: 29313903.

[4] T. A. Anderson, "Heart rate variability: Implications for perioperative anesthesia care," *Current Opinion in Anaesthesiology*, vol. 30, no. 6, pp. 691–697, Dec. 2017, ISSN: 1473-6500. DOI: 10.1097/ACO.0000000000000530. pmid: 28957877.

[5] A. T. Mazzeo, E. La Monaca, R. Di Leo, G. Vita, and L. B. Santamaria, "Heart rate variability: A diagnostic and prognostic tool in anesthesia and intensive care," *Acta Anaesthesiologica Scandinavica*, vol. 55, no. 7, pp. 797–811, Aug. 2011, ISSN: 1399-6576. DOI: 10.1111/j.1399-6576.2011.02466.x. pmid: 21658013.

[6] T. Laitio, J. Jalonen, T. Kuusela, and H. Scheinin, "The role of heart rate variability in risk stratification for adverse postoperative cardiac events," *Anesthesia and Analgesia*, vol. 105, no. 6, pp. 1548–1560, Dec. 2007, ISSN: 1526-7598. DOI: 10.1213/01.ane.0000287654.49358.3a. pmid: 18042846.

[7] R. Brandes, F. Lang, and R. F. Schmidt, Eds., *Physiologie des Menschen: mit Pathophysiologie*, ser. Springer-Lehrbuch. Berlin, Heidelberg: Springer Berlin Heidelberg, 2019, ISBN: 978-3-662-56467-7 978-3-662-56468-4. DOI: 10.1007/978-3-662-56468-4. [Online]. Available: http://link.springer.com/10.1007/978-3-662-56468-4 (visited on 03/20/2022).

[8] S. Standring, Ed., *Gray's Anatomy: The Anatomical Basis of Clinical Practice*, 42nd ed. Elsevier, 2020, ISBN: 978-0-7020-7705-0 978-0-7020-7706-7. [Online]. Available: https://www.elsevier.com/books/grays-anatomy/standring/978-0-7020-7705-0 (visited on 03/20/2022).

[9] R. F. Schmidt and G. Thews, Eds., *Human Physiology*, 2nd ed. Berlin, Heidelberg: Springer Berlin Heidelberg, 1989, ISBN: 978-3-642-73833-3 978-3-642-73831-9. DOI: 10.1007/978-3-642-73831-9. [Online]. Available: http://link.springer.com/10.1007/978-3-642-73831-9 (visited on 03/20/2022).

[10] E. Pierce, *Diagram of the human heart*, Jun. 2, 2006. [Online]. Available: https://commons.wikimedia.org/wiki/File:Diagram_of_the_human_heart_(cropped).svg (visited on 03/21/2022).

[11] Madhero88, *Conduction system of the heart*, Nov. 29, 2013. [Online]. Available: https://commons.wikimedia.org/wiki/File:Conductionsystemoftheheart.png (visited on 03/21/2022).

[12] E. Kaniusas, *Biomedical Signals and Sensors I*, ser. Biological and Medical Physics, Biomedical Engineering. Berlin, Heidelberg: Springer Berlin Heidelberg, 2012, ISBN: 978-3-642-24842-9 978-3-642-24843-6. DOI: 10.1007/978-3-642-24843-6. [Online]. Available: http://link.springer.com/10.1007/978-3-642-24843-6 (visited on 03/29/2022).

[13] ——, *Biomedical Signals and Sensors II*, ser. Biological and Medical Physics, Biomedical Engineering. Berlin, Heidelberg: Springer Berlin Heidelberg, 2015, ISBN: 978-3-662-45105-2 978-3-662-45106-9. DOI: 10.1007/978-3-662-45106-9. [Online]. Available: http://link.springer.com/10.1007/978-3-662-45106-9 (visited on 03/29/2022).

[14] T. Tamura, Y. Maeda, M. Sekine, and M. Yoshida, "Wearable Photoplethysmographic Sensors—Past and Present," *Electronics*, vol. 3, no. 2, pp. 282–302, Apr. 23, 2014, ISSN: 2079-9292. DOI: 10.3390/electronics3020282. [Online]. Available: http://www.mdpi.com/2079-9292/3/2/282 (visited on 04/25/2022).

[15] A. Curtin, *Absorption spectra of oxygenated hemoglobin (HbO2) and deoxygenated hemoglobin (Hb) for Near-infrared wavelengths (NIR)*, Aug. 2, 2012. [Online]. Available: https://commons.wikimedia.org/wiki/File:Oxy_and_Deoxy_Hemoglobin_Near-Infrared_absorption_spectra.png (visited on 04/25/2022).

[16] P. D. Arini, S. Liberczuk, J. G. Mendieta, M. Santa María, and G. C. Bertrán, "Electrocardiogram Delineation in a Wistar Rat Experimental Model," *Computational and Mathematical Methods in Medicine*, vol. 2018, pp. 1–10, 2018, ISSN: 1748-670X, 1748-6718. DOI: 10.1155/2018/2185378. [Online]. Available: https://www.hindawi.com/journals/cmmm/2018/2185378/ (visited on 05/26/2023).

[17] American Society of Anesthesiologists, *Standards for Basic Anesthetic Monitoring*, Dec. 13, 2020. [Online]. Available: https://www.asahq.org/standards-and-guidelines/standards-for-basic-anesthetic-monitoring (visited on 06/20/2022).

[18] R. Buttner and E. Burns. (Mar. 11, 2021). Normal Sinus Rhythm, Life in the Fastlane ECG Library, [Online]. Available: https://litfl.com/normal-sinus-rhythm-ecg-library/ (visited on 08/06/2022).

[19] ——, (Jun. 4, 2021). Sinus Arrhythmia, Life in the Fastlane ECG Library, [Online]. Available: https://litfl.com/sinus-arrhythmia-ecg-library/ (visited on 08/06/2022).

[20] M. Zoni-Berisso, F. Lercari, T. Carazza, and S. Domenicucci, "Epidemiology of atrial fibrillation: European perspective," *Clinical Epidemiology*, vol. 6, pp. 213–220, 2014, ISSN: 1179-1349. DOI: 10.2147/CLEP.S47385. pmid: 24966695.

[21] R. Buttner and E. Burns. (Dec. 23, 2021). Atrial Fibrillation, Life in the Fastlane ECG Library, [Online]. Available: https://litfl.com/atrial-fibrillation-ecg-library/ (visited on 08/06/2022).

[22] ——, (Dec. 23, 2021). Atrial Flutter, Life in the Fastlane ECG Library, [Online]. Available: https://litfl.com/atrial-flutter-ecg-library/ (visited on 08/06/2022).

[23] ——, (Dec. 3, 2021). Ventricular Tachycardia – Monomorphic VT, Life in the Fastlane ECG Library, [Online]. Available: https://litfl.com/ventricular-tachycardia-monomorphic-ecg-library/ (visited on 08/06/2022).

[24] ——, (Dec. 3, 2021). Ventricular Fibrillation, Life in the Fastlane ECG Library, [Online]. Available: https://litfl.com/ventricular-fibrillation-vf-ecg-library/ (visited on 08/06/2022).

[25] ——, (Feb. 8, 2021). AV Block: 2nd degree, Mobitz I (Wenckebach Phenomenon), Life in the Fastlane ECG Library, [Online]. Available: https://litfl.com/av-block-2nd-degree-mobitz-i-wenckebach-phenomenon/ (visited on 11/06/2022).

[26] ——, (Apr. 6, 2021). AV block: 3rd degree (complete heart block), Life in the Fastlane ECG Library, [Online]. Available: https://litfl.com/av-block-3rd-degree-complete-heart-block/ (visited on 11/06/2022).

[27] ——, (Dec. 2, 2021). Premature Atrial Complex (PAC), Life in the Fastlane ECG Library, [Online]. Available: https://litfl.com/premature-atrial-complex-pac/ (visited on 08/06/2022).

[28] ——, (Jun. 2, 2021). Premature Ventricular Complex (PVC), Life in the Fastlane ECG Library, [Online]. Available: https://litfl.com/premature-ventricular-complex-pvc-ecg-library/ (visited on 08/06/2022).

[29] J. Heilman, *A rhythm strip demonstrating bigeminy*, Feb. 10, 2010. [Online]. Available: https://en.wikipedia.org/wiki/File:Bigeminy2010.JPG (visited on 04/27/2022).

[30] D. Nofftz, *Simple ECG of a Supraventricular Bigeminy*, Sep. 25, 2013. [Online]. Available: https://commons.wikimedia.org/wiki/File:Supraventrikulrer_bigeminus.png (visited on 04/27/2022).

[31] I. Cygankiewicz and W. Zareba, "Heart rate variability," in *Autonomic Nervous System*, ser. Handbook of Clinical Neurology 3, R. M. Buijs and D. F. Swaab, Eds., vol. 117, Edinburgh ; London ; New York ; Oxford ; Philadelphia ; St. Louis ; Sydney ; Toronto: Elsevier, 2013, ISBN: 978-0-444-53491-0.

[32] F. Shaffer and J. P. Ginsberg, "An Overview of Heart Rate Variability Metrics and Norms," *Frontiers in Public Health*, vol. 5, p. 258, Sep. 28, 2017, ISSN: 2296-2565. DOI: 10.3389/fpubh.2017.00258. [Online]. Available: http://journal.frontiersin.org/article/10.3389/fpubh.2017.00258/full (visited on 10/17/2022).

[33] T. Kuusela, "Methodological Aspects of Heart Rate Variability Analysis," in *Heart Rate Variability (HRV) Signal Analysis*. CRC Press, Oct. 17, 2012, pp. 9–42, ISBN: 978-1-4398-4980-4 978-1-4665-7605-6. DOI: 10.1201/b12756-4. [Online]. Available: http://www.crcnetbase.com/doi/10.1201/b12756-4 (visited on 10/17/2022).

[34] Task Force of the European Society of Cardiology and the North American Society of Pacing and Electrophysiology, "Heart rate variability: Standards of measurement, physiological interpretation and clinical use.," *Circulation*, vol. 93, no. 5, pp. 1043–1065, Mar. 1, 1996, ISSN: 0009-7322. pmid: 8598068.

[35] S. Laborde, E. Mosley, and J. F. Thayer, "Heart Rate Variability and Cardiac Vagal Tone in Psychophysiological Research – Recommendations for Experiment Planning, Data Analysis, and Data Reporting," *Frontiers in Psychology*, vol. 08, Feb. 20, 2017, ISSN: 1664-1078. DOI: 10.3389/fpsyg.2017.00213. [Online]. Available: http://journal.frontiersin.org/article/10.3389/fpsyg.2017.00213/full (visited on 10/20/2022).

[36] G. E. Billman, "The effect of heart rate on the heart rate variability response to autonomic interventions," *Frontiers in Physiology*, vol. 4, 2013, ISSN: 1664-042X. DOI: 10.3389/fphys.2013.00222. [Online]. Available: http://journal.frontiersin.org/article/10.3389/fphys.2013.00222/abstract (visited on 10/17/2022).

[37] N. M. De Souza, L. C. M. Vanderlei, and D. M. Garner, "Risk evaluation of diabetes mellitus by relation of chaotic globals to HRV," *Complexity*, vol. 20, no. 3, pp. 84–92, Jan. 2, 2015, ISSN: 10762787. DOI: 10.1002/cplx.21508. [Online]. Available: https://onlinelibrary.wiley.com/doi/10.1002/cplx.21508 (visited on 10/17/2022).

[38] E. Watanabe, K. Kiyono, Y. Yamamoto, and J. Hayano, "Heart Rate Variability and Cardiac Diseases," in *Clinical Assessment of the Autonomic Nervous System*, S. Iwase, J. Hayano, and S. Orimo, Eds., Tokyo: Springer Japan, 2017, pp. 163–178, ISBN: 978-4-431-56010-4 978-4-431-56012-8. DOI: 10.1007/978-4-431-56012-8_10. [Online]. Available: http://link.springer.com/10.1007/978-4-431-56012-8_10 (visited on 10/17/2022).

[39] C. B. Weir and A. Jan, "BMI Classification Percentile And Cut Off Points," in *StatPearls*, Treasure Island (FL): StatPearls Publishing, 2023. pmid: 31082114.

[Online]. Available: http://www.ncbi.nlm.nih.gov/books/NBK541070/ (visited on 06/01/2023).

[40] M. Saklad, "Grading of patients for surgical procedures," *Anesthesiology*, vol. 2, no. 3, pp. 281–284, May 1, 1941, ISSN: 0003-3022. DOI: 10.1097/00000542-194105000-00004. [Online]. Available: https://pubs.asahq.org/anesthesiology/article/2/3/281/19041/GRADING-OF-PATIENTS-FOR-SURGICAL-PROCEDURES (visited on 03/20/2022).

[41] American Society of Anesthesiologists, *ASA Physical Status Classification System*, 2014. [Online]. Available: https://www.asahq.org/standards-and-guidelines/asa-physical-status-classification-system (visited on 03/20/2022).

[42] New York Heart Association, "Classification of Functional Capacity and Objective Assessment," in *Nomenclature and Criteria for Diagnosis of Diseases of the Heart and Great Vessels*, M. Dolgin, Ed., 9th ed., Boston, Mass.: Little, Brown and Co, 1994, pp. 253–256, ISBN: 978-0-316-60538-0.

[43] B. E. Ainsworth, W. L. Haskell, S. D. Herrmann, N. Meckes, D. R. Bassett, C. Tudor-Locke, J. L. Greer, J. Vezina, M. C. Whitt-Glover, and A. S. Leon, "2011 Compendium of Physical Activities: A Second Update of Codes and MET Values," *Medicine & Science in Sports & Exercise*, vol. 43, no. 8, pp. 1575–1581, Aug. 2011, ISSN: 0195-9131. DOI: 10.1249/MSS.0b013e31821ece12. [Online]. Available: https://journals.lww.com/00005768-201108000-00025 (visited on 03/20/2022).

[44] T. H. Lee, E. R. Marcantonio, C. M. Mangione, E. J. Thomas, C. A. Polanczyk, E. F. Cook, D. J. Sugarbaker, M. C. Donaldson, R. Poss, K. K. L. Ho, L. E. Ludwig, A. Pedan, and L. Goldman, "Derivation and Prospective Validation of a Simple Index for Prediction of Cardiac Risk of Major Noncardiac Surgery," *Circulation*, vol. 100, no. 10, pp. 1043–1049, Sep. 7, 1999, ISSN: 0009-7322, 1524-4539. DOI: 10.1161/01.CIR.100.10.1043. [Online]. Available: https://www.ahajournals.org/doi/10.1161/01.CIR.100.10.1043 (visited on 03/20/2022).

[45] D. L. Davenport, E. A. Bowe, W. G. Henderson, S. F. Khuri, and R. M. Mentzer, "National Surgical Quality Improvement Program (NSQIP) Risk Factors Can Be Used to Validate American Society of Anesthesiologists Physical Status Classification (ASA PS) Levels:" *Annals of Surgery*, vol. 243, no. 5, pp. 636–644, May 2006, ISSN: 0003-4932. DOI: 10.1097/01.sla.0000216508.95556.cc. [Online].

Available: http://journals.lww.com/00000658-200605000-00009 (visited on 03/20/2022).

[46] S. M. Nehring, A. Goyal, and B. C. Patel, "C Reactive Protein," in *StatPearls*, Treasure Island (FL): StatPearls Publishing, 2022. pmid: 28722873. [Online]. Available: http://www.ncbi.nlm.nih.gov/books/NBK441843/ (visited on 11/06/2022).

[47] M. Stark, C. C. Kerndt, and S. Sharma, "Troponin," in *StatPearls*, Treasure Island (FL): StatPearls Publishing, 2022. pmid: 29939582. [Online]. Available: http://www.ncbi.nlm.nih.gov/books/NBK507805/ (visited on 11/06/2022).

[48] J. H. Sundjaja and S. Pandey, "Cholesterol Screening," in *StatPearls*, Treasure Island (FL): StatPearls Publishing, 2022. pmid: 32809729. [Online]. Available: http://www.ncbi.nlm.nih.gov/books/NBK560894/ (visited on 11/06/2022).

[49] MathWorks, *MATLAB*, version 2022a, Mar. 9, 2022. [Online]. Available: https://mathworks.com/products/matlab.html.

[50] N. H. Nie, C. H. Hull, and D. H. Bent, *IBM SPSS Statistics*, version 28, IBM, May 24, 2021. [Online]. Available: https://www.ibm.com/products/spss-statistics.

[51] MedUni Vienna. (). Department of Anaesthesia, Intensive Care Medicine and Pain Medicine, [Online]. Available: https://www.meduniwien.ac.at/web/en/about-us/organisation/university-departments/department-of-anaesthesia-intensive-care-medicine-and-pain-medicine/ (visited on 06/19/2023).

[52] J. Matta, *Systematical Conception, Design and Development of C++ Software for Transfer of Biomedical Data via the Hardware API of a Clinical Patient Monitor*. Wien, 2018.

[53] F. Kartal, *Development of VREACT, a Tool for Biosignal Acquisition and Visualization Capable of Real-Time Heart Rate Variability Analysis*. Wien, 2018.

[54] A. J. Bukaty and U. Klein, *Perioperative Heart Rate Variability Analysis in Real-time (PHERVR)*, Observational prospective study, NCT02761031, Aug. 20, 2018. ClinicalTrials.gov: NCT02761031. [Online]. Available: https://clinicaltrials.gov/ct2/show/study/NCT02761031 (visited on 06/17/2023).

[55] Microsoft, *Excel Workbook .xlsx*. [Online]. Available: https://support.microsoft.com/en-us/office/file-formats-that-are-supported-in-excel-0943ff2c-6014-4e8d-aaea-b83d51d46247 (visited on 07/09/2022).

[56] A. Atkielski, *ECG of a heart in normal sinus rhythm*, Jan. 13, 2007. [Online]. Available: https://commons.wikimedia.org/wiki/File:SinusRhythmLabels.svg (visited on 05/28/2022).

[57] M. Bachler, C. Mayer, B. Hametner, S. Wassertheurer, and A. Holzinger, "Online and Offline Determination of QT and PR Interval and QRS Duration in Electrocardiography," in *Pervasive Computing and the Networked World*, Q. Zu, B. Hu, and A. Elçi, Eds., red. by D. Hutchison, T. Kanade, J. Kittler, J. M. Kleinberg, F. Mattern, J. C. Mitchell, M. Naor, O. Nierstrasz, C. Pandu Rangan, B. Steffen, M. Sudan, D. Terzopoulos, D. Tygar, M. Y. Vardi, and G. Weikum, vol. 7719, Berlin, Heidelberg: Springer Berlin Heidelberg, 2013, pp. 1–15, ISBN: 978-3-642-37014-4 978-3-642-37015-1. DOI: 10.1007/978-3-642-37015-1_1. [Online]. Available: http://link.springer.com/10.1007/978-3-642-37015-1_1 (visited on 05/23/2022).

[58] Association for the Advancement of Medical Instrumentation, *ANSI/AAMI EC57: Testing And Reporting Performance Results Of Cardiac Rhythm And ST Segment Measurement Algorithms*, 2012. [Online]. Available: https://webstore.ansi.org/Standards/AAMI/ANSIAAMIEC572012R2020 (visited on 04/23/2022).

[59] TU Wien. (). Institute of Biomedical Electronics, [Online]. Available: https://www.tuwien.at/en/etit/bme (visited on 06/19/2023).

[60] T. Madsen, J. H. Christensen, E. Toft, and E. B. Schmidt, "C-Reactive Protein Is Associated with Heart Rate Variability," *Annals of Noninvasive Electrocardiology*, vol. 12, no. 3, pp. 216–222, Jul. 2007, ISSN: 1082-720X, 1542-474X. DOI: 10.1111/j.1542-474X.2007.00164.x. [Online]. Available: https://onlinelibrary.wiley.com/doi/10.1111/j.1542-474X.2007.00164.x (visited on 10/26/2022).

[61] A. Sajadieh, O. W. Nielsen, V. Rasmussen, H. O. Hein, and J. F. Hansen, "C-reactive protein, heart rate variability and prognosis in community subjects with no apparent heart disease," *Journal of Internal Medicine*, vol. 260, no. 4, pp. 377–387, Oct. 2006, ISSN: 0954-6820, 1365-2796. DOI: 10.1111/j.1365-2796.2006.01701.x. [Online]. Available: https://onlinelibrary.wiley.com/doi/10.1111/j.1365-2796.2006.01701.x (visited on 10/26/2022).

[62] N. V. Alen, A. M. Parenteau, R. P. Sloan, and C. E. Hostinar, "Heart Rate Variability and Circulating Inflammatory Markers in Midlife," *Brain, Behavior, & Immunity - Health*, vol. 15, p. 100 273, Aug. 2021, ISSN: 2666-3546. DOI: 10.1016/j.bbih.2021.100273. pmid: 34268499.

[63] A. Haarala, M. Kähönen, C. Eklund, J. Jylhävä, T. Koskinen, L. Taittonen, R. Huupponen, T. Lehtimäki, J. Viikari, O. T. Raitakari, and M. Hurme, "Heart rate variability is independently associated with C-reactive protein but not with Serum amyloid A. The Cardiovascular Risk in Young Finns Study: HEART RATE VARIABILITY, CRP AND SAA," *European Journal of Clinical Investigation*, vol. 41, no. 9, pp. 951–957, Sep. 2011, ISSN: 00142972. DOI: 10.1111/j.1365-2362.2011.02485.x. [Online]. Available: https://onlinelibrary.wiley.com/doi/10.1111/j.1365-2362.2011.02485.x (visited on 12/12/2022).

[64] G. Matchett and P. Wood, "General anesthesia suppresses normal heart rate variability in humans," *Chaos (Woodbury, N.Y.)*, vol. 24, no. 2, p. 023 129, Jun. 2014, ISSN: 1089-7682. DOI: 10.1063/1.4882395. pmid: 24985443.